Spectroscopic modeling of nitro group in explosives

SPECTROSCOPIC MODELING OF NITRO GROUP IN EXPLOSIVES

By

Doris Núñez Quintero

A thesis submitted in partial fulfillment of the requirements for the degree of

MASTER IN SCIENCES

in

CHEMISTRY

UNIVERSITY OF PUERTO RICO
MAYAGÜEZ CAMPUS

2006

Approved by:

Samuel Hernández Rivera, Ph.D. President, Graduate Committee	Date
Ismael Scott, Ph.D. Member, Graduate Committee	Date
Julio G. Briano, Ph.D. Member, Graduate Committee	Date
Gustavo Gutierrez, Ph.D. Representative of Graduate Studies	Date
Francis Patron, Ph.D. Chairperson of the Department	Date

To God who guides me at all times of my life and who carried me every time higher. To my parents, Miguel and Doris, who are my biggest treasure. To my husband, James, for his support, for the good times and moments we have shared together. To my son, Jesús, for teaching me to be a mother.

ACKNOWLEDGMENTS

I acknowledge the guidance of my thesis advisor Dr. Samuel Hernández for his advice and support throughout the development of this study. I would also like to thank the Chemistry Department of the University of Puerto Rico Mayagüez Campus for giving me the opportunity to work in my master degree and supporting me economically during these years. I wish to express my gratitude to James Díaz MS. for his interest in my research and his guidance. I wish to express my gratitude to my friend Oliva Primera for her inconditional help.

The Grant from the center for Chemical Sensors Development of the University of Puerto Rico-Mayagüez sponsored by the Department of Defense, University Research Initiative-Multidisciplinary University Research Initiative (URI-MURI) Program, under grant no. DAAD19-02-1-0257 is also acknowledged.

TABLE OF CONTENTS

LIST OF TABLES

LIST OF FIGURES

LIST OF ABBREVIATIONS

ANN:	Artificial Neural Networks
CLS:	Classical Least Square.
DA:	Discriminant Analysis.
DATB:	2,4,6-Trinitro-1,3-benzenediamine.
DCFT:	Discrete Chirp Fourier Transform.
DNT:	Dinitrotoluene IR Infrared.
DNT:	Dinitrotoluene.
FBI:	Federal Bureau of Investigation.
FFT:	Fast Fourier Transform.
FTIR:	Fourier Transform Infrared.
GA:	Genetic Algorithm.
HMX:	cyclotetramethylenetetranitramine.
HNAB:	2,2',4,4',6,6'-Hexanitroazobenzene.
HNS:	Hexanitrostilbene.
ILS:	Inverse Least Square.
MATB:	Monoaminotrinitroazobenzene.
MLR:	Multiple Linear Regression.
MLR:	Multiple Linear Regression.
NIR:	Near Infrared.
PCA:	Principal Component Analysis
PCR:	Principal Component Regression.
PETN:	Pentaerythritol Tetranitrate.
PLS:	Partial Least Square.
PRESS:	Predicted Residual Error Sum of Square
R:	Correlation Coefficient
RDX:	Ciclotetramethylenetetranitramine.
RMSEP:	Root Mean Square Error of Prediction
SA:	Simulated Annealing.
SNR:	Signal to Noise Ratio.
TATB:	1,3,5-Triamino-2,4,6-Trinitrobenzene.
TNB:	Trinitrobenzene.
TNT:	Trinitrotoluene.

ABSTRACT

In chemometrics Calibration is the process of constructing a mathematical model to relate the output of an instrument to properties of samples. Prediction is the process of using the model to predict spectroscopic properties of a given sample and instrument output. A statistical characterization, based on Discriminant Analysis (DA), of explosive substances allows a characterization and classification of the spectroscopic properties of the effect of nitro group in accordance with the molecular structure. This characterization should help for predicting the nitro group effect in other explosive substances and be a primary actor in sensor design based on IR and Raman Spectroscopies. The goal of this work was to develop a statistical model for the spectroscopic behavior for the nitro group in nitrogen based explosives (nitroexplosives) using DA. The variables used in this analysis were the Raman shift and IR wavenumber (spectral locations) of the symmetric and asymmetric mode of the nitro group. A second group of variables were the absorbance and Raman scattering intensity. Potassium Bromide pellets was used for running the samples in FTIR. The samples were measured at a 4 cm^{-1} resolution and 32 scans. Spectra were collected using Bruker OPUS version 4.2 software, in the range of 400-4000 wavenumbers (cm^{-1}). Raman spectra of samples were collected from neat samples deposited on stainless steel slides (for solids) and in melting point capillary tubes (for liquids). Raman analysis was carried out by using a confocal Renishaw Raman Microspectrometer Model RM2000 equipped with a solid state diode laser system emitting at a wavelength of 532 nm as the excitation source. A statistical model using sixty explosives is presented. In this study was obtained a good model of

calibration using Discriminant Analisis (Linear Discriminant Function) and it was possible to observe, the nitro group behavior in explosives for Raman and Infrared Spectroscopy.

RESUMEN

En Quimiometría, Calibración es el proceso de construir un modelo matemático que relaciona las propiedades de las muestras leídas por un instrumento. Predicción es el proceso de usar el modelo para deducir propiedades espectroscópicas de una muestra dada en un instrumento. Una caracterización estadística, basada en análisis discriminante (DA), de sustancias explosivas seguida de una caracterización y clasificación de las propiedades espectroscópicas del efecto de el grupo nitro de acuerdo con la estructura molecular fue desarrollada. Esta caracterización ayudará a predecir el efecto del grupo nitro en otras sustancias explosivas y será un actor primario en el diseño de un sensor basado en espectroscopías Raman e Infrarrojo. La meta de este trabajo fue desarrollar un modelo estadístico para el comportamiento espectroscópico del grupo nitro en nitro explosivos usando análisis discriminante. Las variables usadas en este análisis fueron el desplazamiento químico en Raman y numero de onda en infrarrojo de los modos simétrico y asimétrico del grupo nitro. Un Segundo grupo de variables fueron la absorbancia e intensidad. Las tabletas de bromuro de potasio fueron usadas para correr las muestras en Infrarrojo. Las muestras fueron medidas a 4 cm^{-1} de resolución y 32 Sans. Los espectros fueron colectados usando Bruker, software OPUS versión 4.2, en el rango de 400-4000 números de onda (cm^{-1}). Los espectros fueron colectados de muestras depositadas sobre placas de acero inoxidable (para sólidos) y de tubos capilares para líquidos. Análisis Raman fue llevado a cabo usando un Reishaw microespectrometro Raman confocal modelo RM2000 equipado con un sistema láser de diodo en estado sólido, emitiendo

longitudes de onda de 532 nm como fuente de excitación. Un modelo estadístico usando 60 explosivos es presentado. En este estudio fue obtenido un buen modelo de calibración usando análisis discriminante (función discriminante lineal) y fue posible observar el efecto del grupo nitro de acuerdo a la clasificación echa en los explosivos por espectroscopías Infrarrojo y Raman.

CHAPTER 1
INTRODUCTION

Explosives are chemical substances that have been used for a long time. An explosive is a compound or mixture used to release, by a chemical reaction, considerable amounts of energy in a confined space and so rapidly that mechanical movement or shattering of surroundings objects is obtained. Ancient Asian alchemists accidentally made the first explosive more than two thousand years ago. By mistake they mixed saltpetre (Potassium Nitrate) and sulfur, and did not add coal, so the mixture actually detonated. Their invention was not used for war; instead of, it was employed for communication. Later the Asians using their explosive technology developed a crude projectile weapon, and then the Arabs stole the Asians knowledge and used it for war.

The explosives can be classified by their performance and uses: Primary explosives (low explosives) undergo a very rapid transition from burning to detonation. They can transmit the detonation to less sensitive explosives. They can be detonated by heat or shock. An example is mercury fulminate, it has a high degree of sensitivity to iniciation to through friction, electric spark or high temperatures and explode whether they are confined or unconfined. Secondary explosives (high explosives) cannot be detonated readily by heat or shock, and they are less sensitive than primary explosives, so they need the later to detonate. Examples are Dinitrotoluene, Trinitrotoluene, cyclotrimethylenetrinitramine, etc. Propellants only burn and do not explode under ordinary conditions. They can be initiated by a flame or

spark. Example are: blackpowder, ammonium nitrate, etc. Dinitrotoluene (DNT) is one of the high explosives that has been used for military purposes since 1902.

1.1 Objectives and Significance

The research objectives of this work are:

- To develop a statistic model of the spectroscopic behavior for the nitro group in explosives using chemometric tools.
- To make an analytical evaluation between two spectroscopic techniques such as Raman and IR about the nitro group behavior in different explosives substances for predicting some properties of NO_2 containing molecules.
- To carry out a spectroscopic study of the nitro group effect in explosives in dependence of the molecular structure.
- To build a database with Thermogalactic Grams software for the used explosives.

1.2 Justification

Calibration is the process of constructing a mathematical model to relate the output of an instrument to properties of samples. Prediction is the process of using the model to predict properties of a sample given and instrument output. Multivariate calibration offers several advantage over univariate approach, such as:

- It is feasible the analysis for multiple components simultaneously.
- Multiple redundance measurements can also provide improved precision in prediction.
- Redundance measurements in multivariate calibration also facilitates fault detection.

A statistical characterization, based in discriminant analysis, of explosive substances will allow a delimitation of the spectroscopic properties of the nitro group effect in accordance with the molecular structure. This characterization should help for predicting the nitro group effect in other explosives. Was select NO_2 because NO_2 give the explosive character to the compound

CHAPTER 2
PREVIOUS WORK

A re-appraisal of the analytical value of Raman Spectroscopy in the investigation of aromatic nitro compounds was provided by Hodge et. al. [1]. Correlations between the frequencies of the nitro vibrations with the electron-donating, withdrawing effect of substituents on the phenyl rings were found. All the compounds examined in this work were of commercial origin and were studied as supplied. Liquids were contained in small sample bottles ($5 \times 25mm$ plastic capped); solids were handled as pellets, lightly pressed into a metal sample holder. All spectra were studied by back-scattering on a spectrometer based on a Perkin-Elmer Model 1710 interferometer and a model 301 Spectron Laser Systems Nd: YAG c/w source. A resolution of 6 cm^{-1} was used and 50 to 100 scans were collected. The authors summarized their results as follows: Aromatics molecules give weak CH stretching modes Nitro compounds are invariably strong scatters with the symmetric N=O stretch the most prominent amongst the modes of the NO_2 group - There are definite correlations to be derived between the frequency of the NO stretching mode and the electron-donating and withdrawing effects of substituents on phenyl rings. The frequency and relative intensity of the highest-frequency CH stretching mode appears to follow the electron density and concentration within the molecule respectively.

Raman spectroscopy, with red (632.8 nm) and near-infrared (785 and 1064nm) excitation sources, was used to obtain high quality spectra of neat explosives by Chaffin et. al. [2]. Samples with dimensions from a minimum size of 10 μm have were analyzed utilizing a Raman microprobe fitted with a charge-coupled device

(CCD) array detector. Little sample fluorescence was observed for 23 of the 32 high explosives using 632.8 nm excitation and all of the samples could be measured with a 1064 nm. Nd: YAG laser the 785 nm radiation source afforded an excellent compromise between sensitivity and fluorescence suppression. The authors used samples of 30 heat explosives and two plastic explosives (C4 and SEMTEX) (0.05-0.1 g) were provided by the Federal Bureau of Investigation (FBI). The spectroscopic instrumentation included Raman spectra were collected using both a Renishaw dispersive Raman spectrometer and a Perkin-Elmer system 2000 FT Raman Spectrometer. The Renishaw Raman Spectrometer was a NIR-optimized spectrometer and utilizes a microscope as the sampling device. It comprised either a Ne:He laser operating at 632.8 nm or a Renishaw-developed diode laser operating at 785 nm. The authors showed that: a NIR Raman Spectroscopic system operating at a wavelength between 785 nm and 1064 nm is probably the optimum system for studies of explosives. With the CCD Raman Spectrometer used for this study, any excitation wavelength up to 860 nm may be used to measure useful spectra of explosives, as the silicon CCD array detector will still allow Raman Spectra to be collected over the wavenumber range $\Delta\nu$= 100-2000 cm^{-1}, where the most important bands for the investigation of nitro-explosives are located.

The theoretical calculations of the structure, internal rotations and vibrations of 2,4,6-trinitrotoluene, TNT were presented by Batchelder and coworkers [3]. For this work a Renishaw micro-raman system 1000 Spectrometer with 785 nm excitation was employed, and used a Nicolet Nexus Spectrometer with a Spectra-Teach Continuum microscope attached for measuring the FTIR spectra. Geometry optimization and frequency analysis of TNT was performed using GAUSSIAN 98. Results obtained of the theoretical analysis of the structure of TNT reveals two stable structures related by internal rotations of 2 or 6 Nitro group and the methyl group.

In situ detection and identification of plastic explosives, used SEMTEX-H for the study [4]. this explosive has two active chemical ingredients: Cyclotrimethylene-Trinitramine or RDX and Penta Erythritol-Tetranitrate or PETN. A Renishaw Raman Microscope was found to be highly specific and capable of identifying explosives samples $1\mu L$ in volume or $1pg$ in mass quantity.

The contamination of soils by energetic materials was studied by Moore [5], employing an InPhote portable Raman system, with 785 nm excitation wavelength, in the 200-2000 cm^{-1} Raman shift detection range and 6-8 cm^{-1} spectral resolution, was coupled the subsample holder using an optical fiber probe, and the spectral data were manipuled using GRAMS/32, the energetic materials were all of (least than) $30\mu m$ grain size to facilitate homogeneous mixing, used HMX, TATB, DATB, PETN, HNS, TNB, TNT, MATB, HNAB and d4-DATB. Multivariate Analysis was shown capable of both extracting the Raman signatures of energetic materials from spectra observed by large fluorescence backgrounds caused by soil components and generating calibration curves for the energetic materials at the percent level; used Principal components Regression (PCR) and Partial Least Square 1 (PLS1) and were performed using three factors and cross validation, with spectral preprocessing by Mean Centering and pathlength normalization, for the entire spectral range recorded. The author sugared that in all training sets investigated, PLS1 performed marginally better than PCR.

Kneipp et. al. used Surface-enhanced Raman Scattering (SERS) from trinitrotoluene (TNT) absorved on colloidal silver and gold in aqueous solutions [6]. Spectra were measured with a fiber optic probe using a diode laser at 830 nm as the excitation source and a charge-coupled device (CCD) as the detection system. Different types of surface-enhanced Raman Spectra and enhancement factors have been observed on these metals, indicating differences in adsorption of TNT on gold and silver. Spectra were measured down to 10-7 M, TNT in colloidal gold solution,

corresponding to a sensitivity of less than $1pg$ TNT. The results demonstrated the potencial at SERS for probing TNT with high sensitivity and specificity, and suggest that SERS on colloidal gold as a powerful method for detection of TNT and similar species at ultratrace levels.

Chemometrics is the application of statistical and mathematical methods to chemical problems to permit maximal collection and extraction of useful information [7]. The development of advanced chemical instruments and processes has led to a need for advanced methods to design experiments, calibrate instruments and analyze the resulting data. Chemometrics includes very useful Multivariate Calibration methods because many common analytical methods provide analyses of multiple species. In these methods, it is assumed that there are a series of mixtures for which the amounts of each component are known and for which a series of properties has been measured. The methods include PCR, PLS, Simulated Annealing (SA), Genetic Algorithm (GA) and artificial neural networks (ANN). Partial Least-Squares has been the most widely applied multivariate calibration method. In this case, the components of the matrix of spectral characteristics are extract so as to maximize the covariance with the measured absorbances in the set of calibration samples. The relationships are developed from the training set and then applied to the set of unknowns. For the unknown sample data, the concentrations of the various constituents in the samples can often be predicted with better accuracy.

The first and most straightforward advantage of multivariate analysis is a noise reduction obtained by using more (redundant) measurements of the same phenomenon [8]. *Rasmus* explain the advantages of use multivariate data analysis and stated that multivariate models are more adequate than univariate models. This strong statement holds in general because it is always possible to discard variables such that a anivariate approach is re-obtained. Thus, a multivariate approach adds opportunities but does not remove any. Multivariate models can handle situations

that can not be handled univariated. In particular, it is possible to incorporate interferents and to have automatic outlier detection when building or using a model. In the future it is expected that demands will be made for effective use of information, fast analysis results, low consumptions of chemicals, and more robust methods that should even work on unforeseen sample matrices.

The progress in the analysis of multicomponent processes and mixtures relies on the combination of sophisticated instrumental techniques and suitable data analysis tools focused on the interpretation of the multivariate responses obtained. *Tauler and de Juan* discussed the argued that the differences in compositional variation, complexity and origin, the raw measurements recorded in a multicomponent chemical system can be very often described with a simple model consisting of the composition-weighted sum of the signals of their pure compounds [9]. Multivariate resolution methods have been the tools designed to unravel this pure compound information from the non-selective mixed original experimental output. The evolution of these chemometrics approaches through the improvement of exploratory tools, the adaptation to work with complex data structures, the ability to introduce chemical and mathematical information in the algorithms and the better quality assessment of the results obtained was revisited. The active research on these chemometrics areas has allowed the successful application of these methodologies to a wide variety at chemical problems.

The UV spectrophotometric analysis of a multicomponent mixture containing paracetamol, caffeine, tripelenamine and salicylamide using multivariate calibration methods such as PCR and PLS was made by Gaetano et. al. [10]. The calibration set was based on 47 reference samples, consisting of quaternary, ternary, binary and single component mixtures, with the aim to develop models able to predict the concentrations of unknown samples containing as many as four components. The

calibration models were optimized by an appropriate selection of the number of factors as well as wavelength ranges to be used for building up the data matrix and excluding any information about the interfering excipients included in pharmaceutics. The PCR and PLS models were compared and their predictive performance was inferred by a successful application to the assays of synthetic mixtures and pharmaceutical formulations. In the experimental part they used a Perkin-Elmer lambda 40P spectrophotometer at the following conditions: scan rate 1nm/s, time response 1s, spectral band 1 nm, data density 1 point nm^{-1} The software UV Winlab 2.79.01 (Perkin Elmer) was used for spectral acquisition. Multivariate calibration consisted of the establishment of a relationship between matrices of chemical data. The methods are based first on a calibration step in which a mathematical model was built, using a chemical data set and a concentration matrix data set. The calibration was followed by a prediction step in which this model was used to estimate unknown concentrations of a mixture from its spectrum. In particular, PCR and PLS techniques are called FACTOR METHODS , because transform the high number of original variables called FACTORS or PRINCIPAL COMPONENTS which are linear combinations of the original variables. The first factors contain useful information, whereas the last ones represent the noise, which has to be discarded and not considered in the modeling.

CHAPTER 3

MULTIVARIATE CALIBRATION AND PREDICTION

Calibration is the process of constructing a mathematical model to related the output of an instrument to properties of samples. prediction is the process of using the model to predict properties of a sample given and instrument output.

Multivariate calibration offers several advantages over a univariate approach as detailed in the following steps:

1. It is possible to analysis for multiple components simultaneously.
2. Multiple redundance measurements can also provide improved precision in prediction. Statistic shows that repeating a measurement n times and calculating a mean value will result in a factor of $\sqrt{n}$ reduction in the standard deviation of the mean. This is commonly termed signal averaging.
3. Redundance measurements in multivariate calibration also facilitated fault detection.

Two main branches for the multivariate methods are: Classical Least Square (CLS) and Inverse Least Square (ILS). The three ILS methods are: Multiple Linear Regression (MLR), Partial Least Square (PLS) and Principal Component Regression (PCR).

PLS and PCR are the most widely used multivariate calibration methods in Chemometrics. This methods make use of the inverse calibration approach, where it is possible to calibrate for the desired component while implicitly modeling the other sources of variation. Estimation of the inverse calibration model involves the inversion of a typically unstable matrix. PLS and PCR solve this inversion problem by replacing the original variables variables with linear combination of the

variables (factors). The difference between PLS and PCR lies in how the factors are calculated.

The most widespread approach is often called PLS1. Although there are several algorithms, the main ones due to *Wold and Marters* [11], the overall principles are fairly straightforward. Instead of modeling exclusively the x variables, two sets of models are obtained as follows:

$$\begin{aligned} x &= T \cdot p + E \\ c &= T \cdot q + f \end{aligned}$$

where q has analogies to loading vector, although is not normalized.

The product of T and P approximates to the spectral data and the product of T and q to the true concentrations; the common link is T. An important feature of PLS is that it is possible to obtain a scores matrix that is common to both the concentrations (c) and measurements (x), Note that T and P for PLS are different to T and P obtained in PCA, and unique sets of scores and loading are obtained for each compound in the dataset. Hence if there are 10 compounds of interest, there will be 10 sets of T, P and q. In this way PLS differs from PCR in which there is only one set of T and P. It is important to recognize that there are several algorithms for PLS available in the literature, and although the predictions of c are the same in each case, the scores and loadings are not. Although the scores orthogonal (as in PCA), the loadings are not (which is an important difference to PCA), and furthermore, the loadings are not normalized, so the sum of square of each p vector does not equal one.

3.1 Root Mean Square Error of Prediction (RMSEP)

Prediction errors is a useful metric selecting the optimum number of factors to include in the model. This is because the models are most often used to predict the concentrations in future unknown samples. There are two approaches for generating a validation set for estimating the prediction error: Interval Validation (Cross-Validation with the calibration data), or external validation (perform prediction on a separate validation set), samples are usually at a premium, and so a cross validation approach is most often used.

The statistical figure at merit used to quantify the error in prediction is the Root Mean Square Error of Prediction (RMSEP)

$$RMSEP = \sqrt{\frac{\sum^{n\ sample} (C_i - \hat{C}_i)^2}{n\ sample}} \tag{3.1}$$

where C_i is the concentration of the ith prediction sample, $\hat{C}_i$ is the predicted concentration for this sample, and n sample is the number of prediction samples. When using a cross validation approach, the original calibration data is divided into calibration and prediction subsets.

3.2 Cross Validation

A complementary series of methods for determining the number of significant factors are based on Cross-Validation. These methods assumed that significant components models "data", cohilst later (and redundant) components model "noise" predicting the concentration of an unknown sample is fairly straightforward.

1. Call the spectrum of sample x_i (a row vector).
2. Subtract the mean of the I-1 samples from this to give $x_i - \bar{x}_i$, where $\bar{x}_i$ is the mean spectrum excluding sample i, if mean centering.

3. Estimate $\hat{t}_i = (x_i - \bar{x}_i)P'$, where P' are the loading obtained from the PCA model using I-1 samples excluding sample i or $\hat{t}_i = x_i P'$ if not mean centered
4. Then calculate ${}^{cv}\hat{C}V_i = \hat{t}_i r + \bar{C}_i$ or $\hat{C}_i = \hat{t}_i r_i$ (uncentred) which is the estimate concentration of sample i using the model based on the Remaining (I-1).

Most methods of Cross-Validation them repeat then repeat the calculation leaving another spectrum out, and so on,until the entire procedure has been repeated over times. The root mean square of these errors is then calculated as follows:

$$E_{cv} = \sqrt{\frac{\sum_{i=1}^{I} ({}^{cv}C_i - \hat{C}_i)^2}{I}} \tag{3.2}$$

The errors often called the Predicted Residual Error Sum of Square or PRESS are calculated by:

$$PRESS_a = \sum_{i=1}^{I}\sum_{j=1}^{J} \left({}^{a,cv}\hat{x}_{ij} - x_{ij}\right)^2 \tag{3.3}$$

this is simply the sum of square difference between the observed and true values for each object using an a PC model. The PRESS errors can then be compared with the RSS (Residual Sum Square) errors for each object for straight PCA (somtimes called the Autopredict on error), given by:

$$RSS_a = \sum_{i=1}^{I}\sum_{j=1}^{J} x_{ij}^2 - \sum_{k=1}^{a} g_k \tag{3.4}$$

$$RSS_a = \sum_{i=1}^{I}\sum_{j=1}^{J} \left({}^{a,auto}\hat{x}_{ij} - x_{ij}\right)^2 \tag{3.5}$$

3.3 Discriminant Analysis

Four of the most popular ways of determining how similar objects are to each other are as follows

3.3.1 Correlation Coefficient

The Correlation Coefficient (r) is the measure of the strength of the linear relationship between two variables, the coefficient reflects the consistency of the effect that a change in one variable has on the other.

$$r = \frac{\sum(x - \bar{x})(y - \bar{y})}{(n-1)\sigma_x \sigma_y} \tag{3.6}$$

3.3.2 Euclidean Distance

The distance between two samples k y l is defined by:

$$d_{kl} = \sqrt{\sum_{j=1}^{J}(x_{kj} - x_{lj})^2} \tag{3.7}$$

Sometimes the equation is presented in matrix format

$$d_{kl} = \sqrt{(x_k - x_l)(x_k - x_l)'} \tag{3.8}$$

3.3.3 Manhattan Distance

This is defined slightly differently to the Euclidean Distance and is given by:

$$d_{kl} = \sum_{j=1}^{J} |x_{kj} - x_{lj}| \tag{3.9}$$

3.3.4 Mahalanobis Distance

The distance between objects k y l is best defined in matrix terms by:

$$d_{kl} = \sqrt{(x_k - x_l)C^{-1}(x_k - x_l)'} \tag{3.10}$$

where C is the variance-covariance matrix of the variables, a matrix symmetric about the diagonal, whose elements represent the covariance between any two variables, of dimensions $j \times j$. Mahalanobis Distance and Linear Discriminant Functions: Many chemometricians use the Mahalanobis distance, sometimes called the "Statistical" distance, between objects. In supervised pattern recognition, a major aim is to define the distance of an object from the centre of a class. There are two principal uses of statistical distances.

1. To obtain a measurement analogous to a score (Linear Discriminant Function)
2. To determine the Mahalanobis distance to the centroid of any given group, a form of class distance. First is to obtain a measurement analogous to a score, often called the single number if there are only two classes.

$$f_i = (\bar{x}_A - \bar{x}_B) \cdot C_{AB}^{-1} \cdot x_i^{'} \tag{3.11}$$

where,

$$C_{AB} = \frac{(N_A - 1) \cdot C_A + (N_B - 1) \cdot C_B}{(N_A + N_B - 2)} \tag{3.12}$$

N_A, represents the number of objects in group A, and C_A, the variance-covariance matrix for this group, with X_A the corresponding centroid. Second, to determine the Mahalanobis distance to the centroid of any given group, a form of class distance. There will be a separate distance to the centre of each group defined for class A, by:

$$d_{iA} = \sqrt{(x_i - \bar{x}_A) \cdot C_A^{-1} \cdot (x_i - \bar{x}_A)'} \tag{3.13}$$

Where x_i, is a row vector for sample i, and $\bar{x}_A$ is the mean measurement (or centroid) for class A.

CHAPTER 4

EXPERIMENTAL TECHNIQUES

Depending on the spectral apparatus used, one differentiates between the various types of spectrometers, subdivided into non-dispersive IR spectrometers in which no variable wavelength selection is possible, dispersive units and Fourier transform (FT) spectrometers. For variable wavelength selection, spectral apparatuses are used such as grating monochromators in dispersive instrument types. In addition, series with sequential filters are possible with which polychromatic light of all wavelengths is broken down into light beams of single wavelengths or, at least, narrow wavelength ranges. In FT spectrometers, the spectral splitting takes place via an interferometer allowing a wavelength-dependent radiation modulation. In most cases, Michelson interferometers are available in which the two beam interferences are converted by mathematical Fourier transform into spectral information. In the non-dispersive IR photometers, interference filters can be used which are based on a multi-beam interference. However, other effects such as optical absorption or reflection may be used in order to filter out more or less narrow-band spectral regions. Another essential element for absorption spectroscopy is a radiation source which should show an as high possible intensity in the wavelength area under investigation. Thermal radiations are mainly used which provide a very broad band, so-called continuum radiation. In contrast, the use of lasers for measuring absorption spectra presumes the use of monochromatic radiation, namely that having an extremely narrow band. This is typically referred to as the laser wavelengths. The purpose of the optical system of a spectrometer is to transmit radiation from the radiation source to the detector, at best without loss. Lens systems of glass or quartz, as used in the visible

and ultraviolet region, are useless in the infrared, because all radiation fractions above 2.0 or 3.8 μm (respectively, below 5000 or 2630 cm^{-1}) are absorbed. It is impractical to make lenses out of IR-transmitting material because of the high cost, possible sensitivity to air moisture and the energy loss near the material-related transmittance limits.

Thus, all IR spectrometer are equipped with mirror optics. The mirrors generally consist of glass, the surface of which is vapor-coated with aluminum or gold. The optical system used is equipped with a sample compartment in which the sample to be measured is placed in the path of the measurement radiation, in part in cells or in corresponding attachments with which measurements techniques other than transmission measurements may be applied. Advantageous for IR spectroscopy is that multiple techniques are available which are adapted to the different sample requirements. For dispersive spectrometers, the sample compartment is situated before the monochromator for the following reasons: The scattered light caused by the sample can be removed by the spectral apparatus when this is placed in succession. The placing of the sample compartment before the monochromator, however, entails the disadvantages that the entire, still not split radiation acts upon the sample, whereby this can heat up considerably through absorption. With FT spectrometers in which the entire spectral range is investigated simultaneously, the sample compartment is placed behind the interferometer, so that the emitted sample radiation remains unmodulated. The detector is used for converting the optical signal into easily measurably electrical signals, as measurements of voltage.

4.1 Dispersive Spectrometers

The monochromator is the essence of a dispersive spectrometer. A monochromator consists of a splitting system, namely the optics and the dispersing element

that splits the radiation: prism or diffraction gratings. Aside from monochromator, there are also so-called polychromators with which several spectral regions can be selected simultaneously. The splitting system, optically included in a monochromator, consists of two narrow slits, which limit the rays at the entry and exit of the monochromator.

4.1.1 Diffraction Grating

While prism monochromators were used almost exclusively earlier, nowadays only diffraction gratings are being used as the radiation-splitting optical elements. By using diffraction gratings, one avoids the difficulties involved with prism materials (hygroscopic, reflection, absorption)and the frequent, complicated prism replacement that was necessary in using larger wavelength ranges. Moreover, gratings produce a much better resolution, constant over wide wavelength ranges. The basic form of diffraction gratings can be obtained by a number of wires ordered parallel and equidistant to each other in one plane. With scratch gratings, slits scratched into a flat glass or metallic surface, on which incident light is diffracted, serves the same purpose. The main fraction of the diffracted radiation disappears by interference erasing. Light of a defined wavelength is observed only in a particular direction, and always when the path length of the light emitted from two neighboring grooves is a multiple of the wavelength. The direction of the emitted light is given by:

$$\sin(a_n) = \frac{n\lambda}{d} \tag{4.1}$$

Whereby, an is the angle measured from the grating perpendicular λ the wavelength in cm, d the grating constant, the distance between two adjacent wires (grooves) in cm and the index $n = 1, 2, 3$ the corresponding ordinal number.

4.1.2 Interference Filters

Another already known dispersion element is recently being used again for very compactly designed instruments. The principle of the interference filter is based on the multiple reflection of a polychromatic light beam within a thin dielectric layer between semipermeable silver layers. Due to interference, all wavelengths are eliminated except a narrow band section. If one designs the dielectric intermediate layer as a wedge and arranges it segmented in the circle of a disc and turns this disc past a slit, then a wavelength selection is obtained as a function of the disc setting. This type of monochromator is found in portable instrument for environmental analysis.

4.1.3 Acousto-Optical Tunable Filters (AOTFS)

A new type of dispersion element called the acousto-optical tunable filter (AOTF), having multiple special applications in the near-infrared region, has been introduced since the mid-eighties. It consists of a double-refracting optical material in which vibrations in the MHz-range are induced. The created acoustic wave runs perpendicular to the optical path of the filter, modulates the refraction index of the crystal and thus creates a type of diffraction grating. Its big advantages are the fact that no movable parts are necessary to tune the filter in a matter of microseconds over a wide spectral range.

4.1.4 Fourier Transform Spectrometers

All commercial mid-infrared (IR) instruments, sold for analytical applications, are based on an interferometric measurement that is they are classified as Fourier Transform Infrared (FTIR) instrument. Today, there are probably no more than 5contrast to this, for near-infrared having experienced an impressive renaissance in analytics dispersive spectrometers are still being widely used.

4.2 Fourier Transform Infrared Spectroscopy

Infrared spectrometers are used to obtain information on the molecular structure of samples, qualitatively and/or quantitatively, without destruction of the molecules. Infrared light is a form at radiation. Infrared spectroscopy is the study of the interaction of infrared light with matter .Light is composed of electric and magnetic waves. These two waves are in planes perpendicular to each other, and the light wave move through space with propagation vector, $\bar{K}$ in a contained plane perpendicular to the planes containing the electric and magnetic waves. It is the electric part of light, called the electric field, vector, that interacts with molecules. The amplitude of the electric field vector changes over time and has the form of a sine wave. The wavelength of a light wave is the distance between adjacent crest or troughs. The magnitude of the propagation vector; $|\vec{K}|$ is know as the wavenumber of a light wave and is defined as the reciprocal of the wavelength, or;

$$|\vec{K}| = W = \frac{1}{\lambda} \tag{4.2}$$

The wavenumber of a light wave is directly proportional to energy as follows:

$$E = hcW$$

where E = light quantum photon energy. c = The speed of light in vacuum ($3.00 \times 10^8 m/s$). h = Planck's constant ($6.63 \times 10^{-34} Joule - second$). W = Wavenumber.

Thus, high wavenumber light has more energy than low wavenumber light. Mid-infrared radiation will be defined as light radiation contained between 400 and $4000 cm^{-1}$. Infrared radiation is another name for heat. All objects in the universe at a temperature above absolute zero give off infrared radiation. When infrared radiation interacts with matter it can be absorbed, causing the chemicals bonds in the material to vibrate. The presence of chemical bonds having a non-zero dipole

moment in a material is a necessary condition for infrared absorbance to occur. The infrared spectra can provide quantitative information as well, such as the concentration of a molecule in a sample. The basis of all quantitative analyses in IR spectroscopy is Beers law, which relates concentration to absorbance, and has the following form:

$$A = \varepsilon lc$$

Where: A = Absorbance. e = Absorptivity. l = Pathlength. c = Concentration.

The performance of any infrared spectrometer is determined by measuring its signal-to-noise ratio (SNR). SNR is calculated by measuring the peak height of a feature in an infrared spectrum (such as a sample absorbance peak), and ratioing it to the level of noise at some baseline point nearby in the spectrum. The SNR can be improved by reducing the noise, since the signal depends only on the concentration, which for a given sample is fixed. noise is a random process thus collecting more sample scans and the averaging the noise is reduced.

$$SNR \propto (N)^{1/2}$$

where N is the number of scans added together, and $\propto$ stands for proportionality.

4.3 FTIR Equipment

Each Fourier Transform Spectrometer is basically composed of the following optical elements: an IR source, an interferometer, beamsplitter and a detector. The beam produced by the IR source passes through an aperture, then eventually trough an optical filter, and enters the interferometer. When the beam exits the interferometer, it is modulated by the scanner (a moving mirror for example). The beam is then led to the sample (where it transmitted or reflected), and finally it

is focused on the detector. The housing of each detector contains a preamplifier (and for some detectors, a programmable gain amplifier). The output signal (an interferogram) of this preamplifier is sent to the main amplifier where it is amplified, filtered and digitized. The digital "signal" is then sent to the acquisition processor (AQP) for further mathematical processes: transformation of the interferogram into a spectrum.

The purpose of an interferometer is to take a beam of light, split it into two beams, and make one of the light beams travel a different distance than the other. The difference in distance traveled by these two light beams is called optical path difference (or optical retardation), δ. The Michelson interferometer consists of four arms. The first arm contains a source of infrared light, the second arm contains a stationary (fixed) mirror, the third arm contains a moving mirror, and the fourth arm is open. At the intersection of the four arms is a beamsplitter, which is designed to transmit half the radiation that impingnes upon it, and reflect half of it. As a result, the light transmitted by the beamsplitter strikes the fixed mirror, and the light reflected by the beamsplitter strikes the moving mirror. After reflecting off their respective mirrors, the two light beams recombine at the beamsplitter, then leave the interferometer to interact with the sample and strike the detector.

An interferogram is a sum of sinusoidal waves, each of which contains information about the wavenumber of a given infrared peak and amplitude information about the peak intensity at that wavenumber. The Fourier transform simply calculates the infrared spectrum from the summed sinusoidal waves in the interferogram. The interferogram is a plot of infrared intensity versus optical path difference, which can be measured in cm^{-1}. The Fourier transform of an interferogram produces a plot of infrared intensity versus inverse centimeters, or cm^{-1} Inverse centimeters are also known as wavenumbers. A plot of infrared intensity versus wavenumber is an infrared spectrum. In a sense, the Fourier transform inverts the interferogram to

produce the infrared spectrum. When an interferogram is Fourier transformed, a single beam spectrum is obtained. A single beam spectrum is a plot of raw detector response versus wavenumber.

The contribution of the instrument by itself to the background spectrum is known as the instrument response function. The overall shape of the spectrum is due to the sensitivity of the detector, transmission and reflection properties of the beamsplitter, emissive properties of the sources , and reflective properties of the mirrors. Common features around 3500 and $1630 cm^{-1}$ are due to atmospheric water vapor, and the bands at 2350 and $667 cm^{-1}$ are due to carbon dioxide A background spectrum must always be run when analyzing samples by FTIR. When an interferogram is measured with a sample in the infrared beam and Fourier transformed, a sample single beam spectrum is produced. It looks similar to the background spectrum except the sample peaks are superimposed upon the instrumental and atmospheric contributions to the spectrum. To eliminate these contributions, the sample single beam spectrum must be ratioed against the background spectrum. This produces a transmittance spectrum as shown by the following equation.

$$\%T = \frac{I}{I_0} \tag{4.3}$$

Where: $\%T$ = Transmittance. I =Intensity measured with a sample in the beam (from the sample single beam spectrum). I_0 =Intensity measure with no sample in the beam (from the background spectrum).

The absorbance spectrum can be calculated from the transmittance spectrum using the following equation

$$A = -\log_{10} T \tag{4.4}$$

Where: T = Transmittance. A = Absorbance.

4.3.1 Definitions

Interferometer: The interferometer is the heart of the spectrometer. The beam entering the interferometer is divided into two beams: one is transmitted (T) to the moving mirror while the second is reflected (R) to the fix mirror. The transmitted part reflects on the moving mirror (where is it thus modulated depending upon the velocity of the scanner) and returns to the beamsplitter where again one part is transmitted back to the source (TT) while the second is reflected (TR) to the sample. It forms an interference pattern called an interferogram.

Sources: The purpose of an infrared source is to provide radiant energy in the infrared region of the electromagnetic spectrum. The simplest infrared source is called an air cooled source. The temperature of the source is maintained by air currents in the spectrometer, hence its name. It consists of an element that may be made up of a coil of nichrome wire or a small ceramic piece. Electricity is passed through the element, and the resistance of the element to the electricity causes it to heat up and give off infrared radiation. Another type of infrared source is the globar. It consists of a rod of silicon carbide, and is resistively heated as in the air cooled source. Globars operate at temperature above 1400 K, so they have the advantage of giving off more infrared radiation than air cooled sources. The disadvantages of globars are the need for cooling water, which is an added expense, and may not be available in some locations.

Beamsplitters: The purpose of the beamsplitter is to divide the light beam in two separate beams at nearly equal intensity. Some of the light reflects off the moving mirror and some of the light reflects off the fixed mirror. Potassium bromide (KBr) is almost universally used as a substrate material in FTIR beamsplitters in the mid IR region (finger print region).Although these beamsplitters are referred to as being made out of KBr, this material does not split the beam since it transmits in the infrared. Instead, a thin coating of germanium is sandwiched between two

pieces of KBr, and it is this Ge coating that divides the beam. It acts similarly to a partially silvered mirror that reflects light but is still partially transparent. The KBr acts as a substrate for the beamsplitter coating and to protect it from the environment. Ge on KBr beamsplitter are usable from 4000 to 400 cm^{-1}, covering the mid-infrared very well. The other material used in mid-infrared beamsplitters is cesium iodide (CsI). This material transmits from 4000 to 200 cm^{-1}, a 200 cm^{-1} wider range than KBr. However, CsI is soft and very hygroscopic, so beamsplitters made from it must be replaced more frequently than KBr.

Detectors: The detector element is usually enclosed behind an infrared transparent window to protect it from the environment. The element is connected to the spectrometer electronics, and its job is to act as a transducer; turning infrared intensity into an electrical signal. The signal is ultimately turned into a voltage, which is amplified, processed, and digitized before being Fourier transformed into a spectrum. The most commonly used detector material in the mid-infrared is deuterated triglycine sulfate (DTGS). The DTGS detector is known as a pyroelectric bolometer and works as follows. Changes in the amount of infrared radiation striking the detector cause the temperature of the DTGS element to change. The dielectric constant of materials such as DTGS changes with temperature. The resultant change in capacitance with temperature is measured as a voltage across the detector element. DTGS detectors equipped with KBr windows cover the midinfrared range from 400 to 4000 cm^{-1}. The advantages of DTGS detectors are that they are simple, inexpensive and robust. The second major detector used in the mid-infrared is the mercury cadmium telluride (HgCdTe) or "MCT" detector. The MCT element consists of an alloy of these three materials, and it is a semiconductor. The detector element absorbs infrared photons, and as aresult electrons are promoted from the valance band (or bonding orbitals) to the conduction band (or anti-bonding orbital). Once electrons are in the conduction band they can respond to an applied

voltage, giving rise to an electrical current. The electrical current is a measure of the number of electrons, and so is directly proportional to the number of infrared photons hitting the detector. The current generated by the detector element is a direct measure of the infrared intensity. The energy difference between the valance band and the conduction band is called the bandgap. Photons with an energy less than the bandgap will be not be detected since they do not promote electrons to the conduction band. Photons with energy greater than the bandgap will promote electrons to the conduction band and will be detected.

4.3.2 Use of Spectral Manipulations

The manipulation of spectra is performed using the software that comes with an FTIR spectrometer, and involves altering or performing a calculation on the original spectrum received from the instrument. The purpose of manipulating a spectrum is to enhance its appearance, or extract more information from it. Several manipulations are applied such as:

Baseline Correction, is used to correct spectra that have sloping or curved baselines so the result is a spectrum with a flat baseline. There are many reasons why a spectrum's baseline may not be flat, including sample scattering, inappropriate choice of background, and instrument drift.

Smoothing, is used on noisy spectra to reduce the noise level, so features that may have been hidden under the noise can be seen more readily. Thus, smoothing enhances the information content of a spectrum. Smoothing also has a cosmetic effect, improving the overall appearance of bad looking data.

Spectral Derivates, the slope of any mathematical function can be determined by calculating its derivative. Since an infrared spectrum is a mathematical function, its derivative can be calculated. The derivative of a spectrum can be taken a number of times, producing derivatives of different orders. For instance, the first derivative of a spectrum is called a first order derivative, the derivative of the

first derivate is called a second order derivative and so on. The simplest way to calculate a spectral derivative is the "point difference" method, where the difference in Y values between successive data points is calculated, then plotted versus wavenumber.

4.3.3 Sampling Technique

The mode of operation used was the Transmission mode. The most popular way of obtaining infrared spectra is to pass the infrared beam directly through the sample. The advantages of this technique are that transmission spectra have high signal-to-noise ratios, and comparatively inexpensive tools are used to prepare the samples for this type of analysis. Another advantage of transmission sampling is that it is a universal technique: it works on solids, liquids, gases and polymers. The major disadvantage of transmission techniques is the "thickness problem". Generally, samples thicker than 20 microns absorb too much infrared radiation, making it impossible to obtain a spectrum. Samples thinner than 1 micron have absorbencies to weak to be detected by the spectrometer. Ideally, samples should be between 1 and 20 microns thick. The challenge in preparing transmission samples is to adjust the thickness or concentration of samples so the appropriate amount of light passes through the sample. Another disadvantage of transmission technique is that time consuming sample preparation may be required. It takes time to melt, squish, or dilute a sample enough so that it transmits the appropriate amount of light.

Potassium bromide (KBr) pellets are used to obtain the infrared spectra of solids, and are particularly well suited to powdered samples. KBr is an inert, infrared transparent material, and acts as a support and a diluent for the sample. Steps to follow for preparing successful KBr pellets are as follows. First, the sample and the KBr must be ground to reduce the particle size to less than 2 microns in diameter. Larger particles will scatter the infrared beam and cause a sloping Baseline. Grinding is traditionally performed with an agate mortar and pestle . A gram or so of KBr

should be placed in the mortar, it should be ground until crystallites can no longer be seen and it becomes somewhat "pasty" and sticks to the sides of the mortar.

There are several problems that may be encountered when making a KBr pellet. An opaque pellet indicates that too much material was used in making the pellet. Opaque pellets will give poor spectra because very little light will pass through them. White spots in a pellet indicate the sample was not ground well enough, or was not dispersed properly in the KBr. Trying to grind for longer time and mixing the sample and KBr more thoroughly. If too little material is placed into the KBr pellets press, the results will be no pellet at all, just little piles of powder. The pressure applied to make the pellet also needs to be controlled, and must be high enough to produce the thin transparent film desired, handling the pellet can be a problem. Pellets are thin and brittle, and can fall out of pellet holders, crack, or disintegrate with the slightest provocation. Care must be exercised in handling them. A good KBr pellet is thin and transparent. KBr is a hygroscopic material, which means it will absorb water directly from the atmosphere. It is critical that the KBr used in making pellets be kept warm and dry, preferably in an oven at 100^oC.

4.3.4 Transmission Spectra of Solids

The techniques best suited for powders or samples than can be ground into a powder are called KBr pellets and mulls. These methods focus on grinding the sample to reduce its particle size, then diluting the sample in an inert matrix so the appropriate amount of light passes through the sample. The second class of transmission sampling methods for solids involves two ways of preparing polymeric samples as thin films for infrared analysis.

Mulls Mulls are another way of obtaining the transmission spectra of solid materials. The sample, usually a powder, is ground in an agate mortar and pestle to achieve a small particle size and avoid scattering. A drop or two of oil, called the "mulling agent" is added, and the mixture is ground some more to disperse

the solid in the oil. The mulling agent is usually mineral oil, which is sold under the trade name Nujol. This technique is called the "Nujol mull" technique because of the prevalence of this brand of mineral oil. To obtained a spectrum, a small amount of the sample/oil slurry is smeared on a KBr window, and a second KBr window is queezed against the first to make a thin film "sandwich". The advantage of mulls over KBr pellets is that mulls are easier and faster to make since there is no time consuming pellet squeezing involved. Mull also well suited to samples that may upon exposure to water. The mulling oil protects the sample from water vapor in the atmosphere since the oil is hydrophobic. KBr is hydrophobic and adsorbs water out of the atmosphere, potentially damaging water sensitive samples. the disadvantage of the mull technique is that the infrared bands of the mulling agent contaminate the spectrum of the sample. The split mull method involves making up two mulls using different mulling agents. The first mull is prepared in Nujol, the second in an oil called Fluorolube. Fluorolube is a mixture of chlorofluorocarbons, long chain alkanes where CH bonds have been replaced by CF and CCl bonds. bonds.

Cast Film Cast films are a way of preparing polymers for infrared analysis. Cast films are made by dissolving the polymer in an appropriate solvent, then placing drops of the solution on a KBr window and allowing the solvent to evaporate. A film of the polymer forms on the KBr window as the solvent evaporates. Drops of polymer are placed on the window at intervals to slowly build up a polymer film of the right thickness. the KBr window and the thin film are then placed in the infrared beam. the background should be run on the same clean KBr window that the polymer is deposited upon. A way of speeding up evaporation of the solvent is to place the KBr window and a paper towel on a hot plate set on low.

4.3.5 Transmission Spectra of Liquids

Capillarity the simplest way to obtain transmission spectra of organic liquids is to place a drop or smear of the sample on a KBr window, place a second window

on top of the first, and place the resulting "sandwich" directly in the infrared beam. this is known as the capillarity thin film method. The advantages of the capillary thin film tachnique is that it produces quality spectra of liquids in a fast and easy manner. It takes only a few seconds prepare samples using this technique. The background spectrum should be run with the sample two KBr windows used in the thin film sandwich. The some problems with the capillary thin film method. Volatile liquids will evaporate to some extent while their spectrum is being obtained. An excellent method of obtaining capillary thin film spectra is to use what is called a demountable cell holder. it is consist of a metal plate that slides into FTIR sample mount, with a hole over which two infrared transparent windows can be placed. the sample is placed between the windows, and a screw ring is used to apply pressure to hold the sample and windows together.

4.3.6 Diffuse Reflectance (DRIFTS)

Diffuse Reflectance Infrared Fourier Transform Spectroscopy (DRIFTS) is used to obtain the infrared spectra of powder and other solid materials. The sample preparation for DRIFTS is similar to that for KBr pellets. The sample and KBr should be ground separately to reduce particle size, either in an agate mortar and pestle.

4.3.7 Attenuated Total Reflectance (ATR)

The attenuated Total Reflectance (ATR) technique is used to obtain the spectra of solids, liquids, semisolids, and thin films. ATR is performed using an accessory that mounts in the sample compartment of an FTIR. At the heart of the accessory is a crystal of infrared transparent material of high refractive index. Typical materials used are zinc selenide, KRS-5 (thallium iodide/thallium bromide), and germanium.

4.3.8 Infrared Microscopy

Infrared microscopy,involves interfacing a visible light microscope with an FTIR to obtain spectra of very small (10 to 250 microns in size) samples. in some microscope designs, the infrared beam passes through a lower aperture, which usually consists of four black knife edges whose position can be adjusted by user. The purpose of the lower aperture is to define the shape of the infrared beam prior to the sample. The optic used in a microscope to focus light on the sample is called a condenser. Samples are typically placed on a microscope X, Y translation stage to allow different parts of the sample to be viewed. The optic used to collect light after it has interacted with the sample is called the objective.

4.4 Raman Spectroscopy

The origin of Raman spectra is markedly different from that of IR spectra. In Raman spectroscopy, the sample is irradiated by intense monochromatic laser beams in the UV-visible or near infrared regions (ν_0), and the scattered light is usually observed in the direction perpendicular to the incident beam. The scattered light consist of two types: one, called RAYLEIGH SCATTERING, is strong and has the same frequency as the incident beam (ν_0), and the other, called RAMAN SCATTERING, is very weak ($\sim 10^{-5}$ of the incident beam) and has frequencies $\nu_0 \pm \nu_m$, where m is a vibrational frequency of a molecule. The $\nu_0 - \nu_m$ and $\nu_0 + \nu_m$ lines are called STOKES and ANTI-STOKES lines, respectively. Thus, in Raman spectroscopy, we measured the vibrational frequency (ν_m) as a shift from the incident beam frequency (ν_0). In contrast to IR spectra, Raman spectra are measured in the UV-visible region where the excitation as well as Raman lines appear. According to classical theory, Raman scattering can be explained as follows: The electric field strength (E) of the electromagnetic wave (laser beam) fluctuates with time (t):

$$|\vec{E}| = E_0 \cos(2\pi\nu_0 t)$$

Where E_0 is the vibrational amplitude and is the frequency of the laser. If a diatomic molecule is irradiated by this light, an electric dipole moment is induced:

$$\vec{P} = \hat{\alpha}\vec{E} = \alpha E_0 \cos(2\pi\nu_0 t) \tag{4.5}$$

Here, $\hat{\alpha}$ is a proportionally constant and is called polarizability. If the molecule is vibrating with a frequency ν_m, the nuclear displacement q is written

$$q = q_0 \cos(2\pi\nu_m t) \tag{4.6}$$

where q_0 is the vibrational amplitude. $\hat{\alpha}$ can be expanded in a tag for series: $(\partial\alpha/\partial q)_0$. Thus, we can write

$$\alpha = \alpha_0 + \left(\frac{\partial\alpha}{\partial q}\right)_0 q_0 + \frac{1}{2}\left(\frac{\partial^2\alpha}{\partial q^2}\right) q_0^2 ... \tag{4.7}$$

Here, α_0 is the polarizability at the equilibrium position, and $(\partial\alpha/\partial q)_0$ is the rate of change of α_0 with respect to the change in q, evaluated at the equilibrium position. Combining the equations 4.5 to 4.7 it is obtained:

$$P = \alpha_0 E_0 \cos(2\pi\nu_0 t) + \left(\frac{\partial\alpha}{\partial q}\right)_0 q_0 E_0 \left[\cos\left\{2\pi(\nu_0 + \nu_m)t\right\} + \cos\left\{2\pi(\nu_0 - \nu_m)t\right\}\right] \tag{4.8}$$

According the classical theory, the first term represents an oscillating dipole that radiates light of frequency ν_0 (Rayleigh scattering), while the second term correspond to the Raman scattering of frequency $\nu_0 + \nu_m$ (anti-Stokes) and $\nu_0 - \nu_m$ (Stokes). If

$(\partial\alpha/\partial q)_0$ is zero, the vibration is not Raman-active. Namely, to be Raman-active, the rate of change of polarizability (α) with the vibration must not be zero. A vibration is IR-active if the dipole moment is changed during the vibration and is Raman -active if the polarizability is changed during the vibration. When a molecule is placed in an electric field (laser beam), it suffers distortion since the positively charged nuclei are attracted toward the negative pole, and electrons toward the positive pole. In actual molecules, such a simple relationship does not hold since both P and E are vectors consisting of three components in the x, y and z directions.

$$\begin{bmatrix} P_x \\ P_y \\ P_z \end{bmatrix} = \begin{bmatrix} \alpha_{xx} & \alpha_{xy} & \alpha_{xz} \\ \alpha_{yx} & \alpha_{yy} & \alpha_{yz} \\ \alpha_{zx} & \alpha_{zy} & \alpha_{zz} \end{bmatrix} \begin{bmatrix} E_x \\ E_y \\ E_z \end{bmatrix} \tag{4.9}$$

The first matrix on the right-hand side in equation 4.9 is called the polarizability tensor. In normal Raman scattering, this tensor is symmetric; $\alpha_{xy} = \alpha_{yx}$, $\alpha_{xz} = \alpha_{zx}$ and $\alpha_{yz} = \alpha_{zy}$. The vibration is Raman-active if one of these components of the polarizability tensor is changed during the vibration.

4.4.1 Instrumentation

The major components in Raman spectrometer are:

1. **Excitation source, which is generally a continuous wave (CW) gas laser**. In excitation source continuous wave (CW) lasers such as Ar^+ (351.1-514.5 nm), Kr^+ (337.4-676.4 nm) and He-Ne (632.8 nm) are commonly used for Raman spectroscopy. More recently, pulsed lasers such as Nd:YAG, diode, and excimer lasers have been used for time-resolved and UV resonance Raman spectroscopy. Lasers are ideal excitation sources for Raman spectroscopy, mainly due to the following characteristics of the laser beam:
    - Single lines from large CW lasers can easily provide 1-2 W power, and pulsed lasers produce huge peak powers of the order of 10-100 MW.

- Laser beams are highly monochromatic (band width, 0.1 cm^{-1}, Ar^{+} laser), and extraneous lines are much weaker. These can be eliminated easily by using filters or premonochromators.
- Laser beams have small diameters (1-2 mm), which can be reduced to $\sim 0.1mm$ in diameter by using simple lens systems.Thus, all the radiant flux can be focused on a small sample, enabling fruitful studies of microliquids ($\sim \mu L$) and crystals ($\sim 1mm^3$). In the case of Raman microscopy, sample areas as small as $\sim 1\mu m$ in diameter can be studied.
- Laser beams are almost completely linearly polarized, and thus are ideal for measurements of depolarization ratios.
- It is possible to produce laser beams in a wide wavelength range by using dye lasers and other devices.

2. **Sample illumination and scattered light collection system**.
3. **Sample holder**.
4. **Monochromador or spectrograph**. In a single monochromator, extraneous light that bounces around the spectrometer ("stray light") overlaps the weak Raman scattered light. This is caused mainly by undiffracted light scattered from the face of the grating. Such stray light could be reduced considerably by arranging two spectrometers in tandem so that the output of one was purified by the second. Thus, the construction of double monochromators began.
5. **Detection system, consisting of a detector, an amplifier and an output device**. Since Raman signals are inherently weak, the problems involved with detection and amplification are severe. More of the very early work was done with photographic detection using long exposure times. This situation has changed considerably since the development of strong laser sources and sensitive detection techniques. Several detection techniques are commonly used such as:

- ***Photon couting***: The Raman scattered light coming out from the exit slit of the monochromator is collected and focused on a photomultiplier (PM) tube, which converts photons into an electrical signal. The PM tube consist of a photocathode that emits electrons when photons strike it; a series of dynodes, each of which emits a number of secondary electrons when struck by an electron; and an anode that collects these electrons as an output signal.
- ***Photodiode Array Detection***: Multichanel photon detectors consist of an array of small photosensitive devices that can convert an optical image into a charge pattern that can be read as a Raman spectrum. Several types of multichannel detectors are commercially available. The silicon vidicon and silicon diode array are based on the silicon diode detector. Vidicon is an image-sensing vacuum tube, and its round target is 16 mm in diameter and contains more than 15,000 photodiodes per square millimeter. The silicon diode array is a linear array of diodes, each of which is 25 m wide and 2.5 mm high. When the dispersed radiation strikes such a multichannel detector, a charge pattern develops that is related to the intensity of radiation along the focal plane, and this charge pattern is detected and ultimately converted into a spectrum.
- ***Charge-Coupled Device Detection*:** The CCD is an optical -array detector based on silicon-metal-oxide semiconductor. The CCD consists of two dimmensional array of 10^6 pixels (silicon diode), each pixel ranging in size from 6 to 30 μm. The major advantages of the CCD relative to other multichannel detectors are the low readout noise, which makes optical intensification unnecessary, and high quantum efficiency and sensitivity in a wide wavelength range (20-1,000 nm). Thus, the CCD coupled with near IR laser excitation (dye laser, diode laser) can be used to measure Raman spectra of fluorescent compounds.

4.5 Raman Microscopy

Raman microscopy was developed in the 1970s. About this time was established the utility of Raman spectroscopy for microanalysis was stablished. The technique provides the capability of obtaining analytical-quality Raman spectra with 1 μm spatial resolution using samples in the picogram range. The sample being studied is placed on the stage of the microscope and is illuminated by light from the transmission illuminator. The focus on the sample is adjusted by viewing from the optical viewpoint and adjusting the objective. The illuminator lamp is switched off and the laser beam is directed to the beam splitter. The optical viewpoints is turned off and the TV camera is switched on by rotating the prism. The scattered light from the sample is collected by the objective and sent into the spectrometer.

The Raman microprobe has provided applications in a number of diverse areas of science. Generally, the areas of applications fall into two major categories:

1. Finger-print identification of microscopic contaminants.
2. Characterization of new materials.

Raman Microscope is a hybrid of optical microscopy and Raman spectroscopy in consequence, has all the concomitant advantages of both techniques. The main purpose of the microscopy is to excite, collect and couple the Raman radiation very efficiently from the sample to raman spectrometer, and to provide a means for sample positioning and viewing at high magnification. The Raman microscope can analyze the vibrational frequency shift at different points of surface. The Renishaw RM2000 Raman Microscopy spectrometer used performs two functions: first, the microscope takes Raman spectra of micron size samples, and second, the microscope produce 2D magnified images using the scattered light only. In this form, a vibrational chemical image of the sample can be obtained in which the spatial distribution of the particles sample can be mapped.

4.5.1 Confocal Raman Microscope

The term "confocal" is used to describe optical systems that limit the light collection to a small volume. This configuration accounts for the ability of the system to provide optical sectioning normal to the surface. Two different approaches to confocal Raman microscopy have been made. The first approach uses the optical configuration with a pinhole as the working principle as illustrated in figure 4–1. The laser excitation beam is first filtered by an illumination pinhole, H1. This initial spatial filter removes the appearance of diffraction rings and speckle noise around the focus spot and results in a clean point source waist that is imaged onto the sample. The scattered Raman radiation is collected by a wide-aperture microscope objective. A notch filter ensures coaxial illumination and light collection by the same objective in the back-scattering configuration. The image of the sample is focused at H2. The exact optical conjugation of H2 with the point source on the sample surface ensures that only the light originating from the sample region, which coincides exactly with the illumination spot, is transmitted to the spectral analyzer and detector. The two effects of spatial filtering, both for illumination and collection, multiply and increase the spatial resolution by eliminating stray light coming from the out-of-focus regions of the sample.

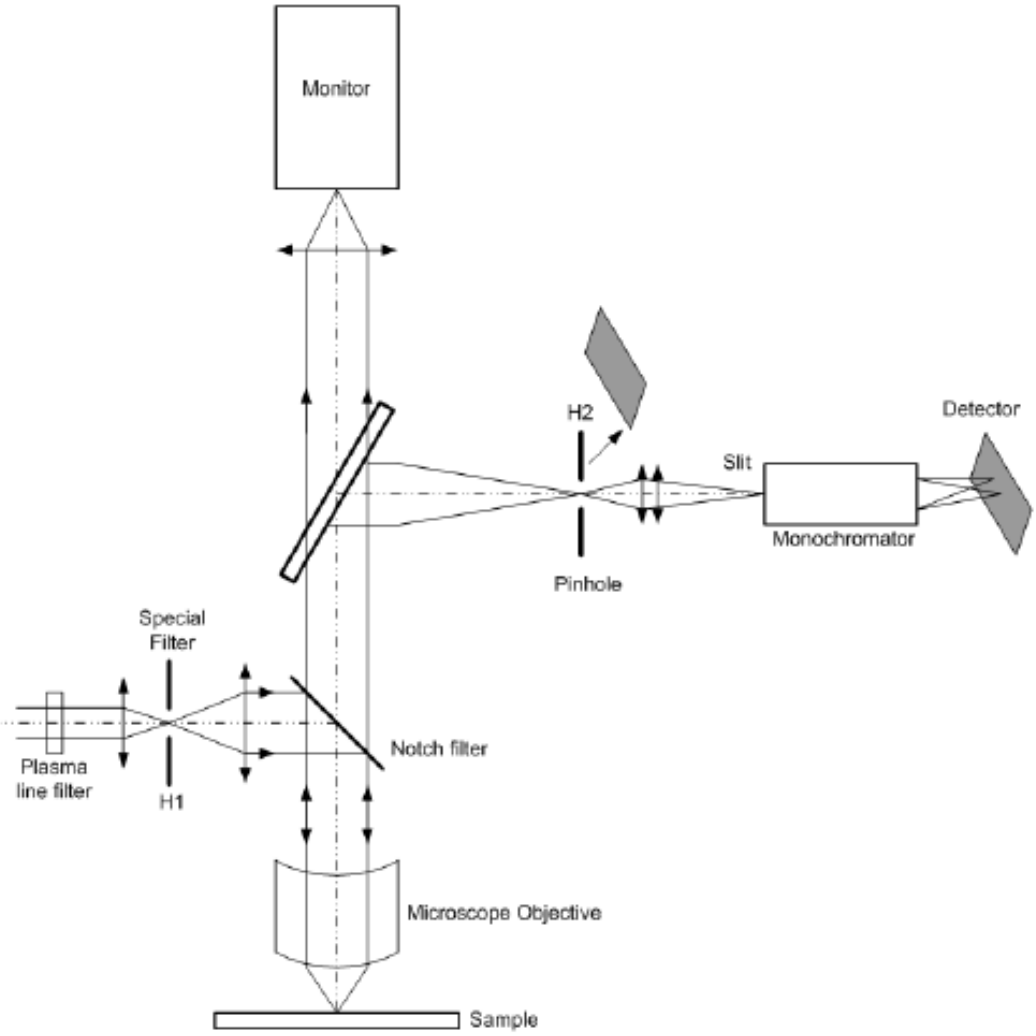

Figure 4–1. Schematic diagram of the working principle of confocal microscopy making use of a real pinhole.

CHAPTER 5
EXPERIMENTS: RAMAN SPECTRA

A Renishaw Raman Microspectrometer RM2000 system was employed for the vibrational spectroscopy measurements. The system was equipped with a Leica microscope and two lasers: Spectra Physics Millennia laser and Renishaw, high power diode laser. The microscope contained objectives with magnifications of 5x, 10x, 20x and 50x. The Millennia laser had a monochromatic excitation source generated by a green diode laser of 532 nm with and a variable output power up to 1 W. The second laser was a Renishaw High Power 785 nm diode laser with a maximum power of 200 mW. The spectra were obtained in the 100-4000 cm^{-1} range and 10 seconds of integration time. A multi channel Charge Coupled Device (CCD) detector and GRAMS software were used for data acquisition.

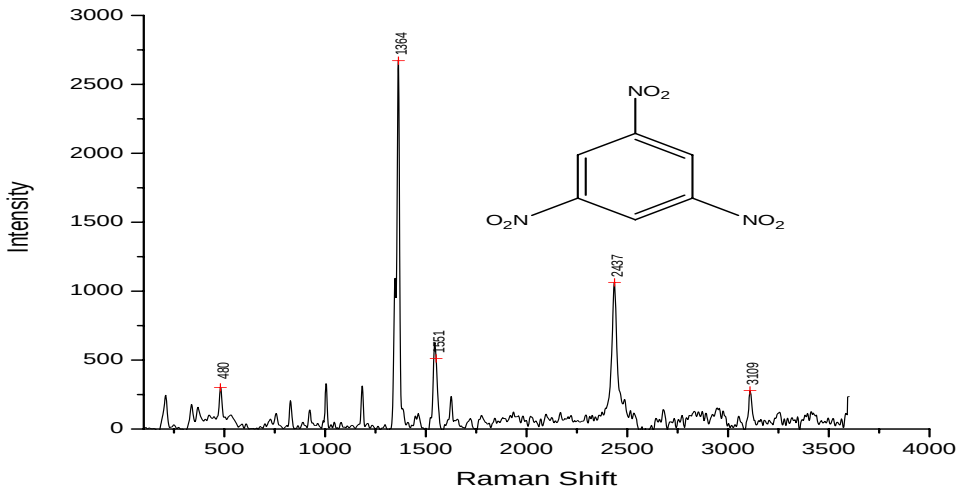

Figure 5–1. Raman Spectrum of 1,3,5-Trinitrobenzene

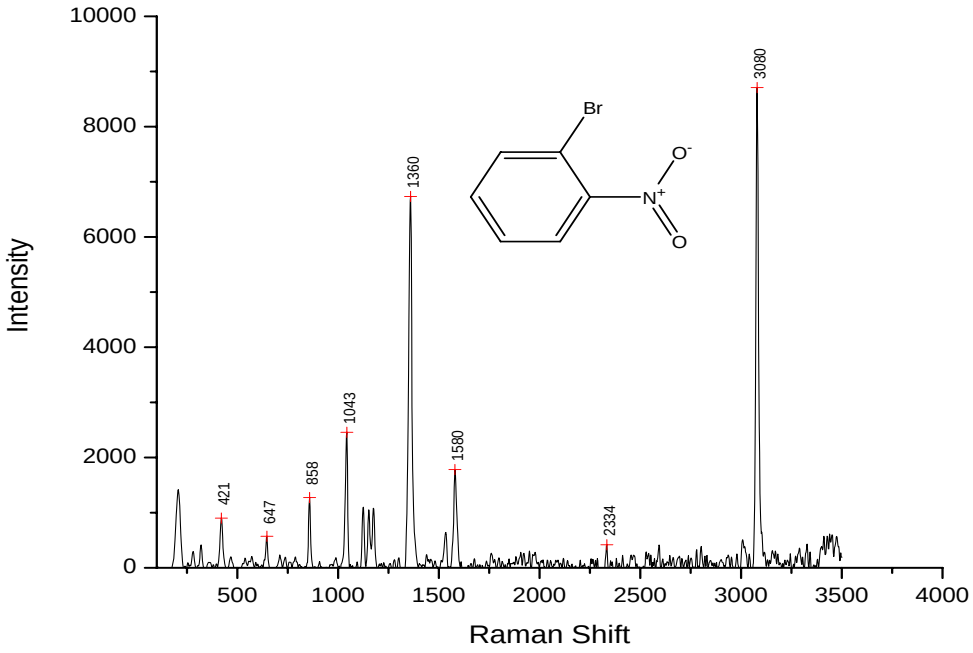

Figure 5–2. Raman Spectrum of 1-Bromo-2-Nitrobenzene

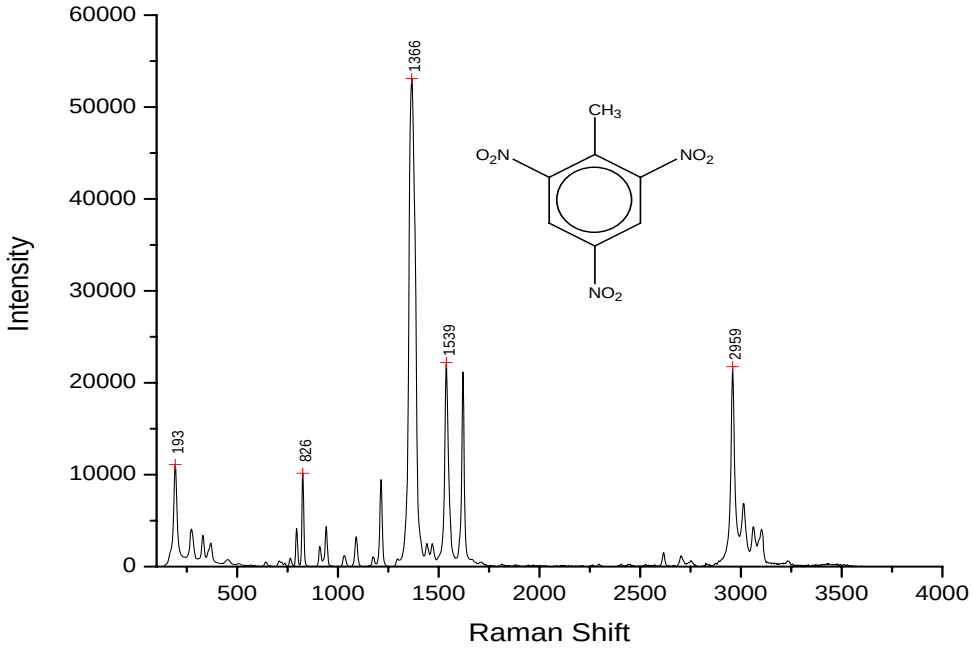

Figure 5–3. Raman Spectrum of 2,4,6-Trinitrotoluene

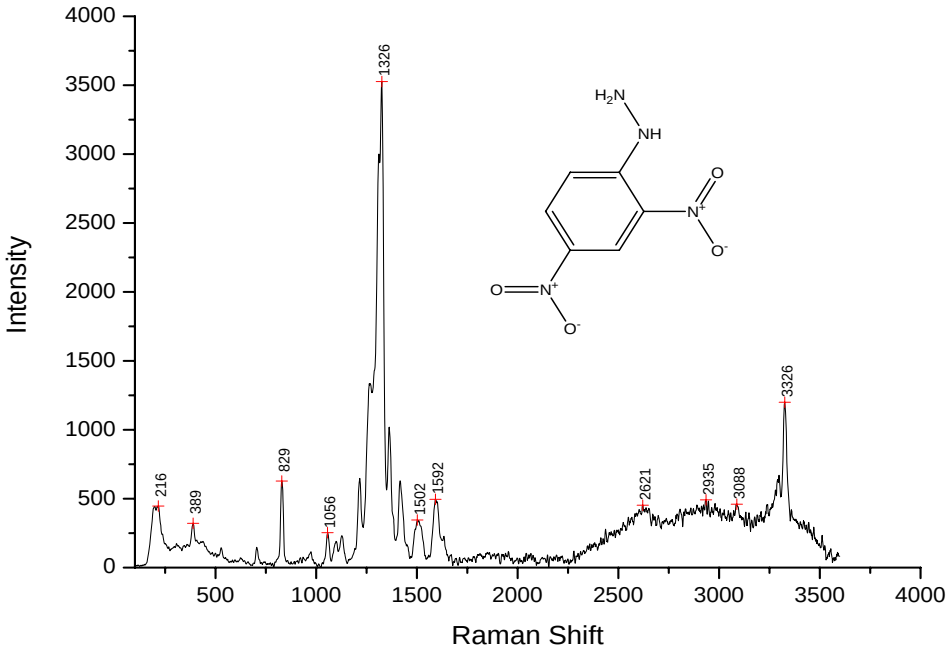

Figure 5–4. Raman Spectrum of 2,4-Dinitrophenylhydrazine

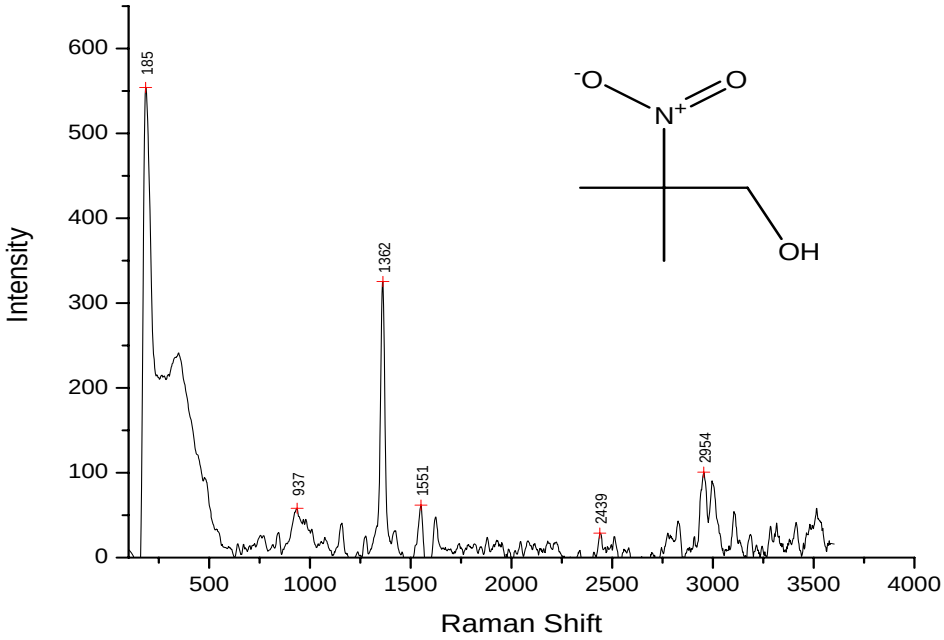

Figure 5–5. Raman Spectrum of 2-Methyl-2-Nitro-1-Propanol

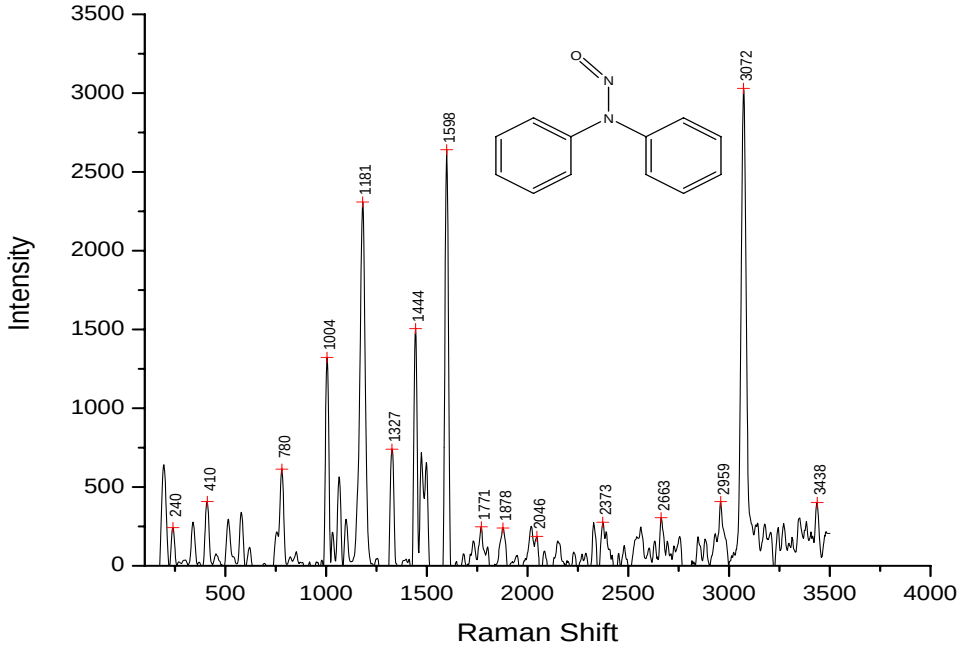

Figure 5–6. Raman Spectrum of n-nitrosodiphenylamine

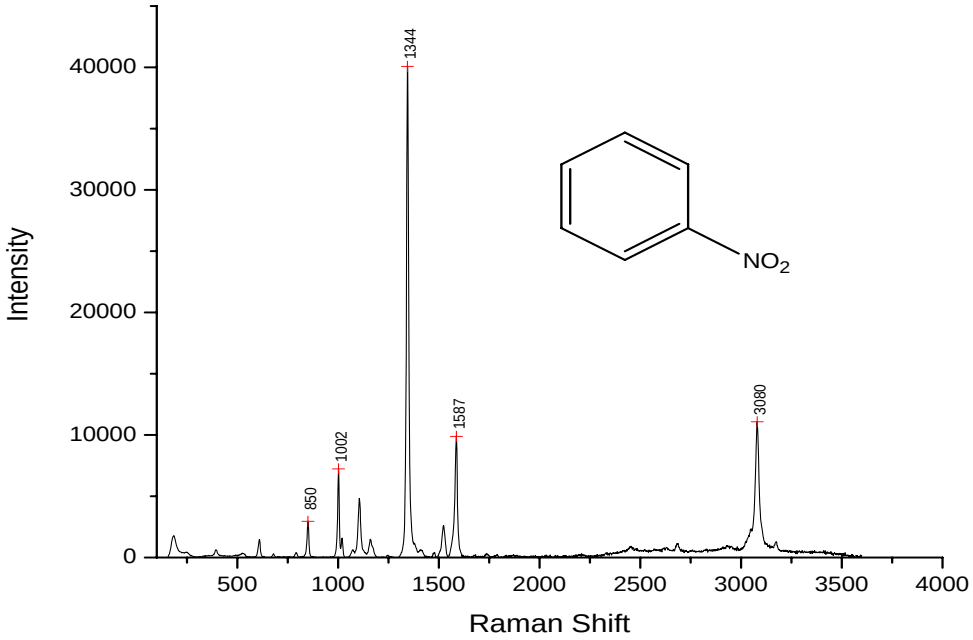

Figure 5–7. Raman Spectrum of Nitrobenzene

CHAPTER 6
EXPERIMENTS: INFRARED SPECTRA

A Bruker Vector-22 spectrometer equipped with a DTGS infrared detector was used to carry out the analysis samples. The KBr pressed disc technique (3.0 mg of sample and 0.1g of KBr) was used for FTIR analysis. The sample was placed in the instrument on a sample holder and spectra were measured at a resolution of $4cm^{-1}$ and 32 scans. The data was obtained using Opus V3.1 (Bruker Optics) Software.

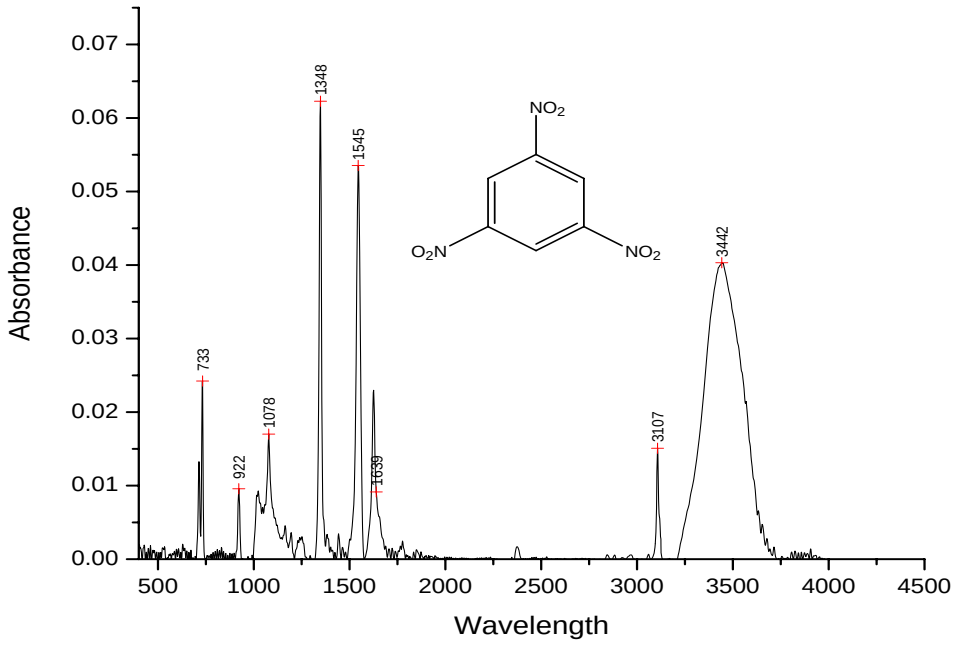

Figure 6–1. Infrared Spectrum of 1,3,5-Trinitrobenzene

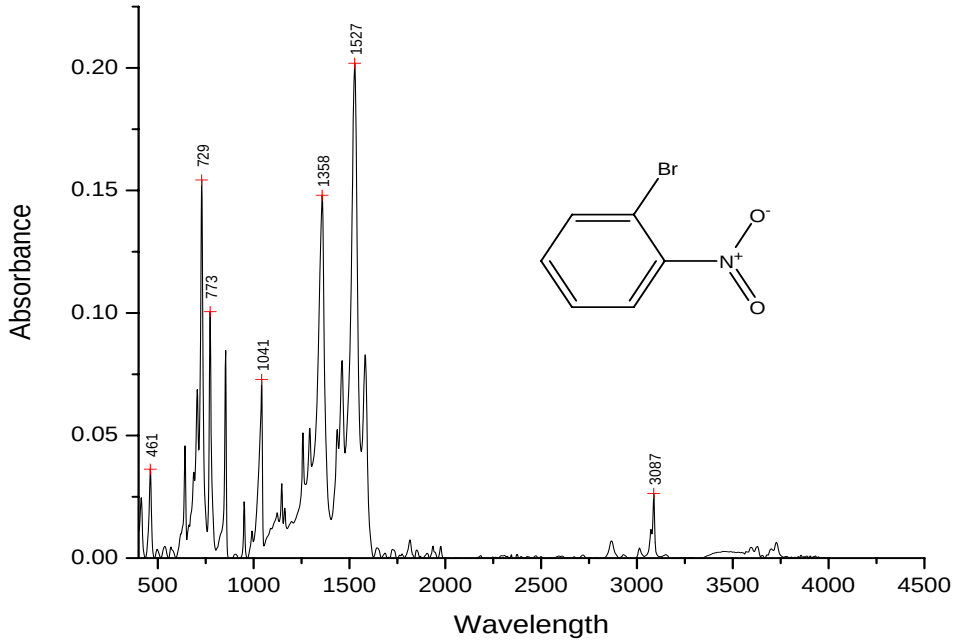

Figure 6–2. Infrared Spectrum of 1-bromo-2-Nitrobenzene

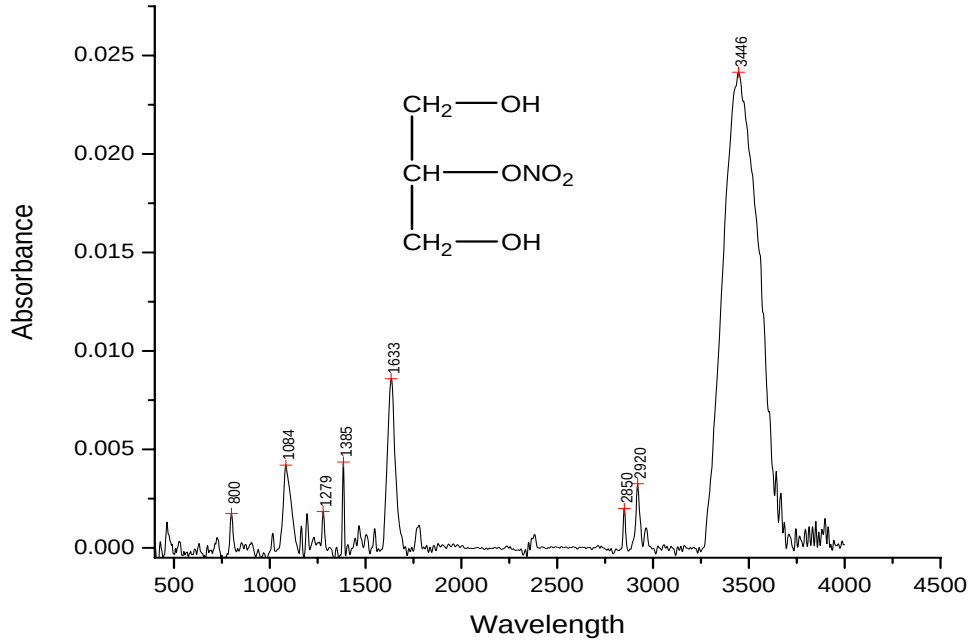

Figure 6–3. Infrared Spectrum of 2-Mononitroglycerin

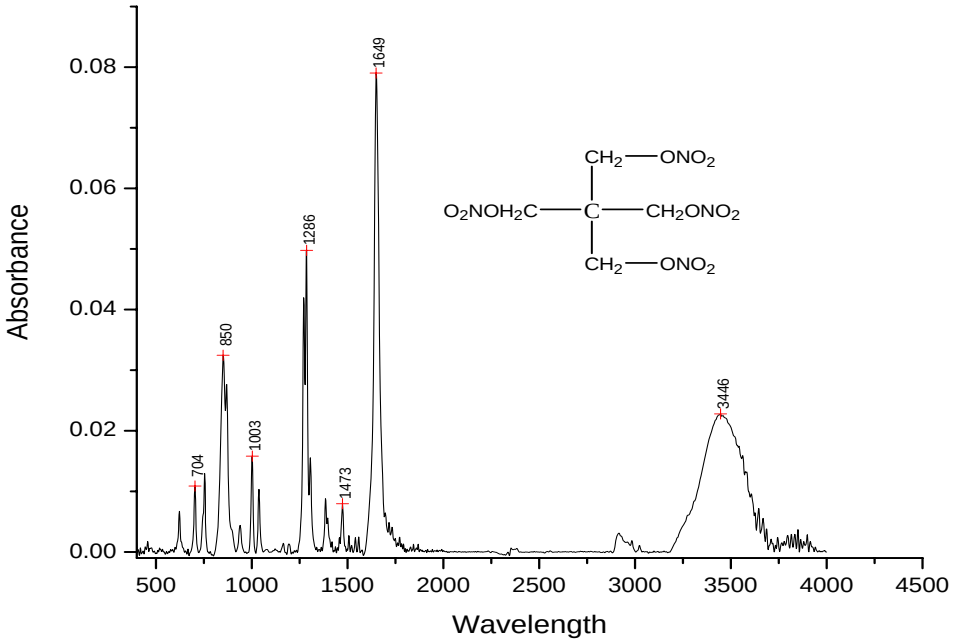

Figure 6–4. Infrared Spectrum of Pentaerytritol Tetranitrate

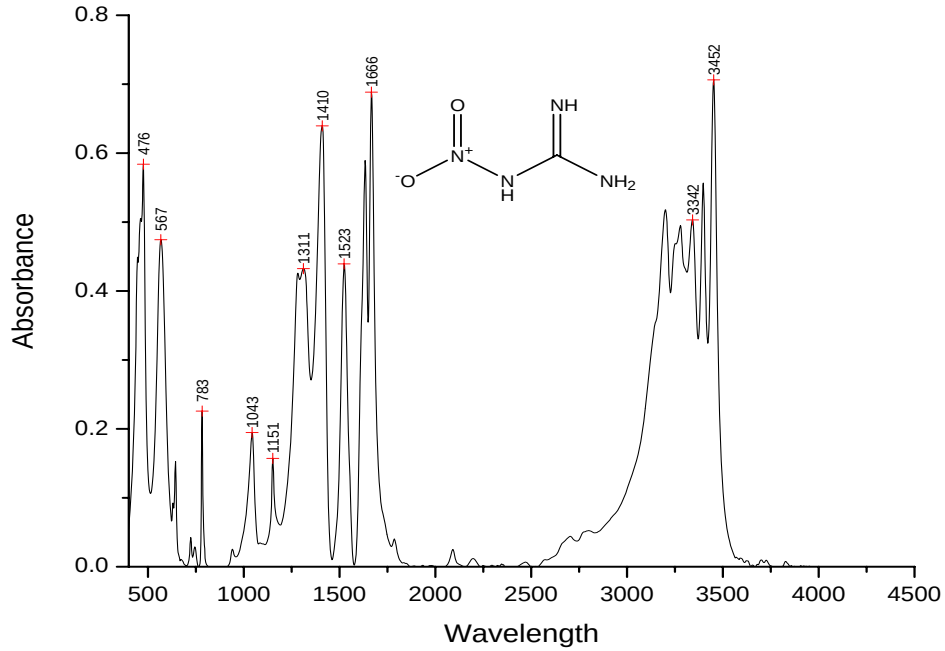

Figure 6–5. Infrared Spectrum of Nitroguanidine

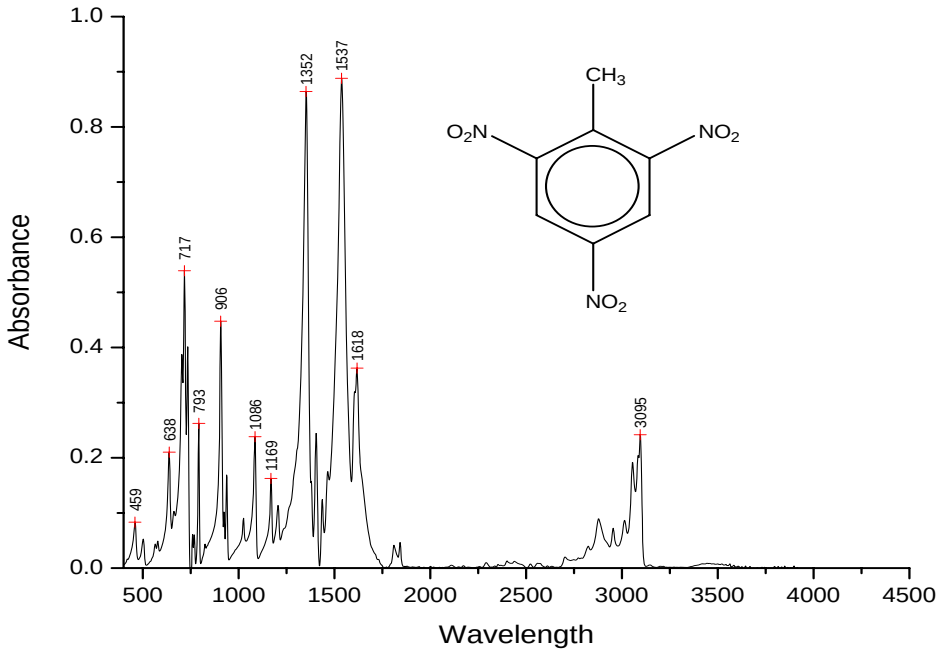

Figure 6–6. Infrared Spectrum of 2,4,6-Trinitrotoluene

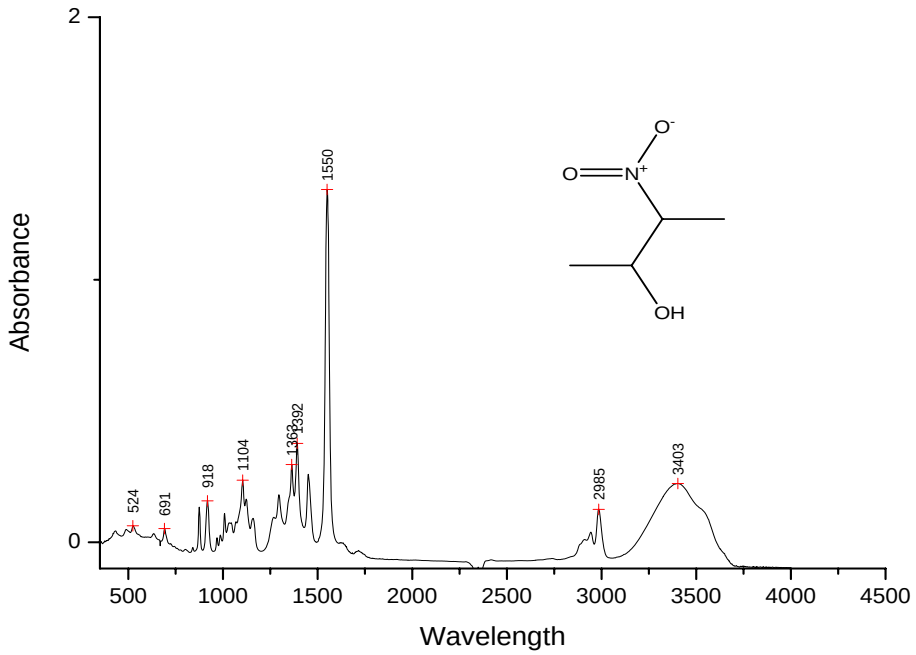

Figure 6–7. Infrared Spectrum of 3-nitro-2-butanol

CHAPTER 7
MODELING AND RESULTS

7.1 Discriminant Analysis for Infrared Data

The infrared spectra was modeled statistically using MINITAB software based in Linear Discriminant Function (LDF). The multivariate analysis was made for predicted spectroscopic behavior and it can be used to predict the group for the each explosive substance used in the work. The group means the type of substance according to the classification given in table 7–1. The predictors were the Wavelength Symmetric and Asymmetric modes.

Type	Group number	Quantity
$O-NO_2$	1	8
$N-NO_2$	2	3
$C-NO_2$	3	3
$Ring-NO_2$	4	47

Table 7–1. Classification of explosives substance used in this work for Infrared techniques.

The equation used in this model is:

$$LDF = m_i^{'} S_p^{-1} x - 0.5 m_i^{'} S_p^{-1} m_i + ln(p) \tag{7.1}$$

where,

x= column vector of length p containing the values of the predictors for this observation (note, this column vector is stored as one row)

m_i = column vector of length p containing the means of the predictors calculated from the data in group i

$m_i^{'}$=transpose vector of m_i

S_p = pooled covariance matrix

$ln(p)$ = natural log of the prior probability

The Constant row in table 7–2 is the term $-0.5 m_i^{'} S_p^{-1} m_i$ in the equation 7.1 for each group, the row "WSym" are the coefficient for wavelength in Symmetric mode, "WAsym" are the coefficient for wavelength in Asymmetric mode. For a given x vector predictor, the group with the smallest squared distance has the largest LDF. The table 7–3 shows the statistical distance between groups.

Groups				
–	1	2	3	4
Constant	-17832	-18352	-19217	-18365
Wsym	18.479	19.471	20.999	20.509
Wasym	7.307	6.833	6.078	5.958

Table 7–2. Linear Discriminant Function for Groups in Infrared Spectra

Groups				
–	1	2	3	4
1	0.000	53.313	347.654	290.753
2	53.313	0.000	128.717	102.575
3	347.654	128.717	0.000	19.391
4	290.753	102.575	19.391	0.000

Table 7–3. Squared Distance Between Groups for Infrared

The scatter plots for the sample in infrared technique are shown in the figures 7–4 and 7–5. These plots show a clear linear statistical behavior of the data. The data was plotted using MINITAB software and the groups are clearly identifiable.

7.1.1 Summary of results for Infrared

The table 7–4 shows the statistical results for Infrared technique. The model was made with 61 like sample size. This table shows a P-value de zero that is less than 0.05, since it is conclude that the model is significative highly. As future works, It is recommendable to increase the groups number including other nitro explosives

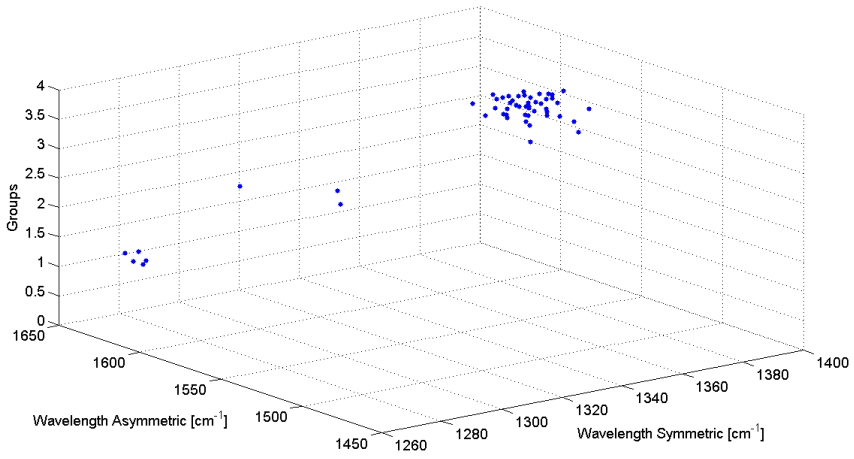

Figure 7–1. Data of Group vs WSym, WAsym for Infrared Technique

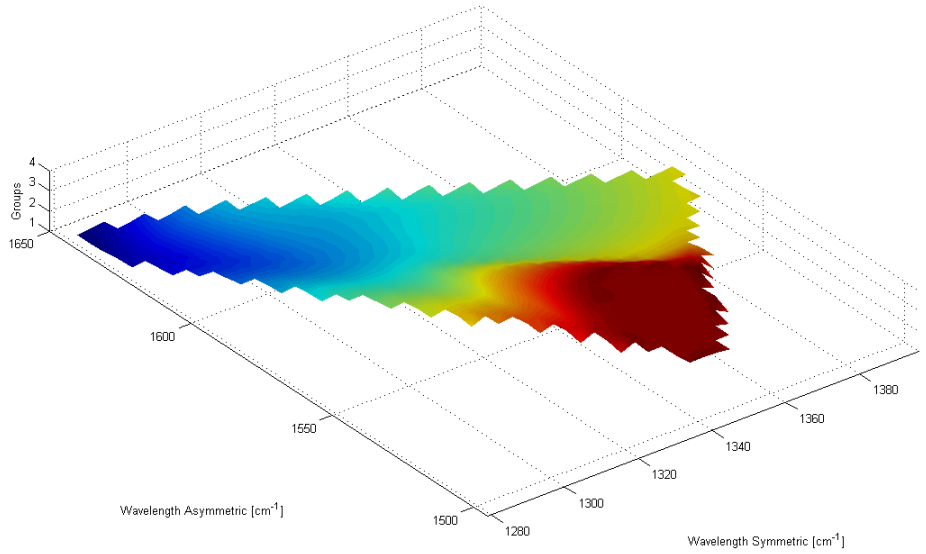

Figure 7–2. Surface Plot of Group vs WSym, WAsym for Infrared Technique

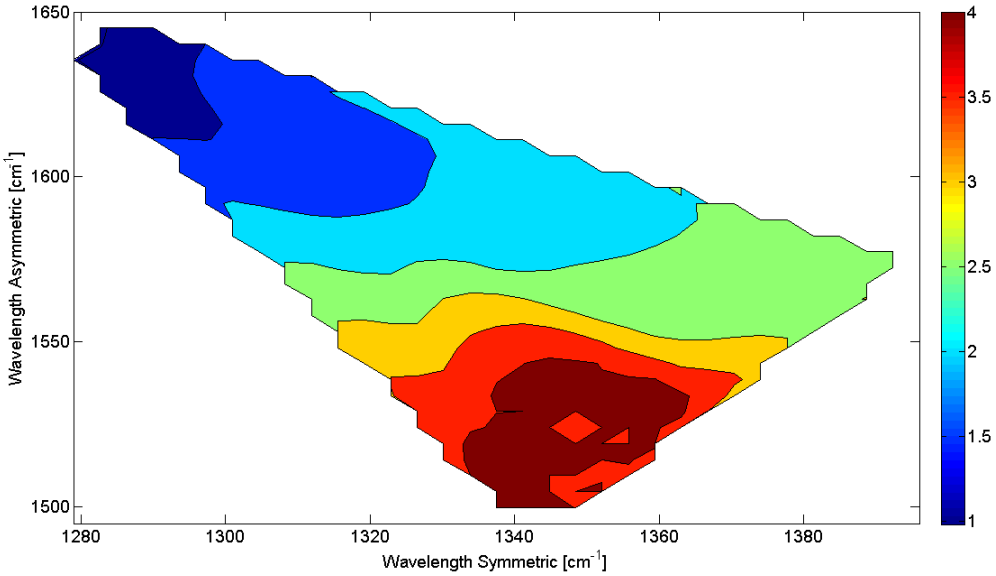

Figure 7–3. Contour Plot of Group vs WSym, WAsym for Infrared Technique

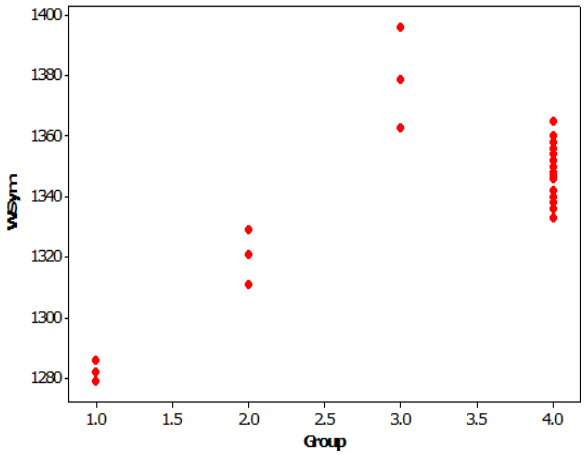

Figure 7–4. Scatter Plot of Symmetric Wavelength vs Groups

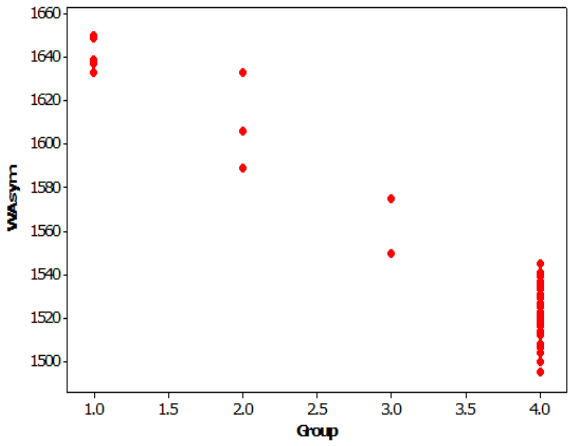

Figure 7–5. Scatter Plot of Asymmetric Wavelength vs Groups

with other molecular structures. The model was tested using nine explosives, the results is shown in the table 7–5

	True Groups			
Put into Group	1	2	3	4
1	8	0	0	0
2	0	3	0	0
3	0	0	3	0
4	0	0	0	47
Total N	8	3	3	47
N correct	8	3	3	47
Proportion	1.000	1.000	1.000	1.000
Results	N = 61	N Correct = 61	% Correct = 100%	P-Value=0.000

Table 7–4. Summary of results for Infrared

Substance	Wsym	Wasym	True Groups	Predicted Group
RDX	1267	1590	2	2
2-nitro-1,4-diaminobenzene	1329	1500	4	4
4-nitrothyophenol	1336	1504	4	4
5-nitro-4-amino-1,3-dimethylbenzene	1327	1516	4	4
5-nitro-2-aminotoluene	1317	1508	4	4
4,4-dinitrodiphenylamine	1324	1500	4	4
2,4-nitrophenyl hydrazine	1319	1515	4	4
3-methyl 2-nitroanysole	1373	1527	4	4
nitrobenzene	1360	1527	4	4

Table 7–5. Validation for Infrared

Type	WSym	WAsym	Group
1,2,4-butanetriol trinitrate	1279	1639	1
1,3-dinitroglyceryn	1279	1639	1
1-Mononitroglycerin	1282	1637	1
2-mononitroglycerin	1279	1633	1
pentaerytritol tetranitrate	1286	1649	1
1,2-Dinitroglycerin	1282	1650	1
1,2-Pentanediol Dinitrate	1282	1637	1
1,2-Propanediol Dinitrate	1282	1637	1
nitroguanidine	1311	1633	2
n-nitrosodiphenylamine	1321	1589	2
n-nitroso-n-ethylurea	1329	1606	2
trans-b-nitrostirene	1396	1575	3
3-nitro-2-butanol	1363	1550	3
n-nitrosomethylethylamine	1379	1550	3
3-nitrophtalic anhydride	1354	1537	4
m-nitroacetophenona	1350	1527	4
m-nitroaniline	1338	1518	4
m-nitrobenzaldehide	1352	1537	4
m-nitrobenzylamina hydrocl	1356	1541	4
m-nitrodimethylaniline	1340	1529	4
m-nitrophenol	1352	1537	4
nitrophenol	1348	1495	4
o-nitroaniline	1346	1508	4
p-nitroacetanilide	1348	1504	4
p-nitrobenzaldehide	1346	1539	4
p-nitrobenzamide	1336	1514	4
p-nitrobenzylamine hydrochlorid	1348	1523	4
n-metyl-p-nitroaniline	1338	1539	4
n-methyl-o-nitroaniline	1356	1520	4
m-nitroanisole	1360	1533	4
p-nitrotertbutylbenzene	1347	1521	4
o-nitrotoluene	1347	1523	4
2-nitro-1,4-dimethylbenzene	1346	1527	4
o-nitroanisole	1352	1523	4
3-nitro-o-xylene	1352	1526	4
1,3,5-trinitrobenzene	1348	1545	4
2,4,6-tnt	1352	1537	4
2-AMINO-4,6-DNT	1346	1531	4
3,4-DNT	1346	1527	4
4-amino-2,6dnt	1358	1535	4
n-(2,4-dinitro-1-naphtyl)benzen	1360	1531	4
o-dinitrobenzene	1365	1533	4
2,6-dinitrotoluene	1354	1533	4
2,4-dinitrotoluene	1338	1520	4
1-nitronaphtalene d7	1350	1516	4
2,2'-dinitrodiphenylamine	1336	1514	4
2,4-dinitrodiphenylamine	1338	1506	4
2-nitrobyphenyl	1356	1527	4
4,4-Dinitrobyphenyl	1342	1514	4
2,2'-dinitrobiphenyl	1336	1500	4
2,4-dinitro-1-naphtol-7-sulfonic acid	1346	1525	4
4-nitrobyphenyl	1346	1516	4
1-BROMO-2-NITROBENZENE	1358	1527	4
1-iodo-2-nitrobenzene	1333	1522	4
1-IODO-4-NITROBENZENE	1342	1512	4
2,4-dinitro-5-fluoroanilne	1348	1512	4
o-nitrobenzyl bromide	1342	1525	4
p-nitrobenzyl bromide	1348	1539	4
p-nitrobenzyl chloride	1350	1539	4
o-nitrobenzyl chloride	1348	1533	4
2,4-dinitrofluorobenzene	1354	1533	4

Table 7–6. Classification of explosives substance using Infrared technique.

7.2 Discriminant Analysis for Raman Data

The Raman spectra was modeled statistically using MINITAB software based in Linear Discriminant Function (LDF). The multivariate analysis was made for predicted spectroscopic behavior and it can be used to predict the group for the each explosive substance used in the work as is shown in the table 7–7.

Group	Type	Quantity
1	$N - NO_2$	4
2	$C - NO_2$	3
3	$Ring - 1 - NO_2$	34
4	$Ring - 2,3 - NO_2$	11

Table 7–7. Classification of explosives substance used in this work for Raman techniques.

The "Constant" row in table 7–8 is the term "$-0.5 m_i^{'} S_p^{-1} m_i$" in the equation 7.1 for each group, the row "ShiftSym" are the coefficient for Raman Shift in Symmetric mode, "ShiftASym" are the coefficient for Raman Shift in Asymmetric mode. Figure 7–7. Surface Plot of Group vs Raman Shift in symmetric and asymmetric mode.

Groups				
–	1	2	3	4
Constant	-17393	-17966	-18375	-17880
ShiftSym	12.925	13.646	13.582	13.716
ShiftAsym	11.535	11.292	11.607	11.174

Table 7–8. Linear Discriminant Function for Groups in Raman Spectra

Groups				
–	1	2	3	4
1	0.000	47.519	39.636	62.097
2	47.519	0.000	11.788	1.828
3	39.636	11.788	0.000	22.416
4	62.096	1.828	22.416	0.000

Table 7–9. Squared Distance Between Groups for Raman

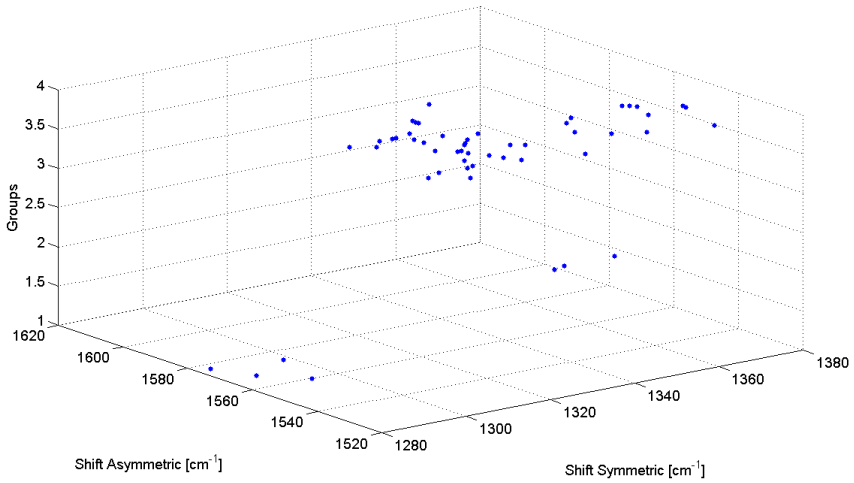

Figure 7–6. Data of Group vs Symmetric and Asymmetric Shift for Raman Technique

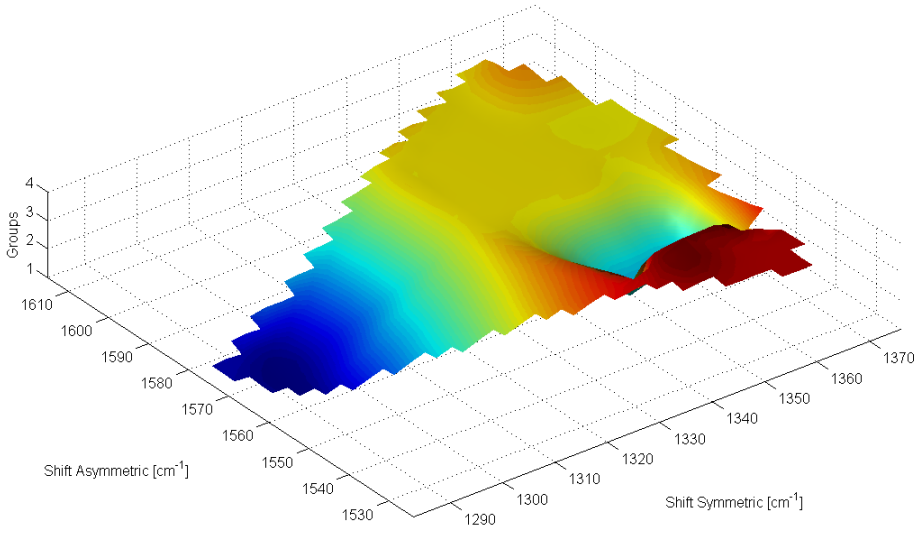

Figure 7–7. Surface Plot of Group vs Symmetric and Asymmetric Shift for Raman Technique

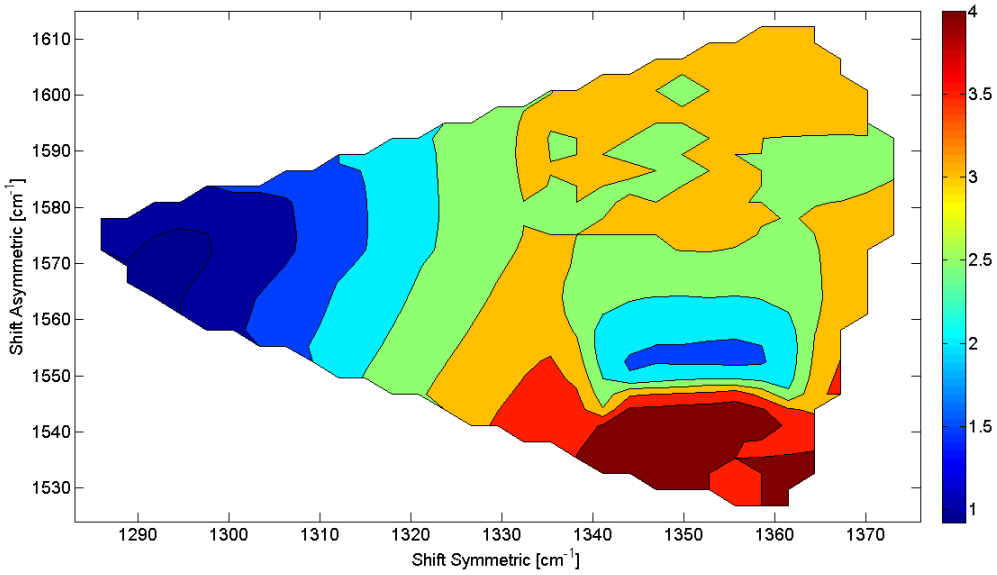

Figure 7–8. Contour Plot of Group vs Symmetric and Asymmetric Shift for Raman Technique

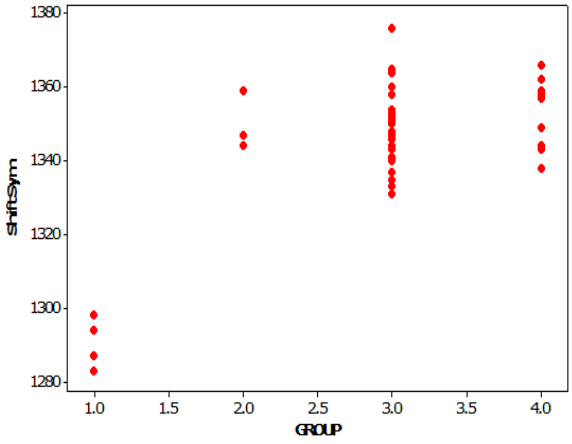

Figure 7–9. Scatter Plot of Symmetric Shift vs Groups

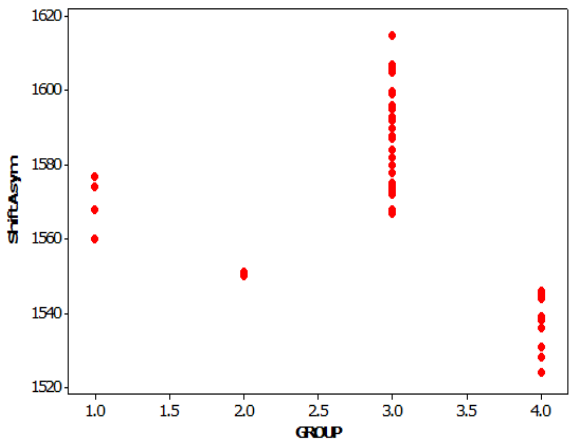

Figure 7–10. Scatter Plot of Asymmetric Shift vs Groups

7.2.1 Summary of results for Raman

The table 7–10 shows the statistical results for Infrared technique. The model was made with 52 as sample size. This table shows a P-value de 0.05 that is less than 0.05, since it is conclude that the model is significative highly. As future works, It is recommendable to increase the groups number including other nitro explosives with other molecular structures.

	True Groups			
Put into Group	1	2	3	4
1	4	0	0	0
2	0	3	1	2
3	0	0	33	0
4	0	0	0	9
Total N	4	3	34	11
N correct	4	3	33	9
Proportion	1.000	1.000	0.971	0.818
Results	N = 52	N Correct = 49	% Correct = 95%	P-Value=0.050

Table 7–10. Summary of results for Raman

The model was tested using nine explosives, the results is shown in the table 7–11

substance	ShiftSym	ShiftAsym	True Group	Predicted Group
2,4-dinitrophenylhydrazine	1326	1502	4	4
2,6-dnt	1362	1524	4	4
3,4-dnt	1357	1538	4	4
1-nitropropane	1360	1550	2	2

Table 7–11. Validation for Raman

NAME	ShiftSym	ShiftAsym	GROUP
N-nitroso arcosine	1294	1560	1
nitroguanidine	1283	1577	1
HMX	1287	1568	1
RDX	1298	1574	1
2-methyl-2-nitro-1-propanol	1359	1551	2
3-nitro-2-butanol	1344	1550	2
n-nitrosomethylethylamine	1347	1551	2
3-methyl-2-nitroanisole	1376	1588	3
m-nitroanisole	1351	1587	3
p-nitroanisole	1337	1596	3
p-nitrobenzyl hidrochloride	1354	1607	3
m-nitroaniline	1354	1590	3
m-nitrobenzylamine hydrochlorid	1358	1592	3
methyl-m-nitrobenzoate	1352	1588	3
m-nitrotoluene	1347	1584	3
nitrobenzene	1344	1587	3
o-nitrotoluene	1344	1578	3
3-nitro-o-xilene	1351	1575	3
2-methyl-5-nitrophenylisocyanate	1354	1606	3
p-nitrotoluene	1344	1599	3
2-nitro-1,4-diaminobenzene	1341	1573	3
5-nitro-4-amino-1,3-dimethylbenzene	1365	1568	3
m-nitrodimethylaniline	1337	1567	3
o-nitroaniline	1353	1572	3
p-nitrobenzamide	1340	1599	3
4-nitroacetanilide	1333	1599	3
4-nitrothiophenol	1331	1572	3
m-nitrobenzaldehyde	1350	1578	3
p-nitrobenzaldehyde	1346	1596	3
m-nitrophenol	1352	1595	3
4-nitrobiphenyl	1343	1599	3
2-nitrobyphenyl	1364	1615	3
2,2'-dinitrobyphenyl	1358	1582	3
p-nitrodiphenyl eter	1348	1600	3
p-nitrobenzyl chloride	1354	1605	3
1-bromo-2-nitrobenzene	1360	1580	3
1-iodo-4-nitrobenzene	1343	1574	3
o-nitrobenzyl chloride	1348	1584	3
1-iodo-2-nitrobenzene	1335	1574	3
o-nitrobenzyl bromide	1348	1582	3
p-nitrobenzyl bromide	1346	1593	3
o-nitroanisole	1343	1531	4
1,3,5-tnb	1357	1546	4
3,4-dnt	1357	1538	4
o-dinitrobenzene	1366	1538	4
2,4,6tnt	1366	1539	4
2,4-dnt	1349	1528	4
4,6-dinitro-o-cresol	1338	1536	4
3,5-dinitro-4-methyl benzoic	1359	1544	4
2,6-dinitrotoluene	1362	1524	4
n-nitronaphtalene-d7	1344	1545	4
2,4-dinitrofluorobenzene	1358	1545	4

Table 7–12. Classification of explosives substance using Raman technique.

CHAPTER 8
CONCLUSIONS

1. The model presented is useful for making predictions of the data obtained.
2. Three major classes of explosives, the nitrate esters containing the "$R-O-NO_2$" group, the nitro-aromatic containing the "$Ar-NO_2$" group and the nitramines containing the "$R-N(NO_2)-R$" group, may be distinguished on the basis of their Raman and Infrared spectra. Group frequencies (cm^{-1}) of NO_2 in vibrational spectroscopic for asymmetrical mode stretch were: $C-NO_2 = 1534-1603$, $Ar-NO_2 = 1487-1555$, $O-NO_2 = 1620-1640$ and $N-NO_2 = 1550-1630$ and for mode symmetrical stretch were $C-NO_2 = 1297-1388$, $Ar-NO_2 = 1318-1357$ and $N-NO_2 = 1250-1300$.
3. Nitro compounds show a narrow dispersion of points with respect of the symmetric mode for infrared ($1280-1400cm^{-1}$) and Raman spectra ($1280-1375cm^{-1}$). The asymmetric mode exhibits a wider distribution in Infrared is ($1490-1650cm^{-1}$) and Raman is ($1520-1615cm^{-1}$).
4. The contour map is an excellent tool for the visualization of the classification and identification and was used effectively for this purpose.
5. Significant progress has been achieved in the creation of a spectroscopic library of explosives using vibrational spectroscopy.

BIBLIOGRAPHY

[1] Passingham C., Hendra P.J., Hodges C., and Willis H.A. *The Raman Spectra of Some Aromatic Nitro Compounds*. *Spectrochimica Acta*, 47A(9/10):1235–1245, April 1991.

[2] Lewis I.R., Daniel Jr N.W., Chaffin N.C., Griffiths P.R., and Tungol M.W. *Raman Spectroscopic Studies of Explosive Materials: Towards a fieldable Explosives Detector*. *Spectrochimica Acta part A*, 51, 1995.

[3] Clarkson J., Batchelder W., Smith adn D., Smith D., and Coats A. *A Theoretical Study of the Structure and Vibrations of 2, 4, 6-Trinitrotoluene*. *Journal of Molecular Structure*, 648, 2003.

[4] Cheng C., Kirkbride T.E., Batchelder D.N., Lacey R.J., and Sheldon T.G. *In Situ Detection and Identification of Trace Explosives by Raman Microscopy*. *Journal of Forensic Sciences*, 40(1):31–37, 1995.

[5] Moore D.S. *Determination of Energetic Materials in Soil Using Multivariate Analysis of Raman Spectra*. *Fresenius J. Anal. Chem.*, 369, 2001.

[6] Kneipp K., Wang Y., Dasari R., Feld M., Gilbert B., Janni J., and Steinfeld J. *Near-Infrared Surface-enhanced Raman Scattering of Trinitrotoluene on Colloidal Gold and Silver*. *Spectrochimica Acta part A*, 51, 1995.

[7] Hopke P. *The Evolution of Chemometrics*. *Analytica Chimica Acta*, 500, 2003.

[8] Bro R. *Multivariate calibration. What is in chemometrics for the analytical chemist? .* *Analytica Chimica Acta*, 500, 2003.

[9] de Juan A. and Tauler R. *Chemometrics Applied to Unravel Multicomponent Processes and Mixtures Revisiting Latest Trends in Multivariate Resolution*. *Analytica Chimica Acta*, 500, 2003.

[10] Ragno G., Ioele G., and Risoli. A. *Multivariate Calibration Techniques Applied To The Spectrophotometric Analysis Of One-To-Four Component Systems. Analytica Chimica Acta*, 512, 2004.

[11] Brereton R. G. *Chemometrics, Data Analysis for the Laboratory and Chemical Plant.* John Wiley and Sons Ltd, England, 2002.

[12] Lin-Vien D., Colthup N. B., Fateley W. G., and Grasselli J. G. *The Handbook of Infrared and Raman Characteristic Frequencies of Organic Molecules.* . Academic Press, 1991.

[13] Baranska H., Labudzinska A., and Terpnski J. *Laser Raman Spectrometry Analytical Applications.* Ellis Horwood, 1987.

[14] Silverstein R. M., Webster F. X., and Kiemle D. J. *Spectrometric Identification of Organic Compouds.* Wiley, 2005.

[15] Kramer R. *Chemometric Techniques for Quantitative Analysis.* Marcel Dekker, New York, 1998.

[16] Beebe K., Pell R., and Beth M. *Chemometrics: A practical Gide.* John Wiley and Sons, inc., 1998.

[17] Otto M. *Chemometrics. Statics and Computer Application in Analytical Chemistry.* Wiley-VCH, Federal Republic of Germany., 1999.

[18] Huberty C. J. *Applied Discriminant Analysis.* Wiley-Interscience, New Jersey, 1994.

[19] Schrader B. *Infrared and Raman Spectroscopy. Methods and Applications.* Schrader, B., New York, 1995.

[20] Zerner M. C. *Review of Computational Chemistry.* VCH, New York, 1991.

[21] Paramonov G. K. and Saalfrank P. *Infrared-laser induced vibrational excitation of relaxing adsorbates: Quantum dynamical aspects. J. Chem. Phys.*, 110(13):6500, 1999.

[22] Mukamel S. *Principles of Nonlinear Spectroscopy*. Oxford University Press, Oxford, 1995.

[23] Rodolfa K. T. and Cremers D. A. *Capabilities of Surface Composition Analysis Using a Long Laser-Induced Breakdown Spectroscopy Spark*. *Society for Applied Spectroscopy*, 58(4):367–375, 2004.

[24] Marquardt B. J., Stratis D. N., Cremers D. A., and Angel S. M. *Novel Probe for Laser-Induced Breakdown Spectroscopy and Raman Measurements Using an Imaging Optical Fiber*. *Society for Applied Spectroscopy*, 52(9):1148–1153, 1998.

[25] Torres P., Mercado L., Cotte I., Hernández S. P., Mina N., Santana A., Chamberlain R. T., Lareau R., and Castro M. E. *Vibrational Spectroscopy Study of β and α RDX Deposits*. *American Chemical Society*, 108:8799–8805, 2004.

[26] Tafipolskya M.A., I.V. Tokmakovb, and Shlyapochnikova V.A. *Structure and Vibrational Spectra of Dinitromethane and Trinitromethane*. *Journal of Molecular Structure*, 510:149156, 1999.

[27] P. G. Datskos, N. V. Lavrik, and M. J. Sepaniakb. *Detection of Explosive Compounds with the Use of Microcantilevers with Nanoporous Coatings*. *American Scientific Publishers*, 1:2532, 2003.

[28] Steinfeld J. I. and Wormhoudt J. *Explosives Detection: A Challenge for Physical Chemistry*. *Annu. Rev. Phys. Chem.*, 49:203–232, 1998.

[29] Sylvia J. M., Janni J. A., J. D. Klein, and Spencer K. M. *Surface-Enhanced Raman Detection of 2,4-Dinitrotoluene Impurity Vapor as a Marker To Locate Landmines*. *Analytical Chemistry*, 72(23):5834–5840, 2000.

[30] Psillakis E., Mantzavinos D., and Kalogerakis N. *Development of a Hollow Fibre Liquid Phase Microextraction Method to Monitor the Sonochemical Degradation of Explosives in Water*. *Analytica Chimica Acta*, 501:310, 2004.

[31] Pinnaduwage L. A., Yi D., Tian F., and Thundat T. *Adsorption of Trinitrotoluene on Uncoated Silicon Microcantilever Surfaces. American Chemical Society*, 20:2690–2694, 2004.

[32] Lewis I. R., N. W., Jr. D., and Griffiths P. R. *Interpretation of Raman Spectra of Nitro-Containing Explosive Materials. Part I: Group Frequency and Structural Class Membership. Society for Applied Spectroscopy*, 51(12):1854–1867, 1997.

[33] Lewis M. L., Lewis I. R., and Griffiths P. R. *Anti-Stokes Raman Spectrometry with 1064-nm Excitation: An Effective Instrumental Approach for Field Detection of Explosives. Society for Applied Spectroscopy*, 58(4):420–427, 2004.

[34] Courtecuisse S., Cansell F., Fabre D., and Petitet J. P. *Comparative Raman spectroscopy of nitromethane-h3 , nitromethane-d3 , and nitroethane up to* $20GPa$. *Journal Of Chemical Physics*, 108(17):7350–7355, 1998.

[35] Atkins P. W. *Physical Chemistry.* Freeman, sixth edition, 1997.

[36] Metz C. R. *Schaum's Outline of Theory and Problems Physical Chemistry.* McGraw-Hill, second edition, 1998.

[37] Carey F. A. and Sundberg R. J. *Advanced Organic Chemistry: Structure and Mechanisms: Part A.* Springer, fourth edition, 2004.

[38] Carey F. A. and Sundberg R. J. *Advanced Organic Chemistry: Structure and Mechanisms: Part B.* Springer, fourth edition, 2004.

[39] Sourisseau C. *Polarization Measurements in Macro- and Micro-Raman Spectroscopies: Molecular Orientations in Thin Films and Azo-Dye Containing Polymer Systems. American Chemical Society*, 104:3851–3891, 2004.

[40] Naal Z., Park J.H., S. Bernhard, Shapleigh J. P., Batt C. A., and Abrun H. D. *Amperometric TNT Biosensor Based on the Oriented Immobilization of a Nitroreductase Maltose Binding Protein Fusion. Analytical Chemistry*, 74(1):140–148, 2004.

[41] Barshick S. A. and Griest W. H. *Trace Analysis of Explosives in Seawater Using Solid-Phase Microextraction and Gas Chromatography/Ion Trap Mass Spectrometry*. *Analytical Chemistry*, 70(14):3015–3020, 1998.

[42] Yakovlev V. V., Scarel G., Aita C. R., and Mochizuki S. *Short-range order in ultrathin film titanium dioxide studied by Raman spectroscopy*. *Applied Physics Letters*, 76(9):1107–1109, 2000.

BIOGRAPHICAL SKETCH

Doris Núñez Quintero was born on October 14nd, 1976, in Barranquilla, Colombia. Doris is the daughter of Miguel Angel Núñez and Doris Quintero. In October 2001 she received her B.S. degree in Pharmaceutical Chemistry from the Universidad del Atlántico, Barranquilla Campus. In January of 2003, she started her graduate education. She worked under the supervision of Dr. Samuel P. Hernández.

APPENDIX A
RAMAN SPECTRA

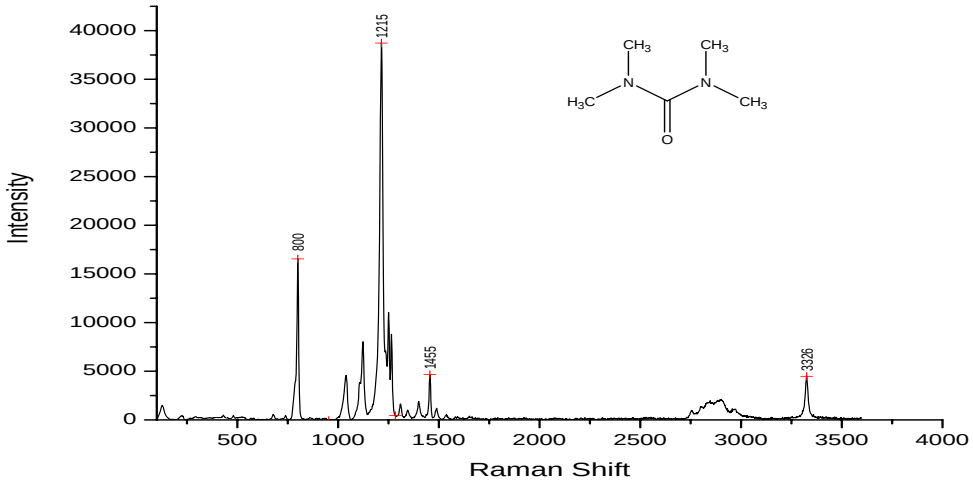

Figure A–1. Raman Spectrum of 1,1,3,3-Tetramethylurea

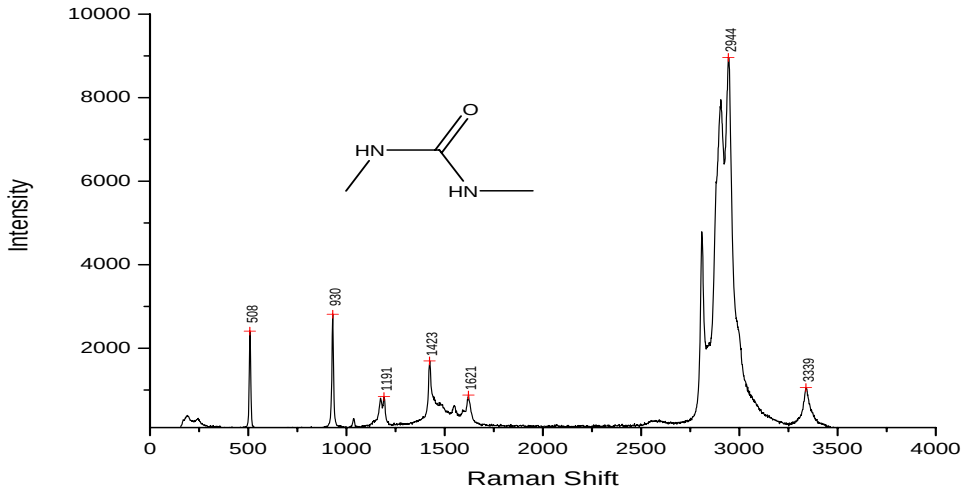

Figure A–2. Raman Spectrum of 1,3-Dimethylurea

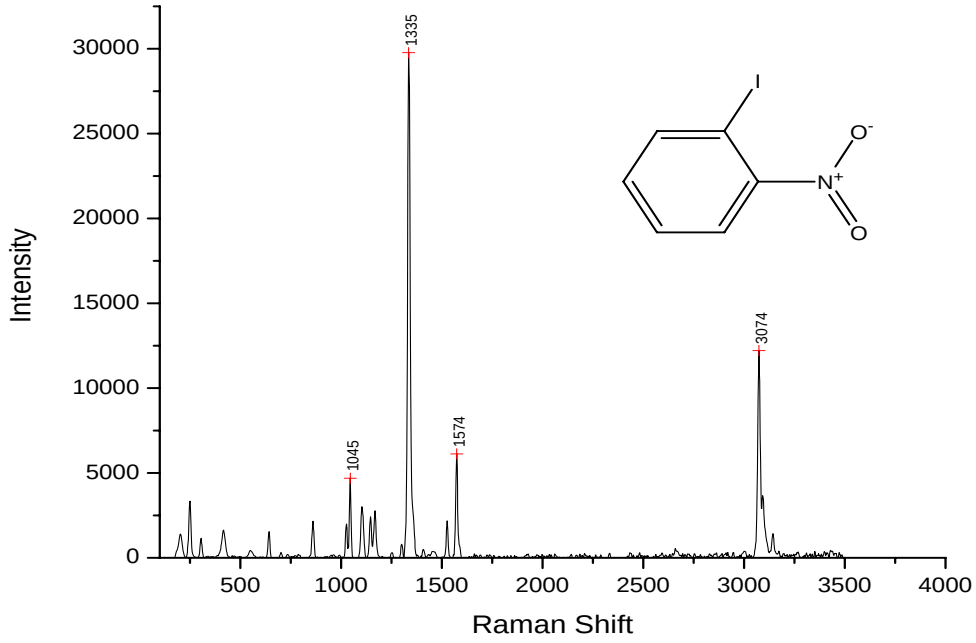

Figure A–3. Raman Spectrum of 1-Iodo-2-Nitrobenzene

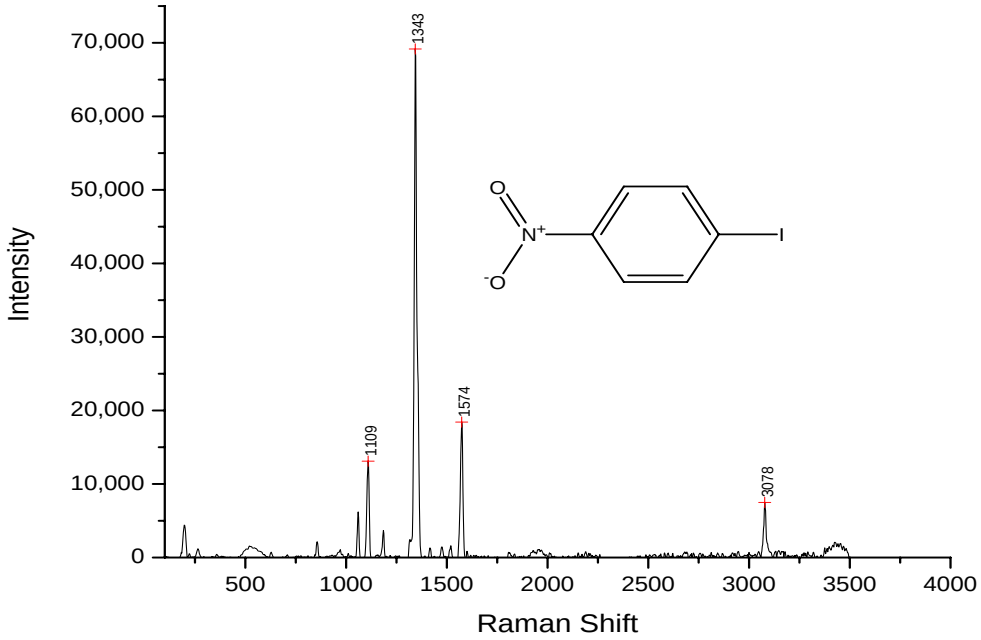

Figure A–4. Raman Spectrum of 1-Iodo-4-Nitrobenzene

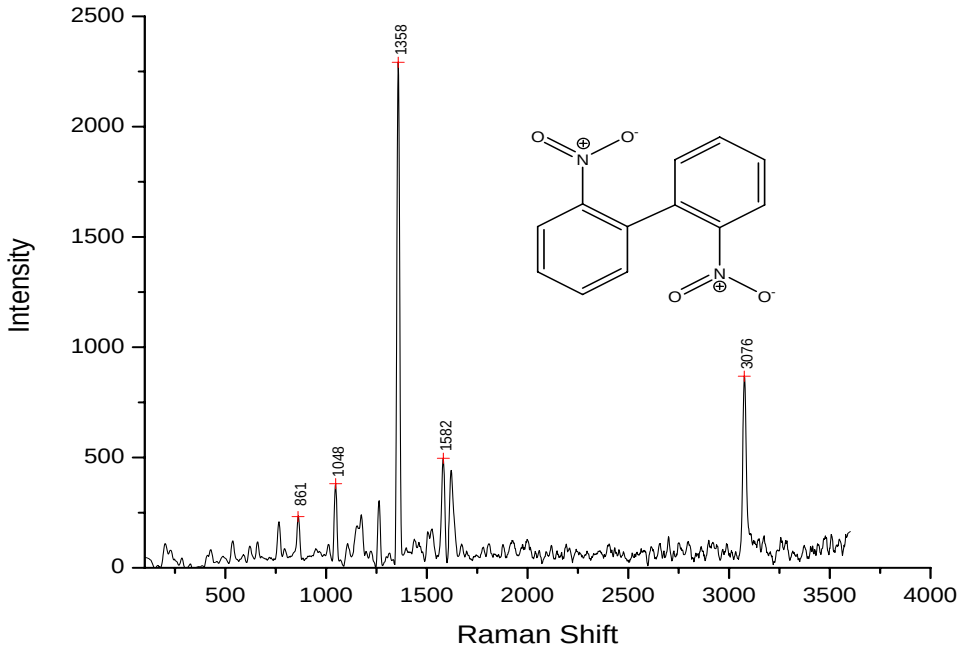

Figure A–5. Raman Spectrum of 2,2-Dinitrobyphenyl

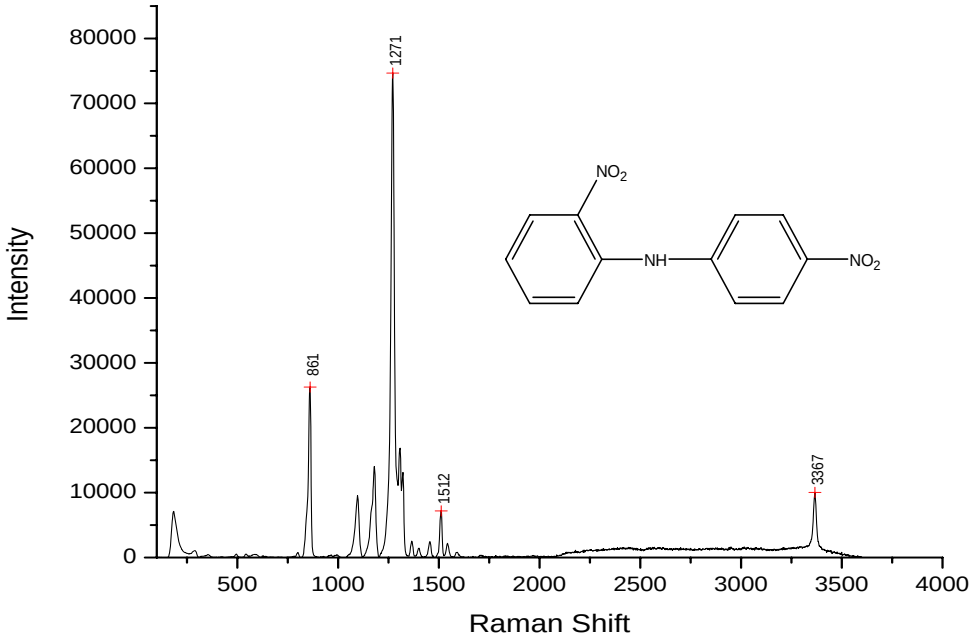

Figure A–6. Raman Spectrum of 2,4'-Dinitrodiphenylamine

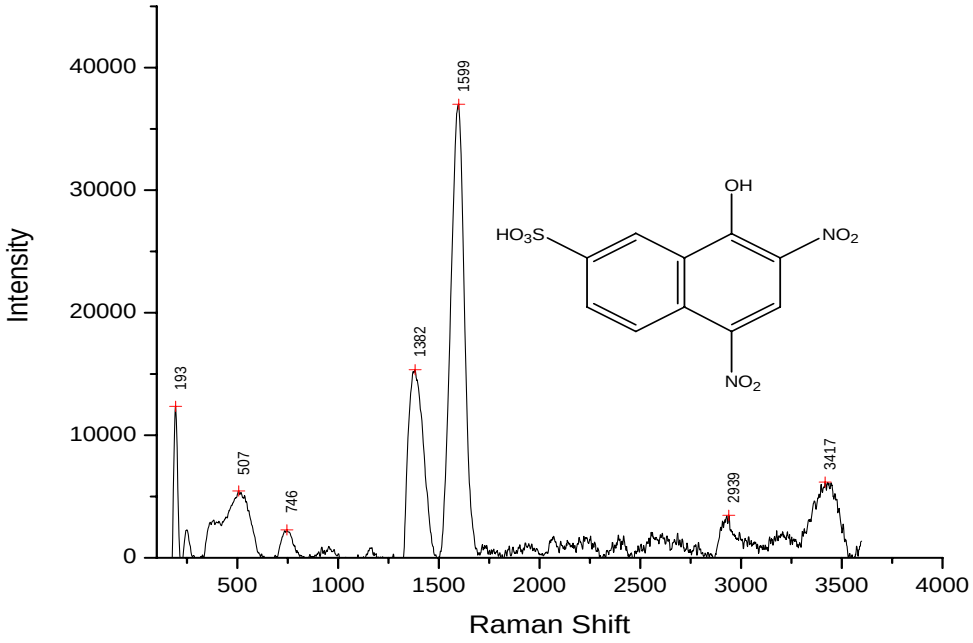

Figure A–7. Raman Spectrum of 2,4-Dinitro-1-Naphtol-7-Sulfonic Acid

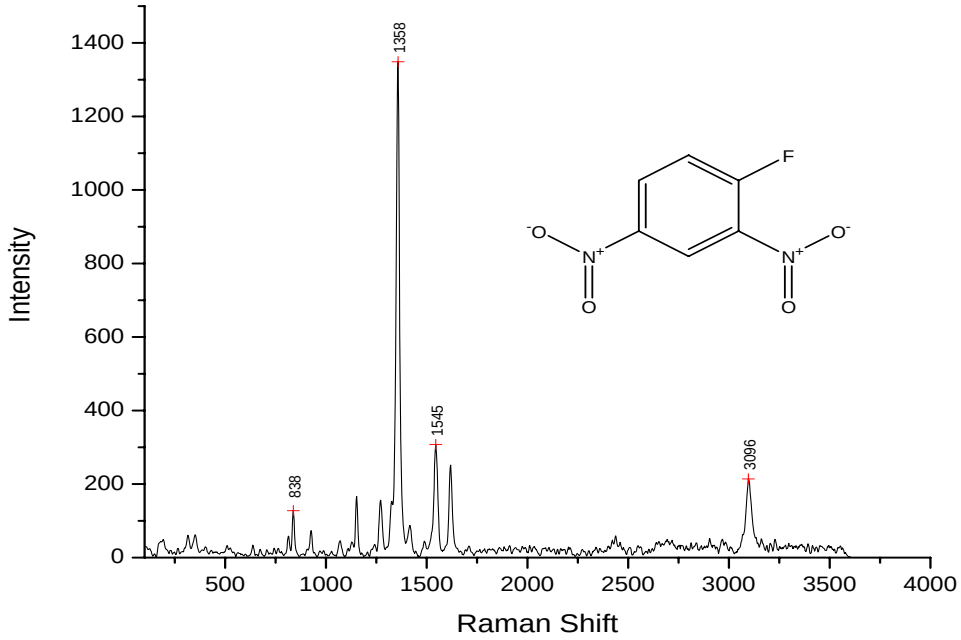

Figure A–8. Raman Spectrum of 2,4-Dinitrofluorobenzene

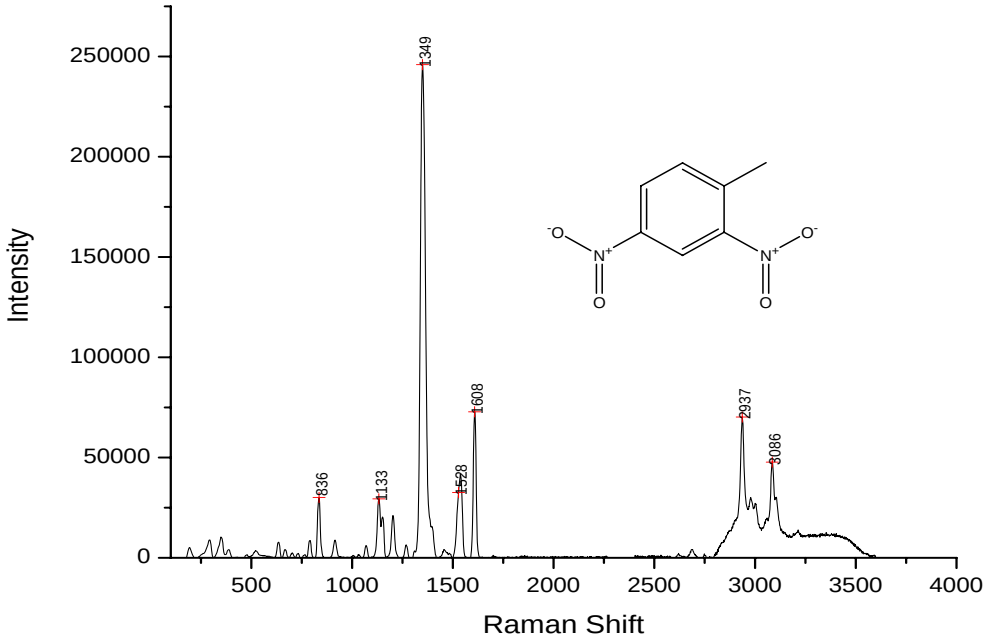

Figure A–9. Raman Spectrum of 2,4-Dinitrotoluene

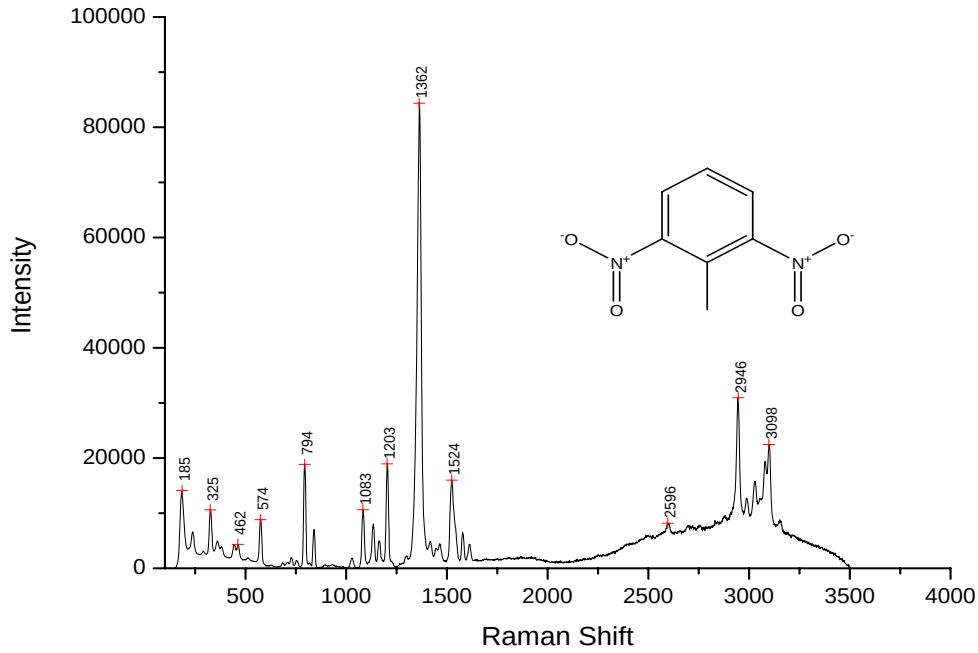

Figure A–10. Raman Spectrum of 2,6-Dinitrotoluene

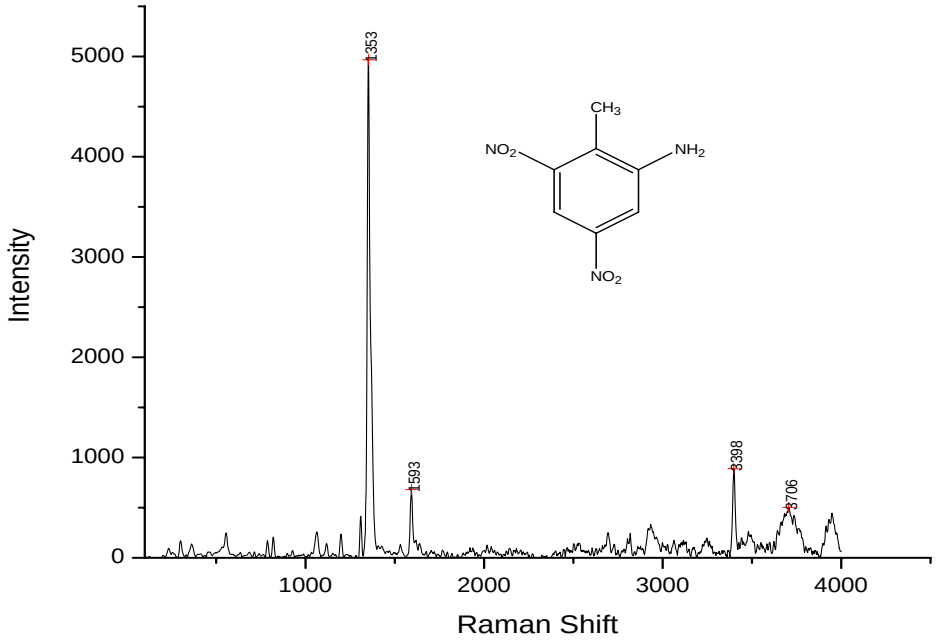

Figure A–11. Raman Spectrum of 2-Amino-4,6-Dinitrotoluene

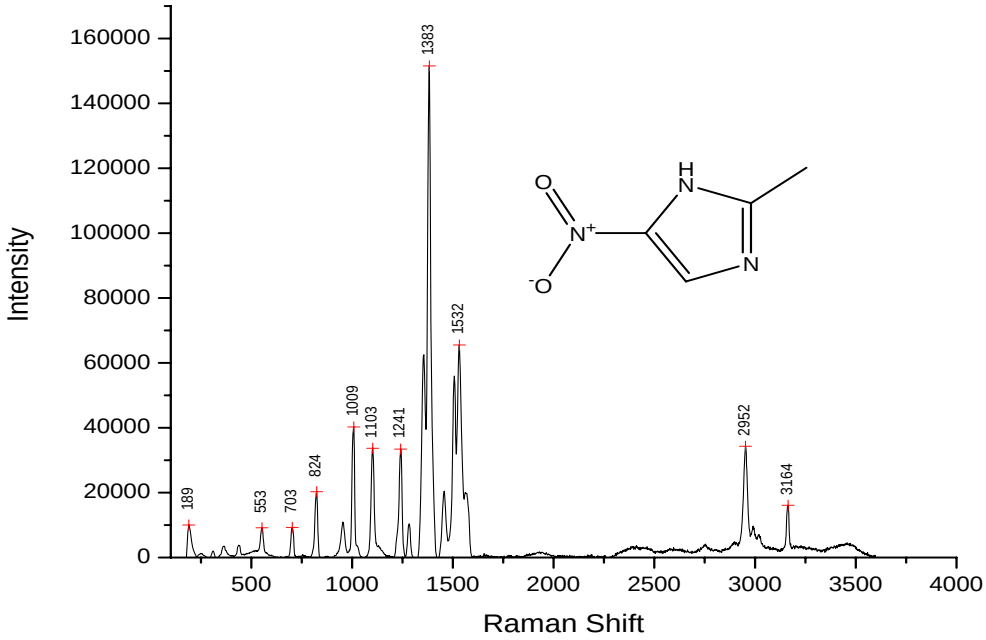

Figure A–12. Raman Spectrum of 2-Methyl-5-Nitroimidazole

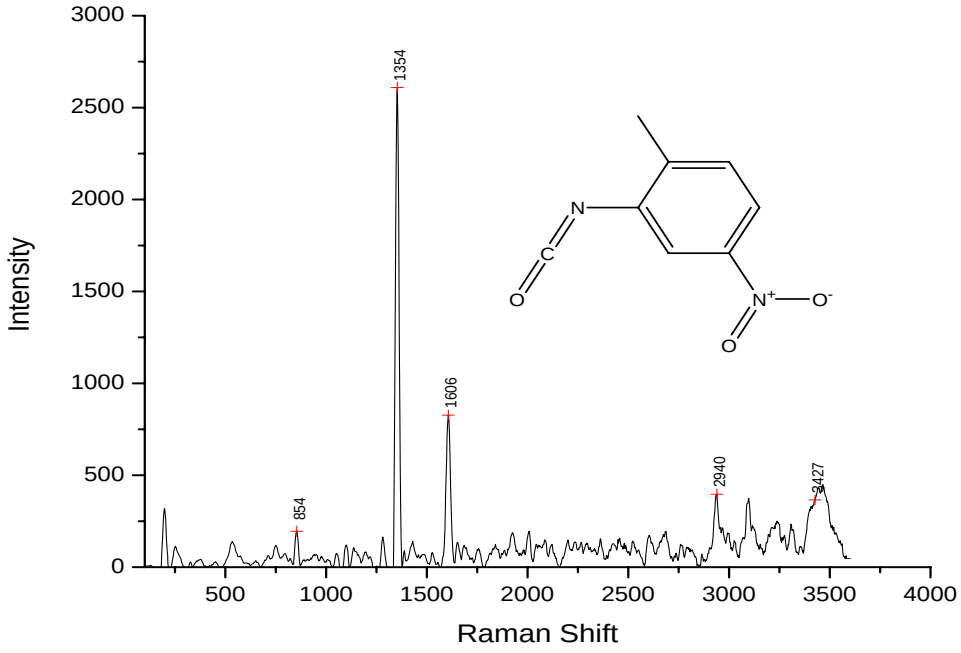

Figure A–13. Raman Spectrum of 2-Methyl-5-Nitrophenylisocianate

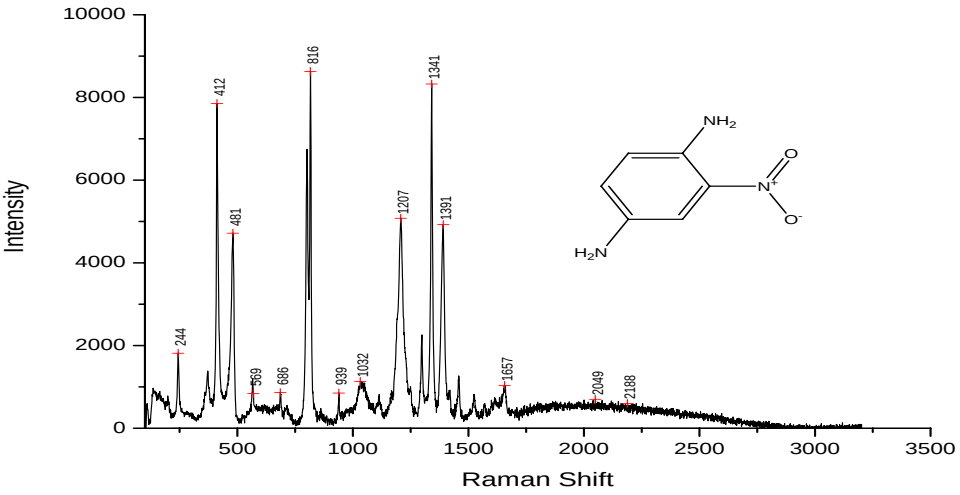

Figure A–14. Raman Spectrum of 2-Nitro-1,4-Diaminobenzene

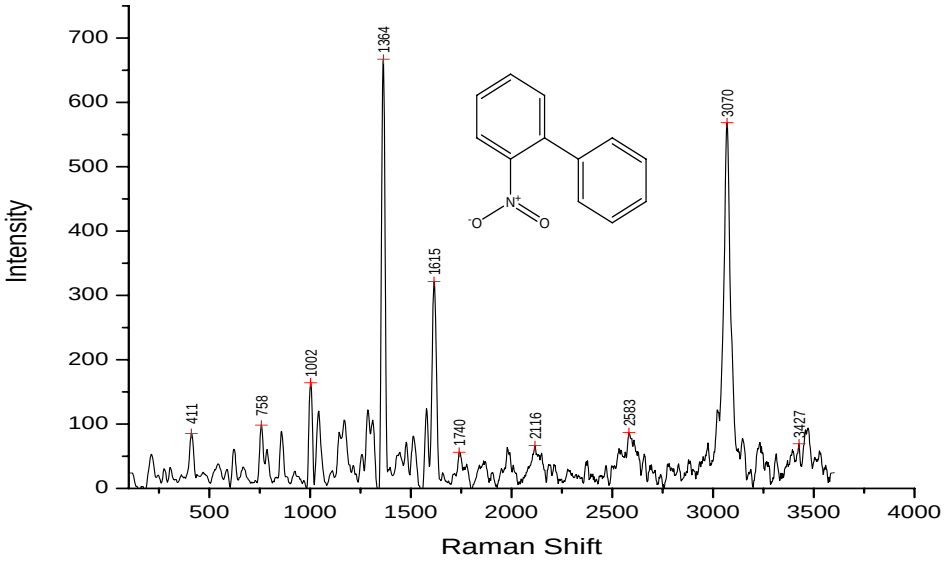

Figure A–15. Raman Spectrum of 2-Nitrobiphenyl

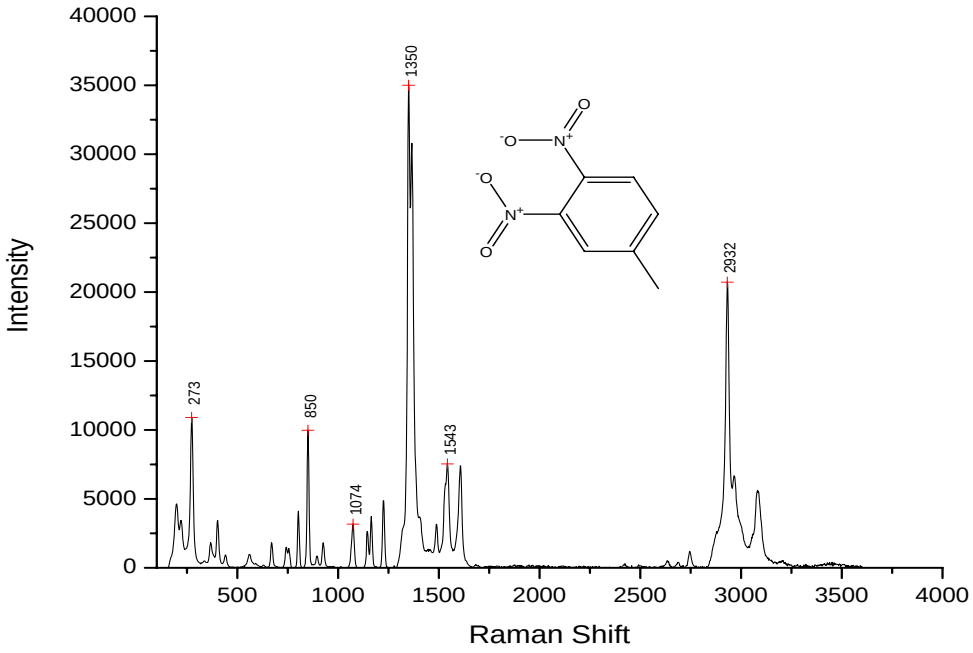

Figure A–16. Raman Spectrum of 3,4-Dinitrotoluene

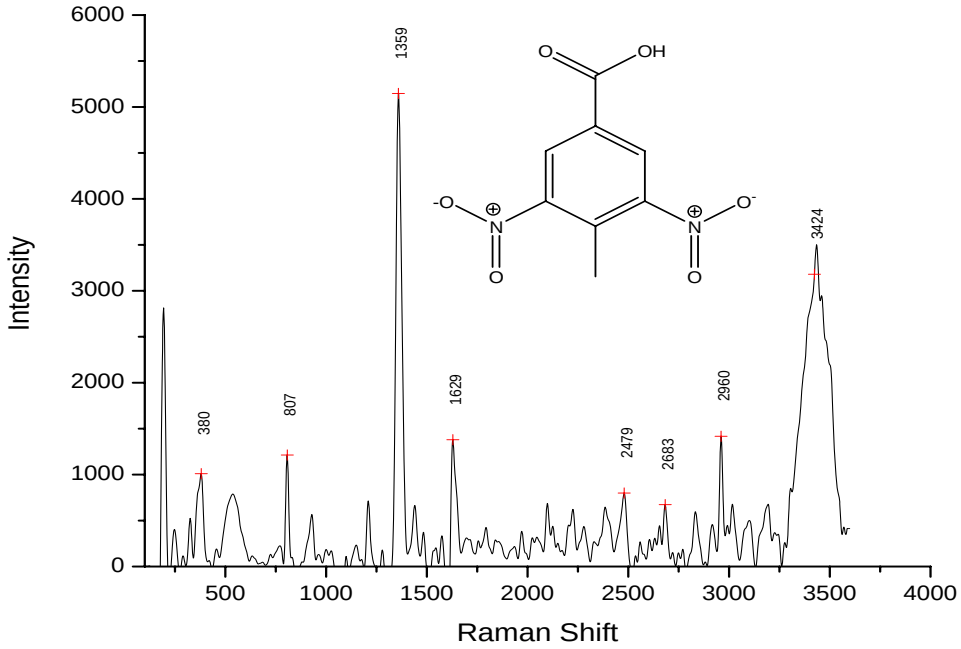

Figure A–17. Raman Spectrum of 3,5-Dinitro-4-Methyl Benzoic Acid

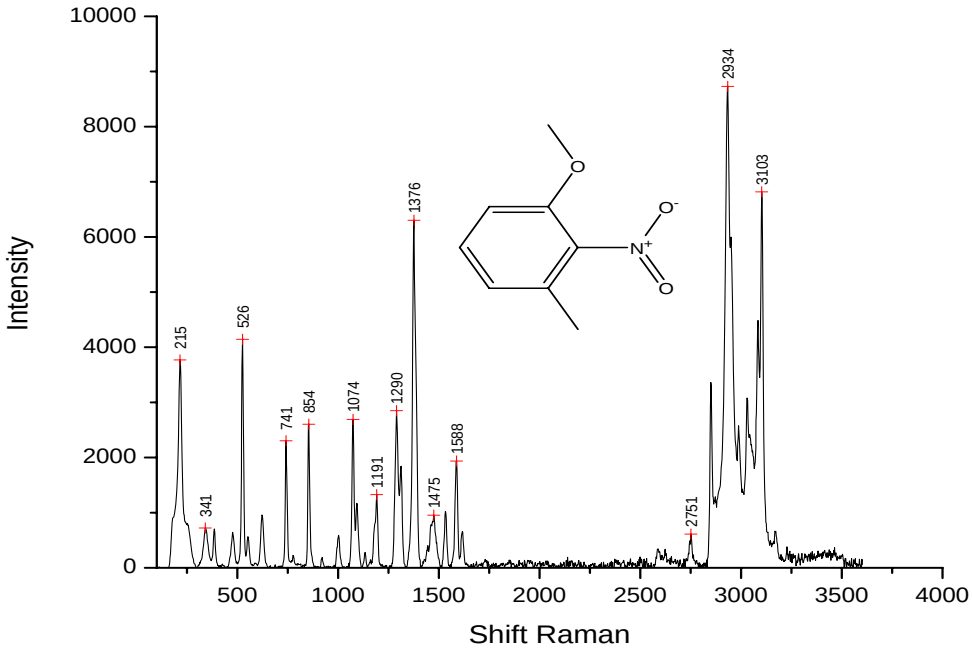

Figure A–18. Raman Spectrum of 3-Methyl-2-Nitroanisole

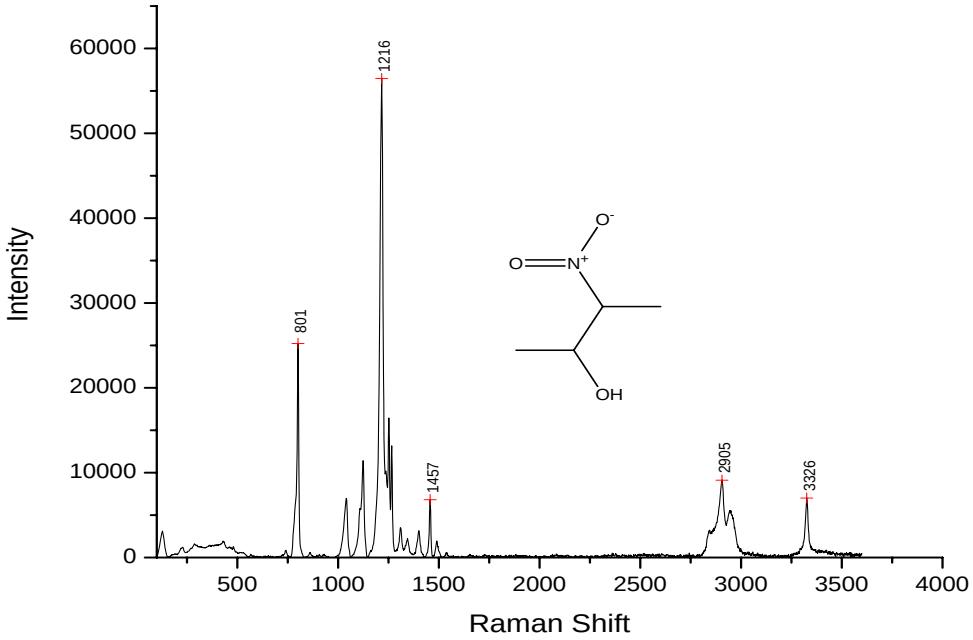

Figure A–19. Raman Spectrum of 3-Nitro-2-Butanol

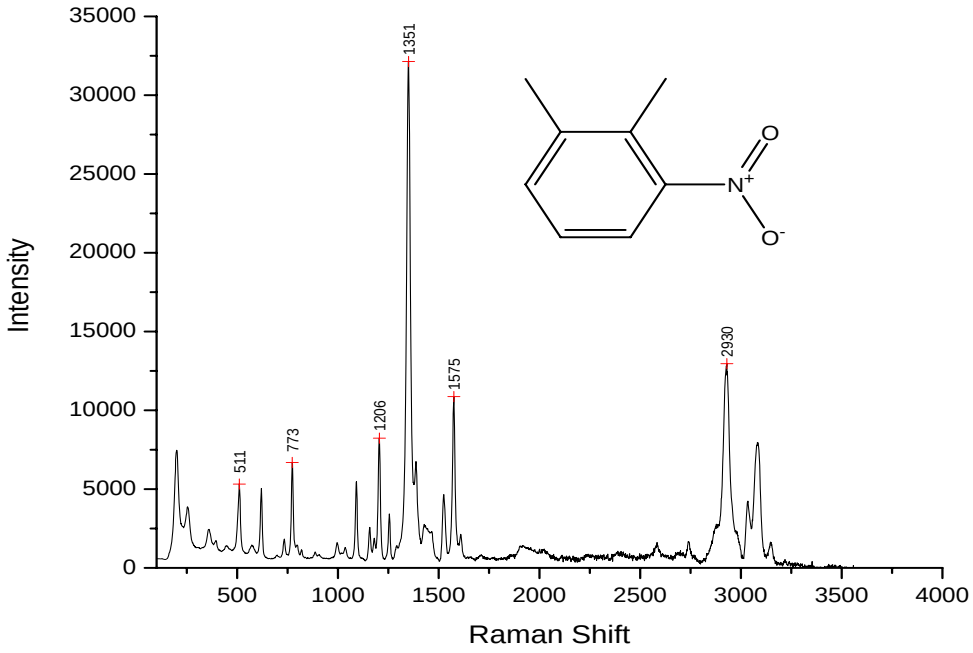

Figure A–20. Raman Spectrum of 3-Nitro-o-Xylene

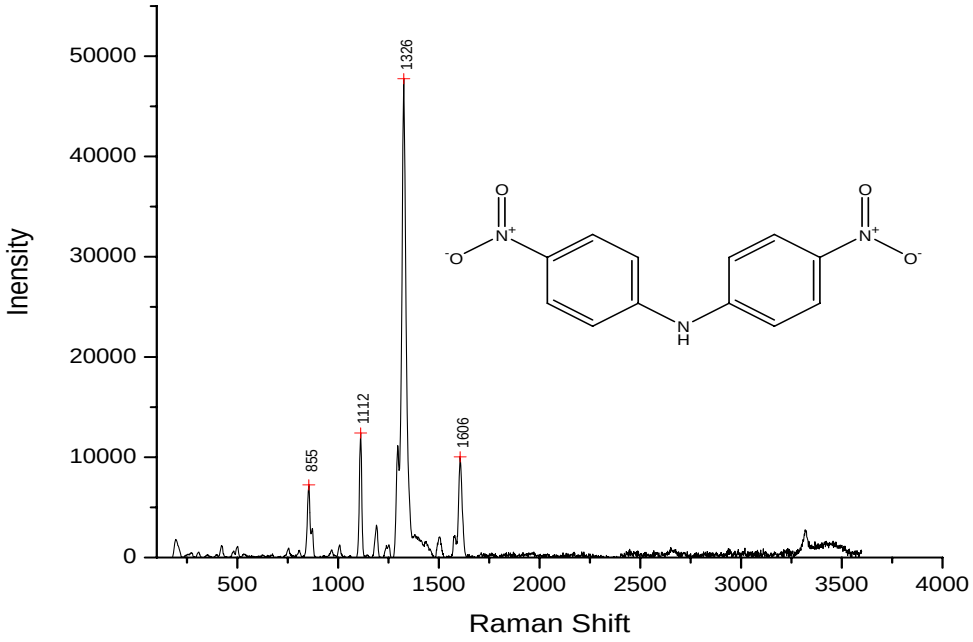

Figure A–21. Raman Spectrum of 4,4'-Dinitrodiphenylamine

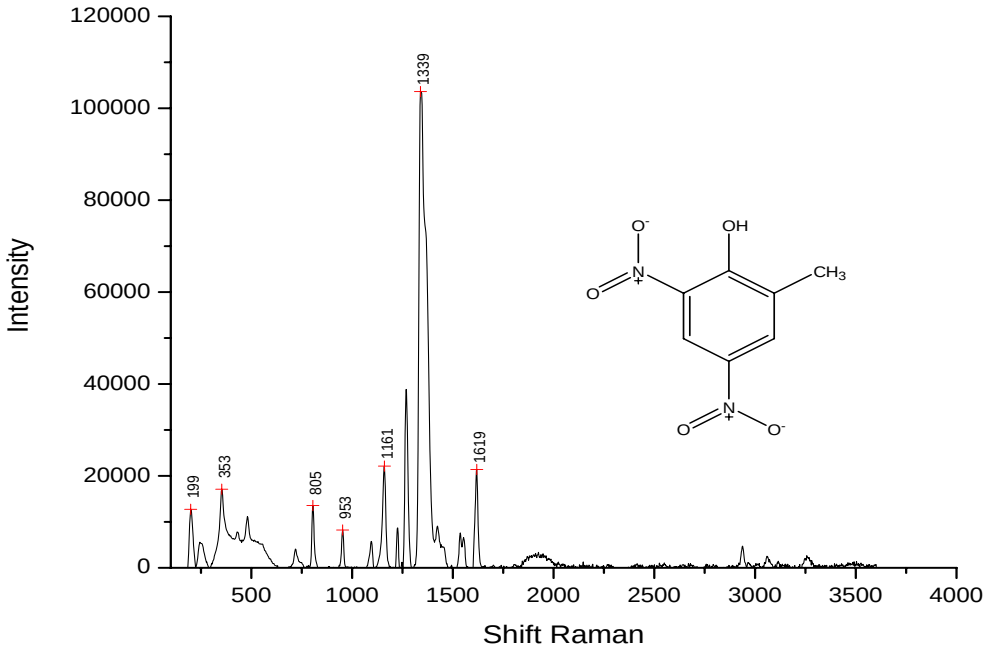

Figure A–22. Raman Spectrum of 4,6-Dinitro-o-Cresol

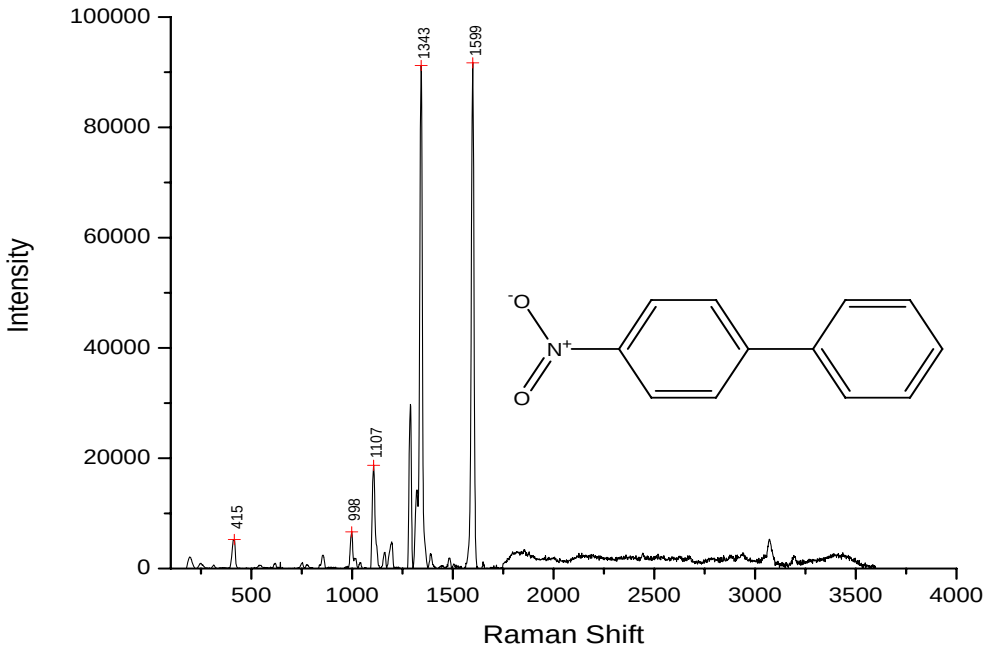

Figure A–23. Raman Spectrum of 4-Nitrobiphenyl

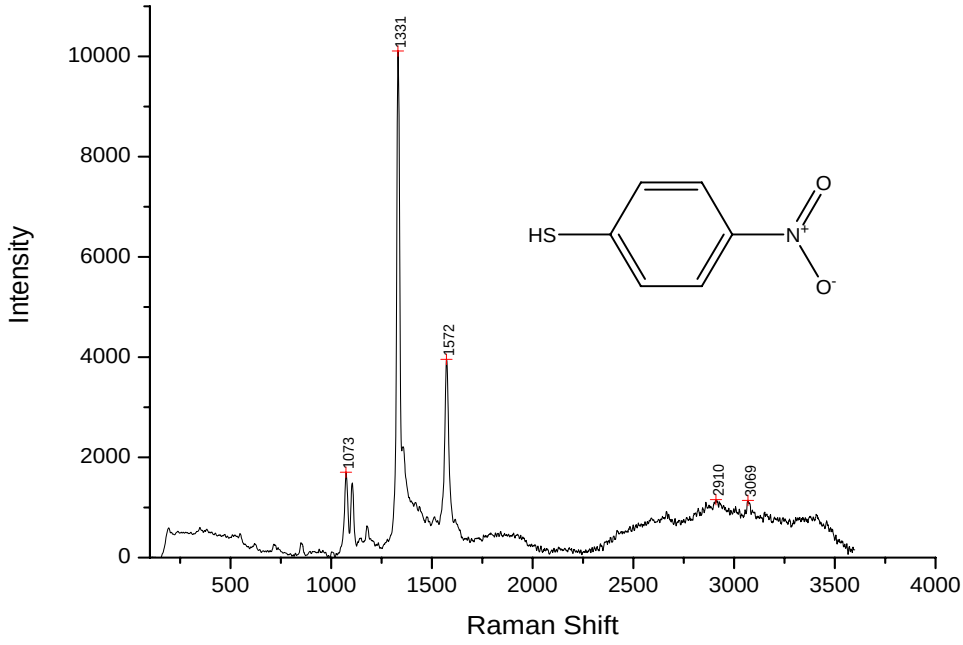

Figure A–24. Raman Spectrum of 4-Nitrothiophenol

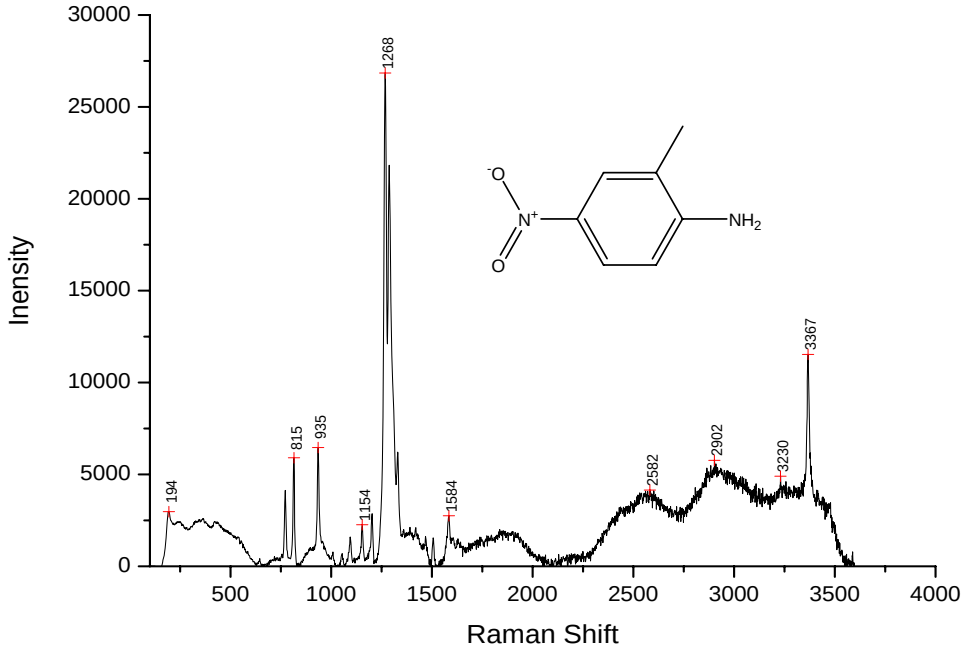

Figure A–25. Raman Spectrum of 5-Nitro-2-Aminotoluene

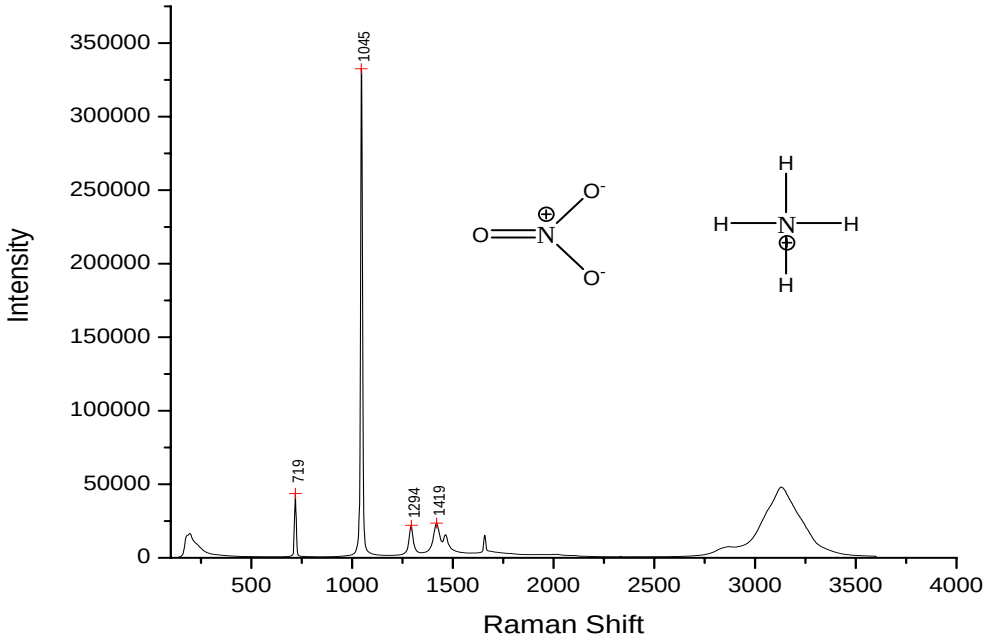

Figure A–26. Raman Spectrum of Ammonium Nitrate

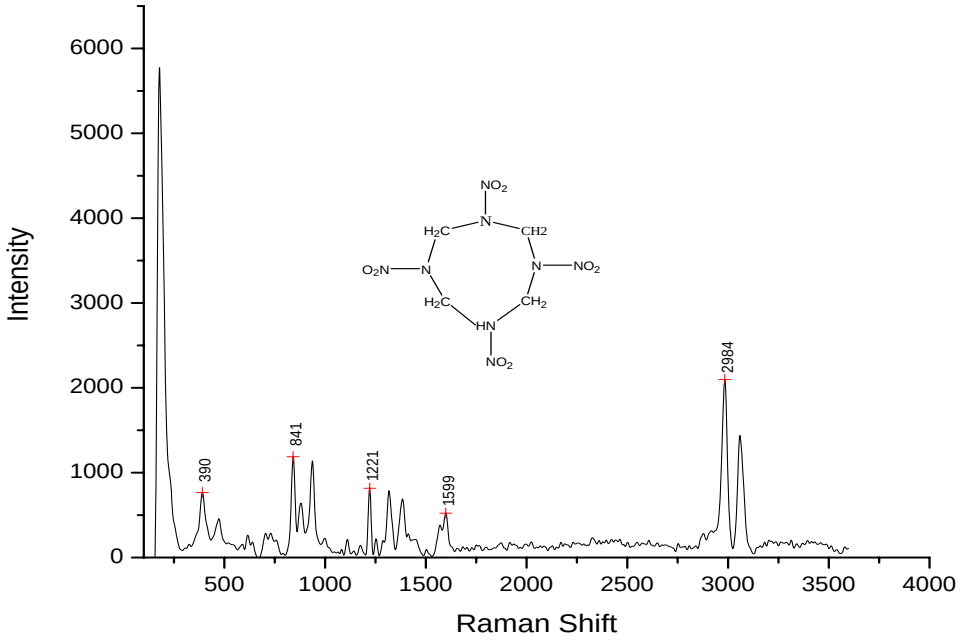

Figure A–27. Raman Spectrum of HMX

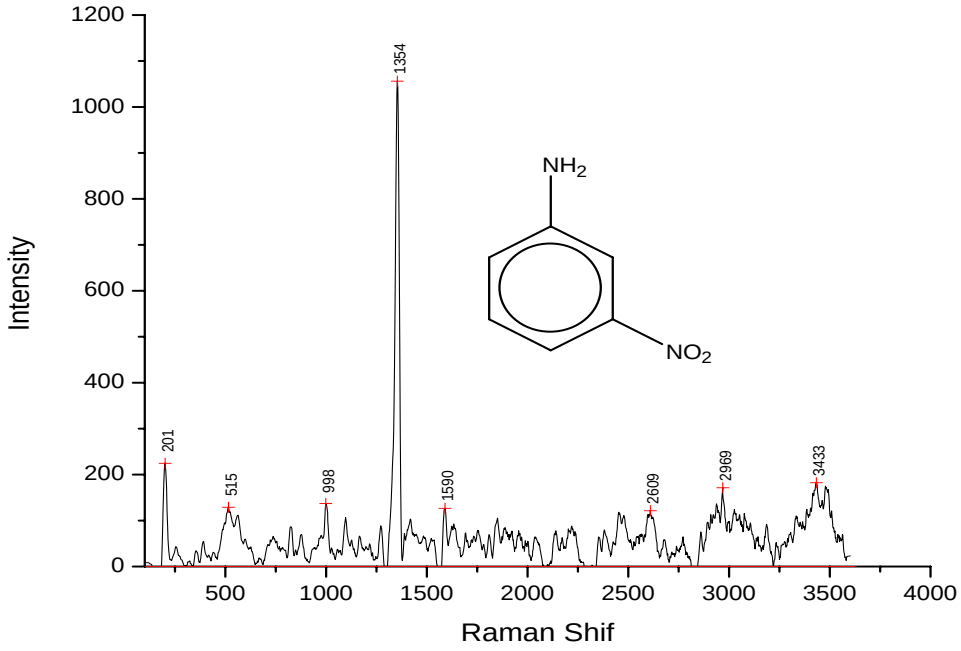

Figure A–28. Raman Spectrum of m-nitroaniline

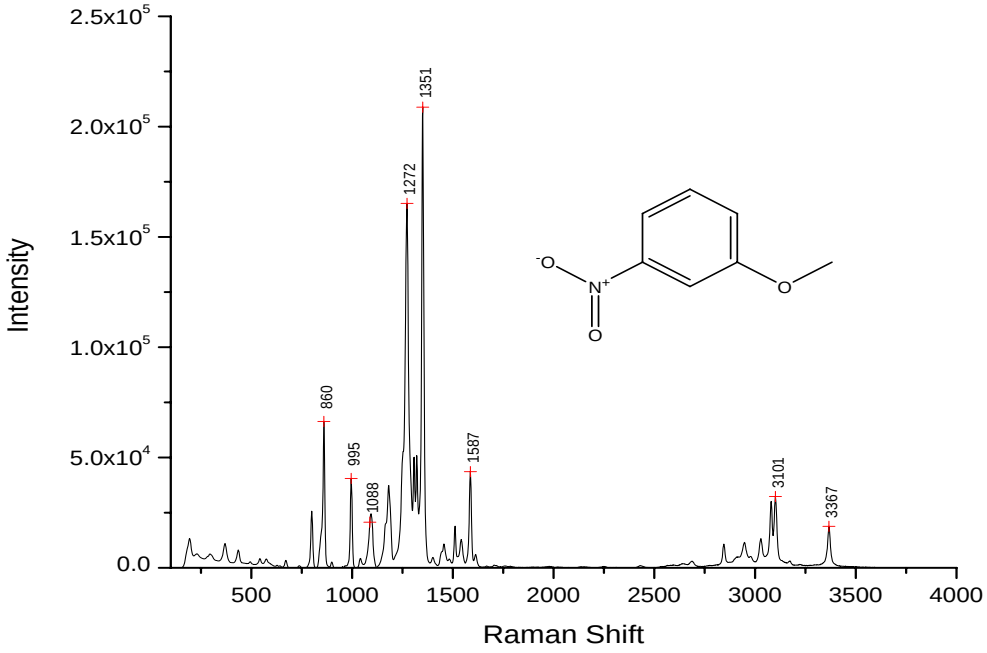

Figure A–29. Raman Spectrum of M-Nitroanisole

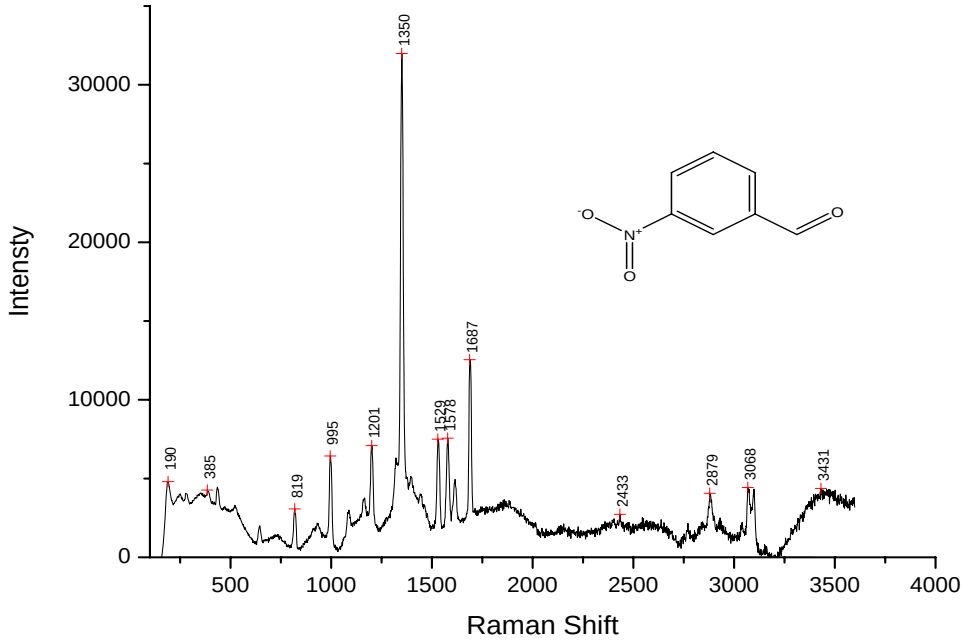

Figure A–30. Raman Spectrum of m-Nitrobenzaldehyde

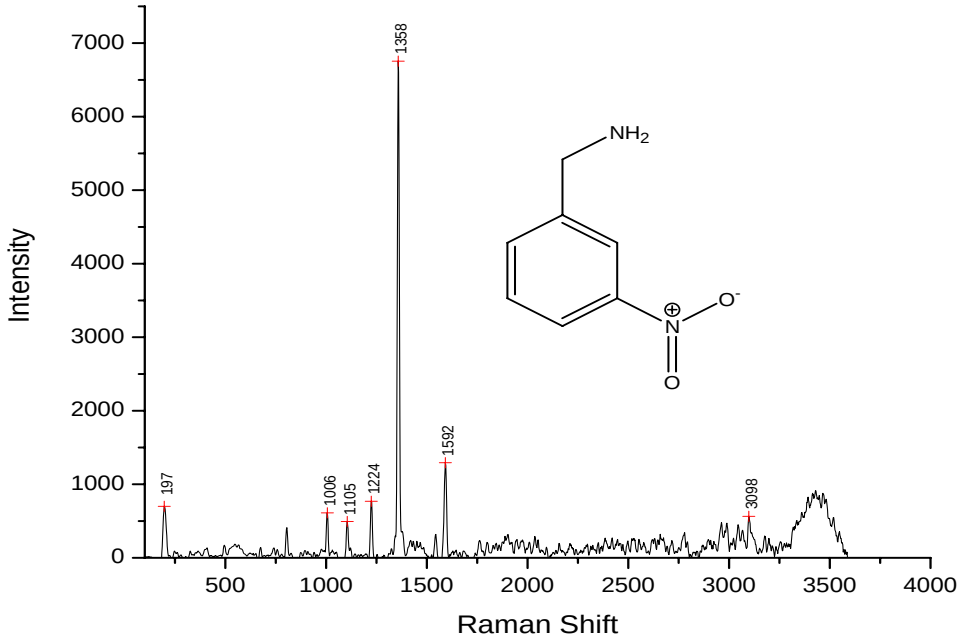

Figure A–31. Raman Spectrum of m-Nitrobenzylamine Hidrochloride

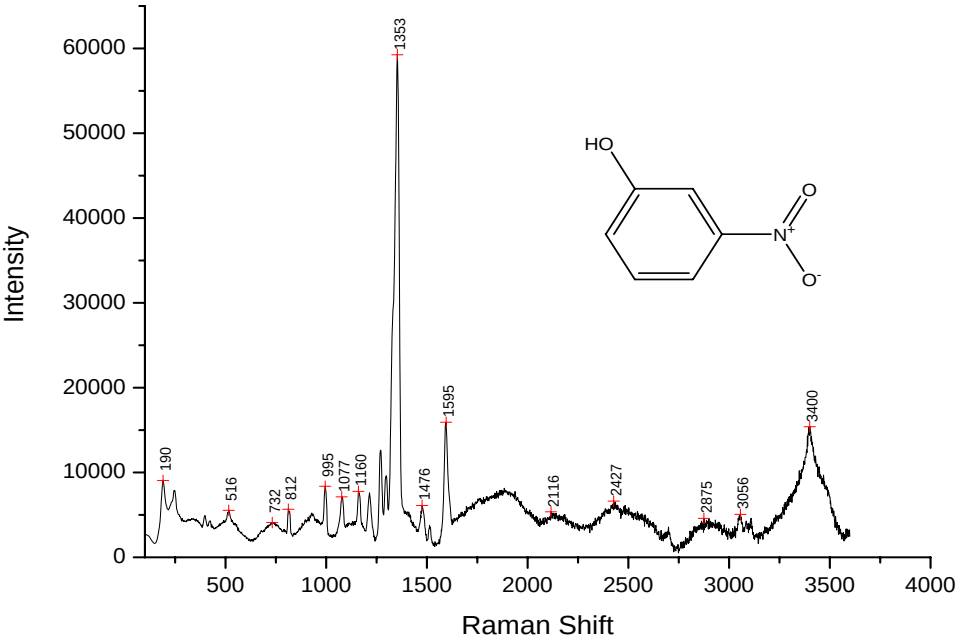

Figure A–32. Raman Spectrum of m-Nitrophenol

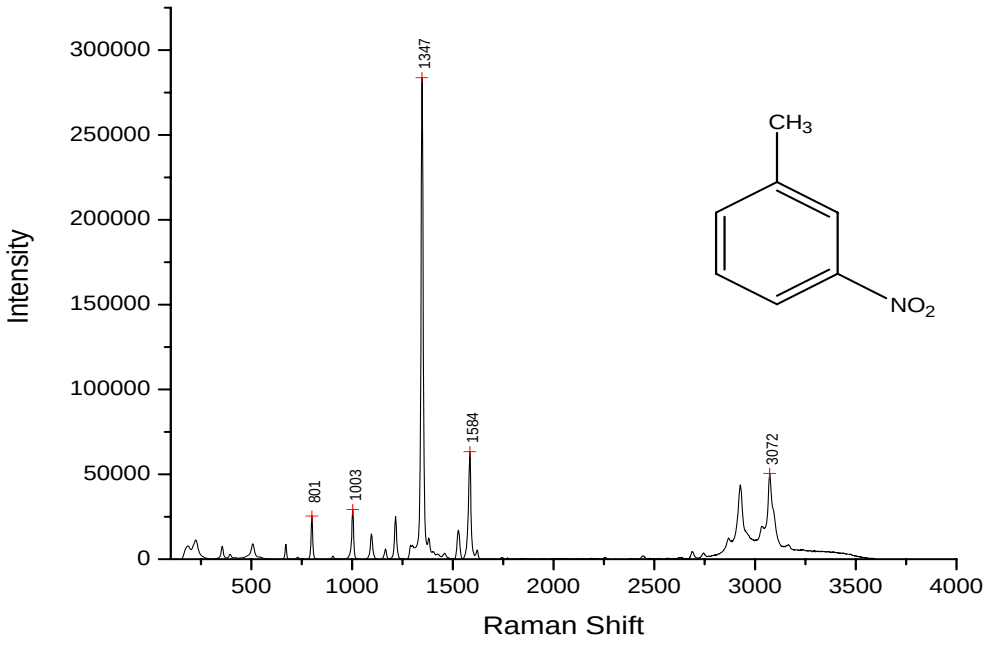

Figure A–33. Raman Spectrum of m-Nitrotoluene

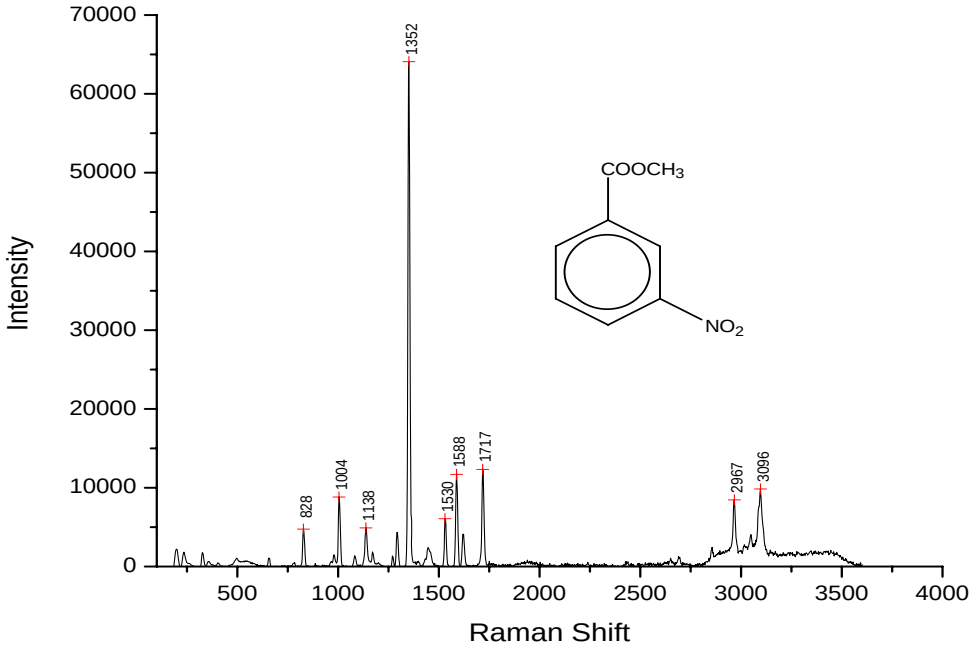

Figure A–34. Raman Spectrum of Methyl-m-Nitrobenzoate

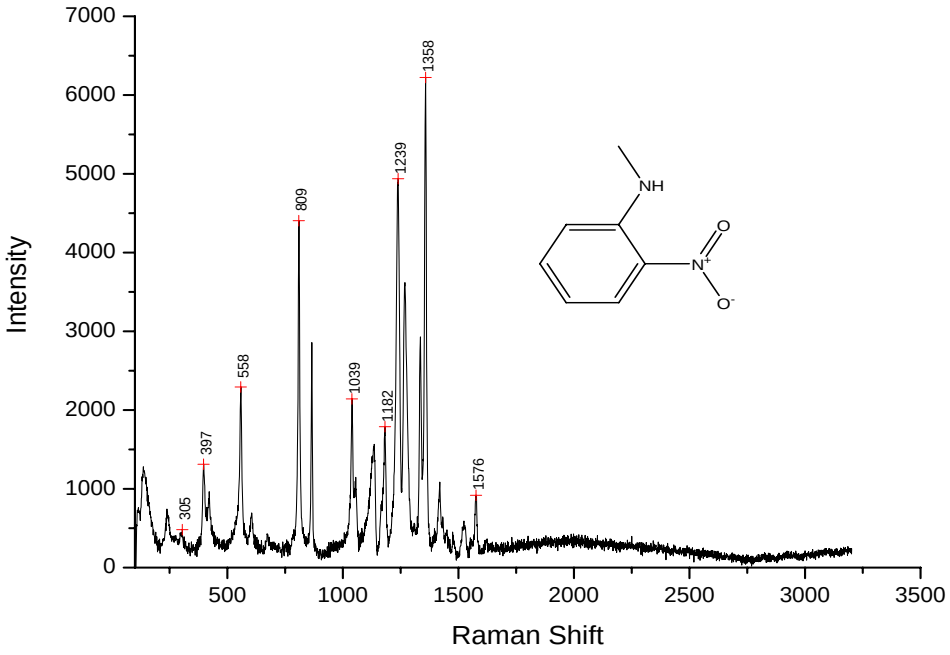

Figure A–35. Raman Spectrum of n-Methyl-o-Nitroaniline

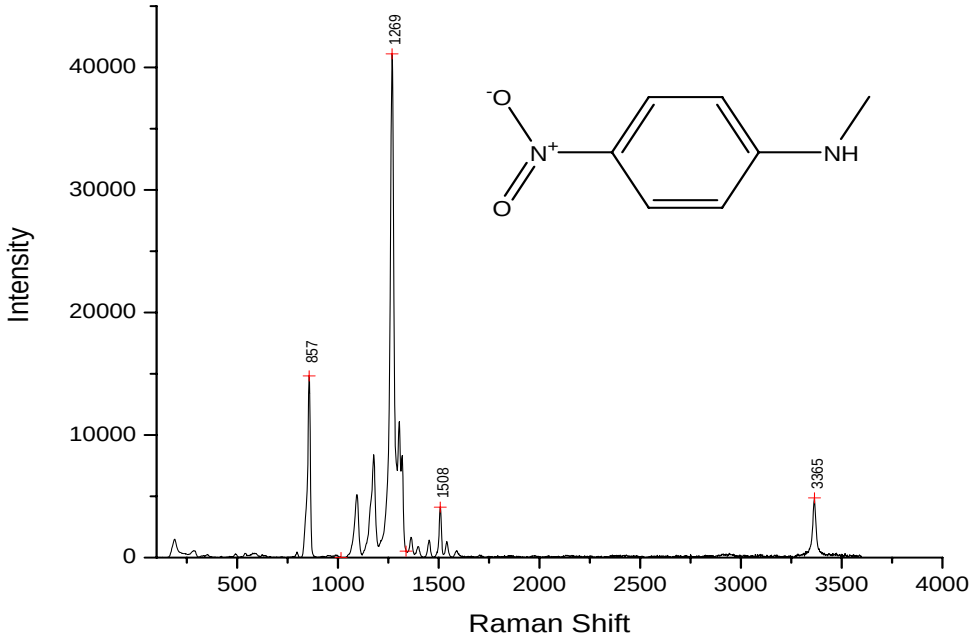

Figure A–36. Raman Spectrum of n-Metyl-p-Nitroaniline

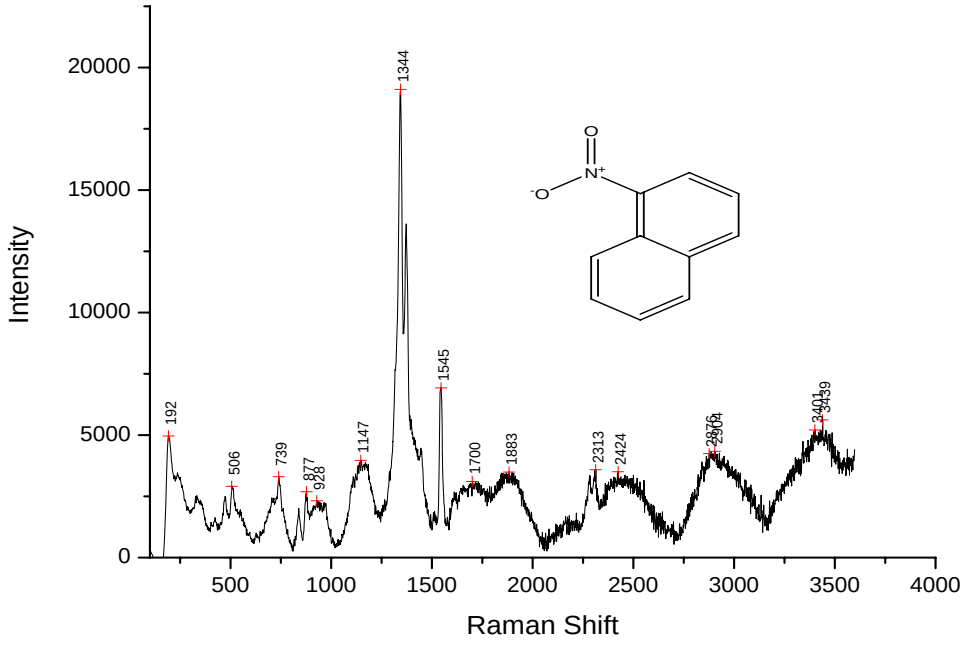

Figure A–37. Raman Spectrum of n-Nitronaphthalene-d7

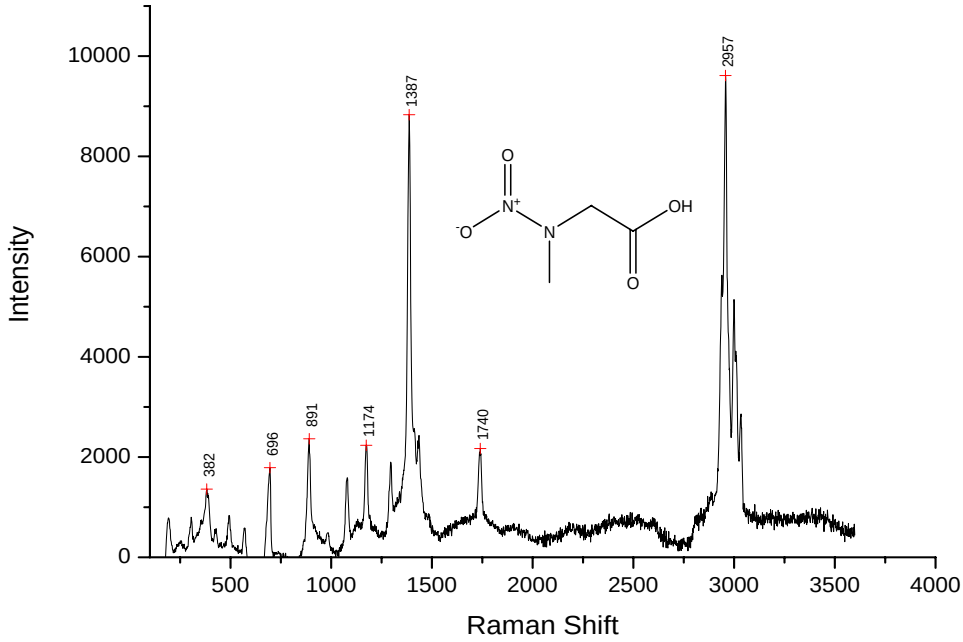

Figure A–38. Raman Spectrum of n-Nitrosarcosine

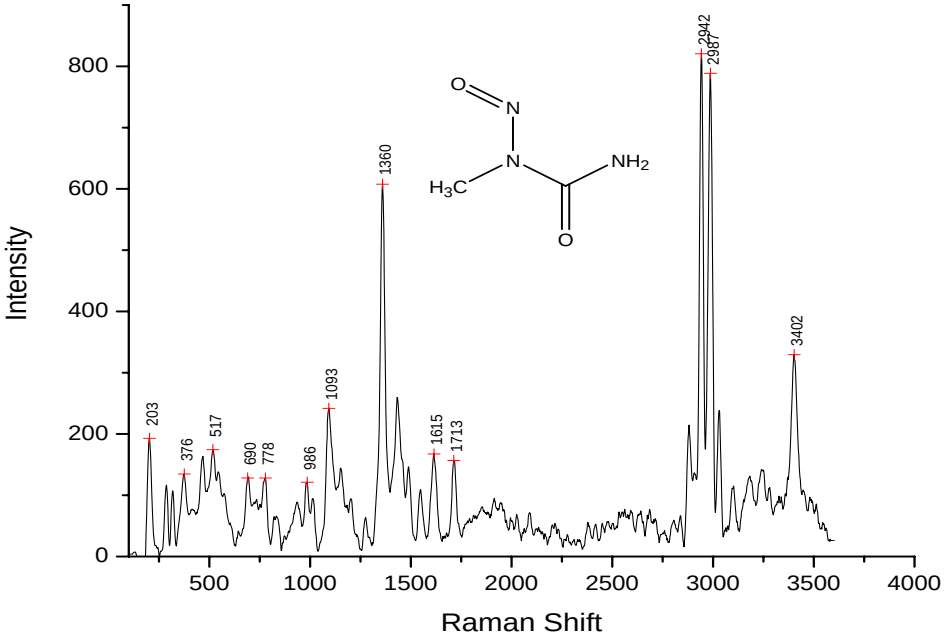

Figure A–39. Raman Spectrum of n-Nitroso-n-Ethylurea

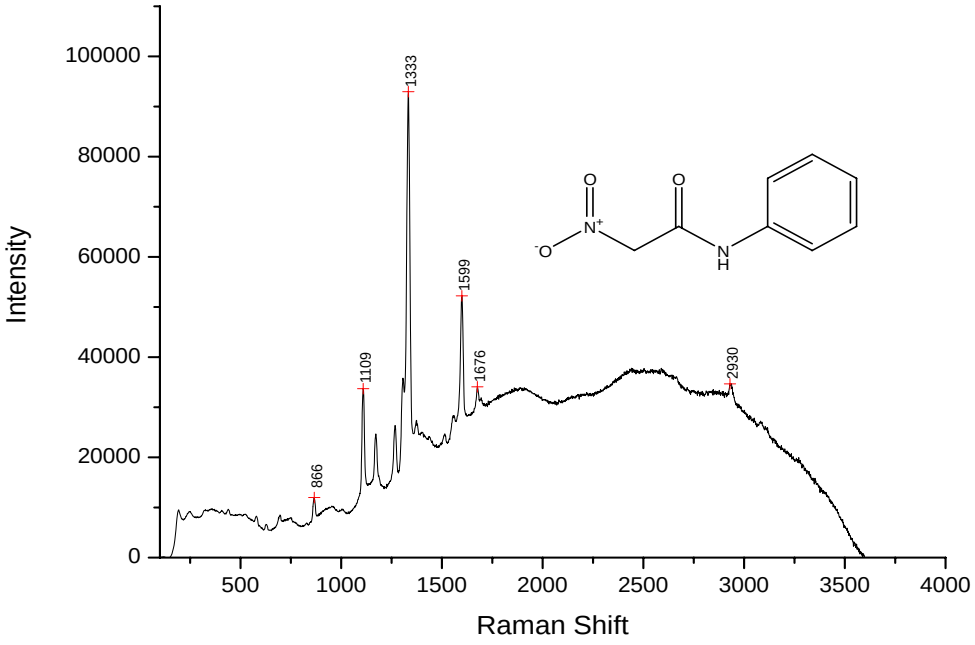

Figure A–40. Raman Spectrum of Nitroacetanilide

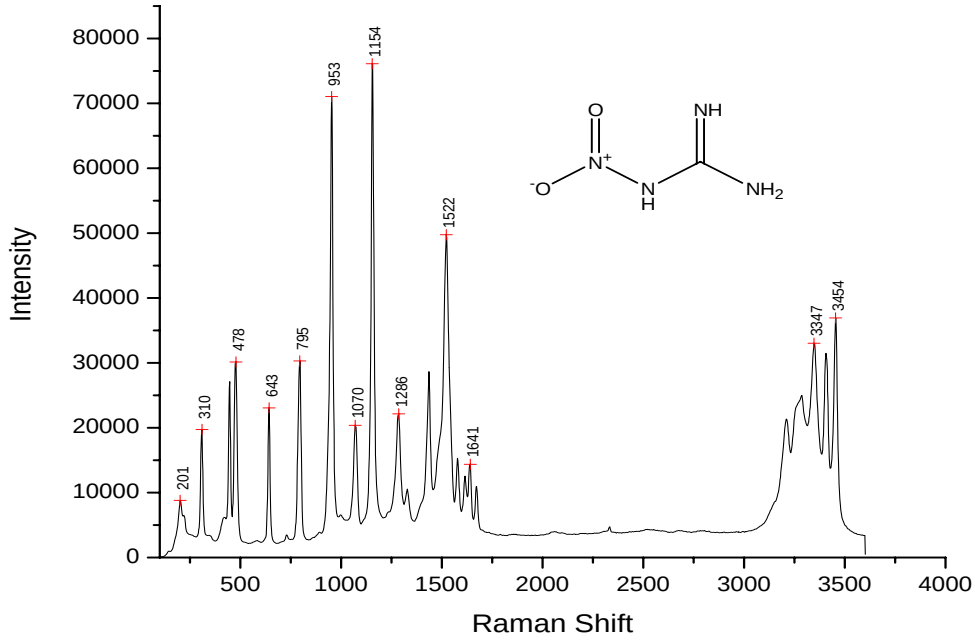

Figure A–41. Raman Spectrum of nitroguanidine

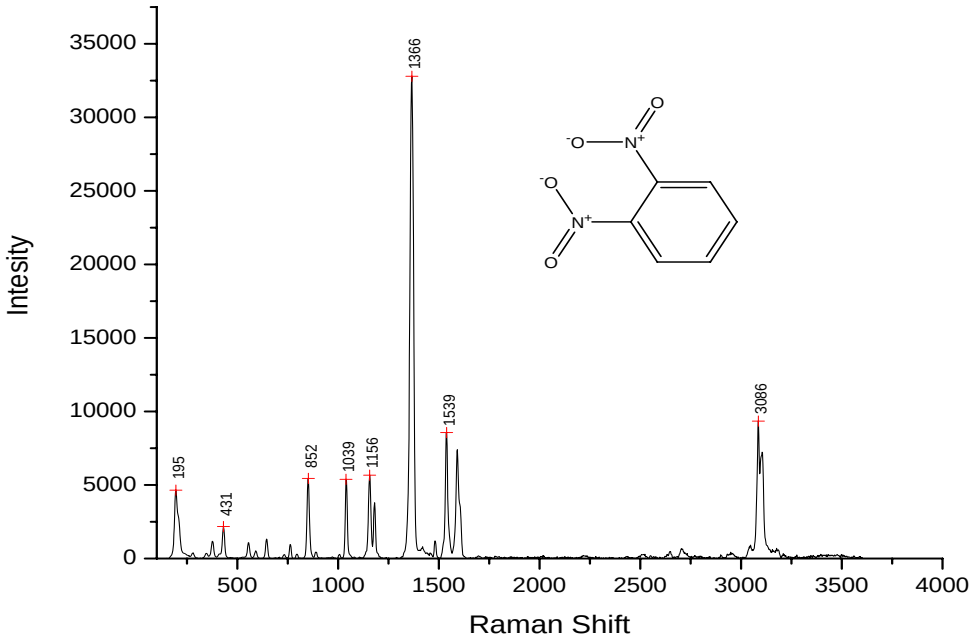

Figure A–42. Raman Spectrum of o-Dinitrobenzene

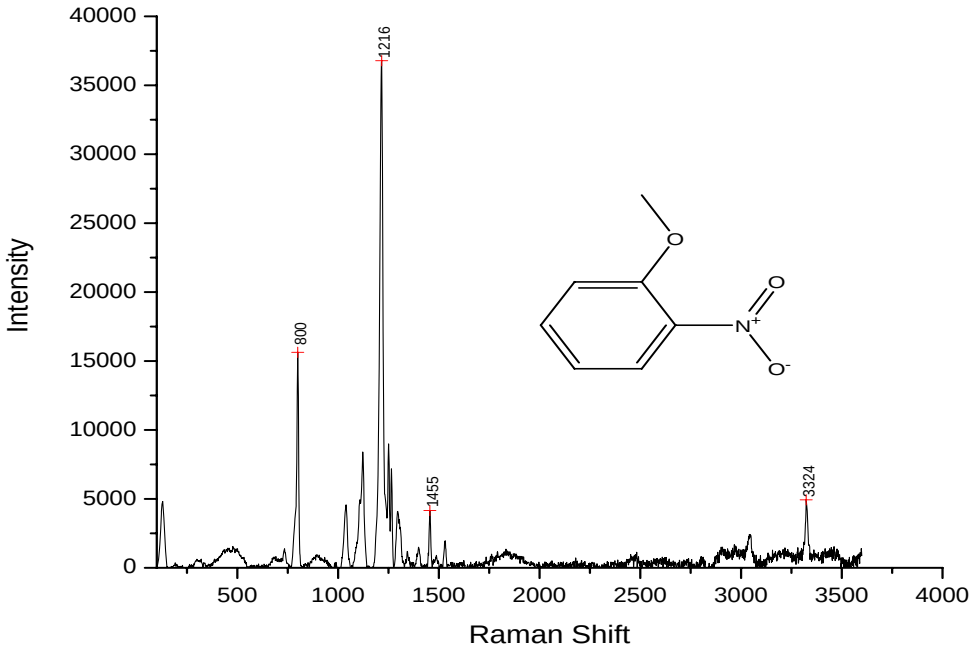

Figure A–43. Raman Spectrum of o-Nitroanisole

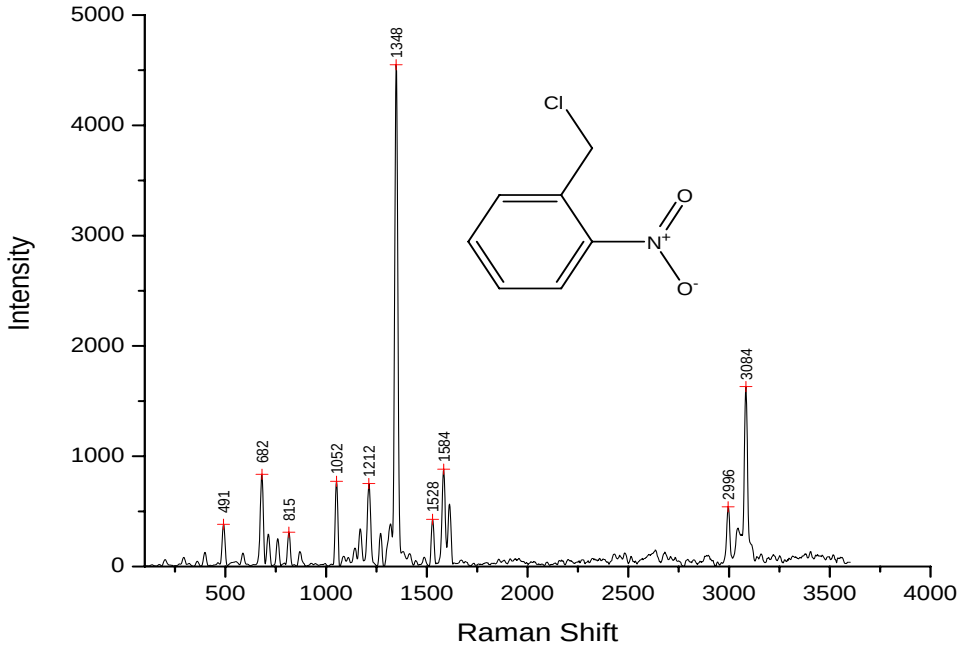

Figure A–44. Raman Spectrum of o-Nitrobenzyl Chloride

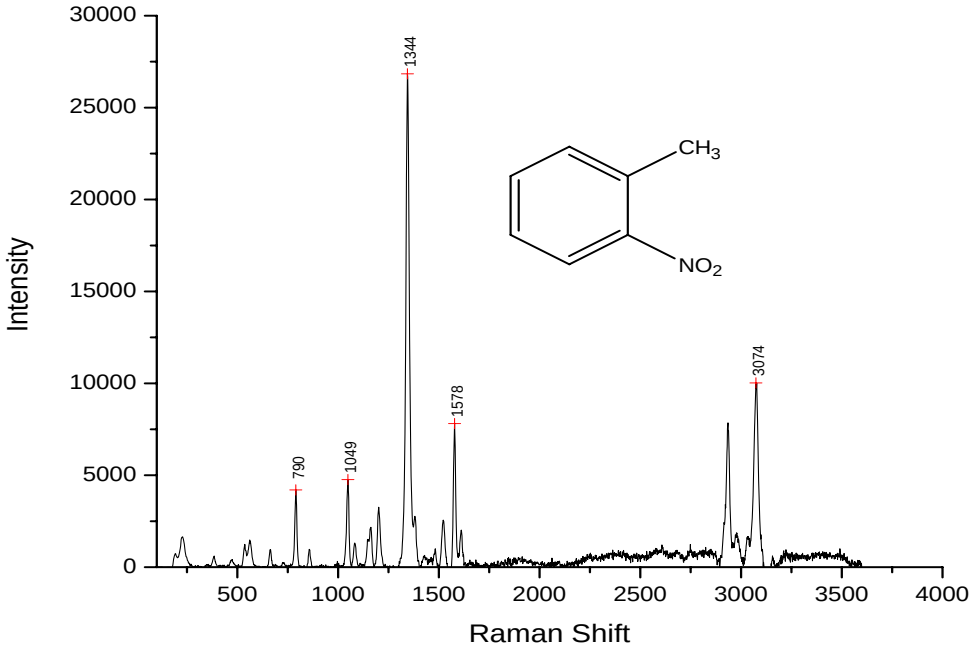

Figure A–45. Raman Spectrum of o-Nitrotoluene

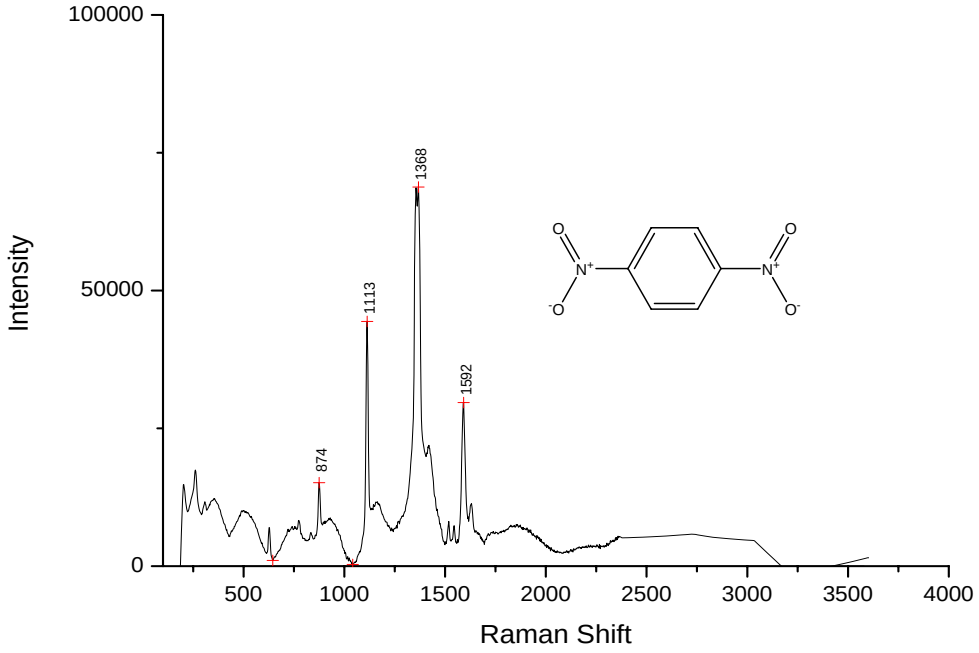

Figure A–46. Raman Spectrum of p-Dinitrobenzene

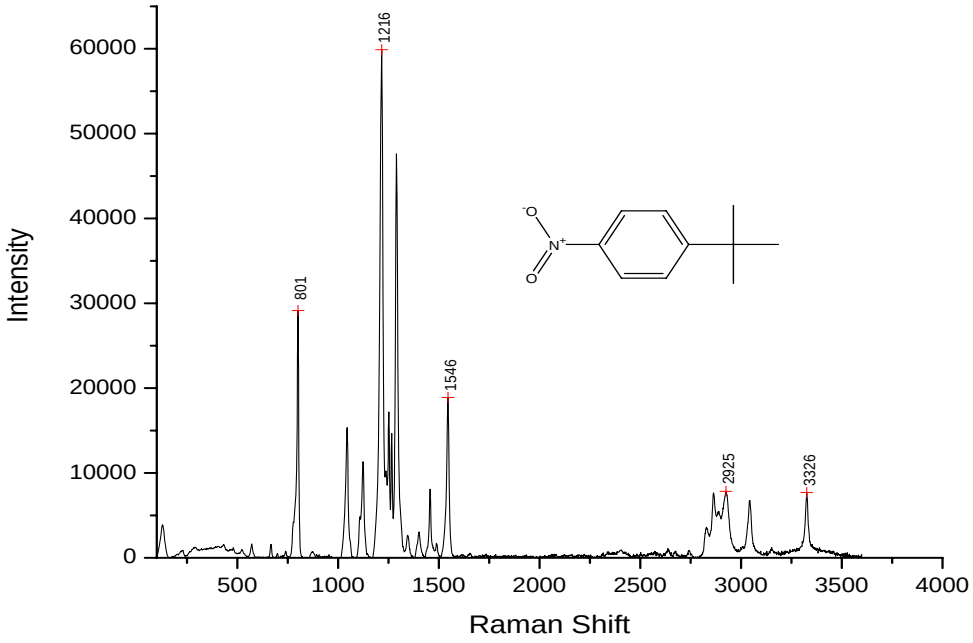

Figure A–47. Raman Spectrum of p-Nitro-Tert-Butylbenzene

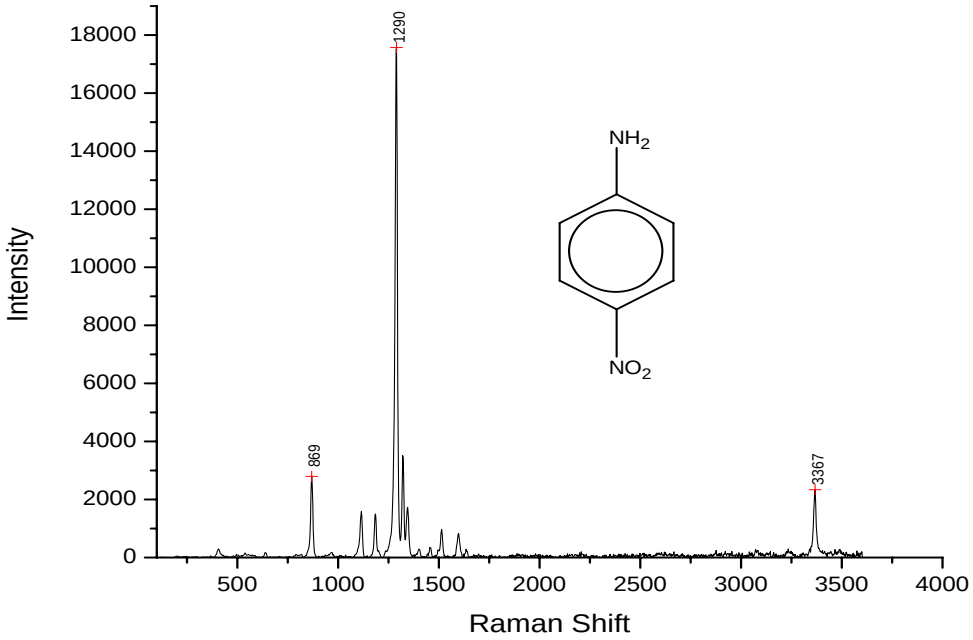

Figure A–48. Raman Spectrum of p-nitroaniline

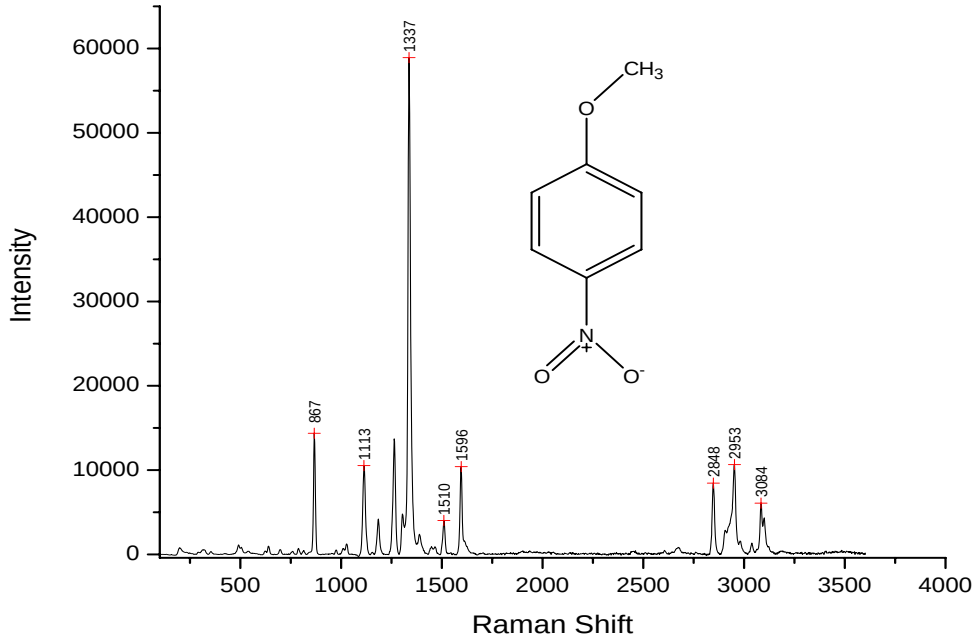

Figure A–49. Raman Spectrum of p-Nitroanisole

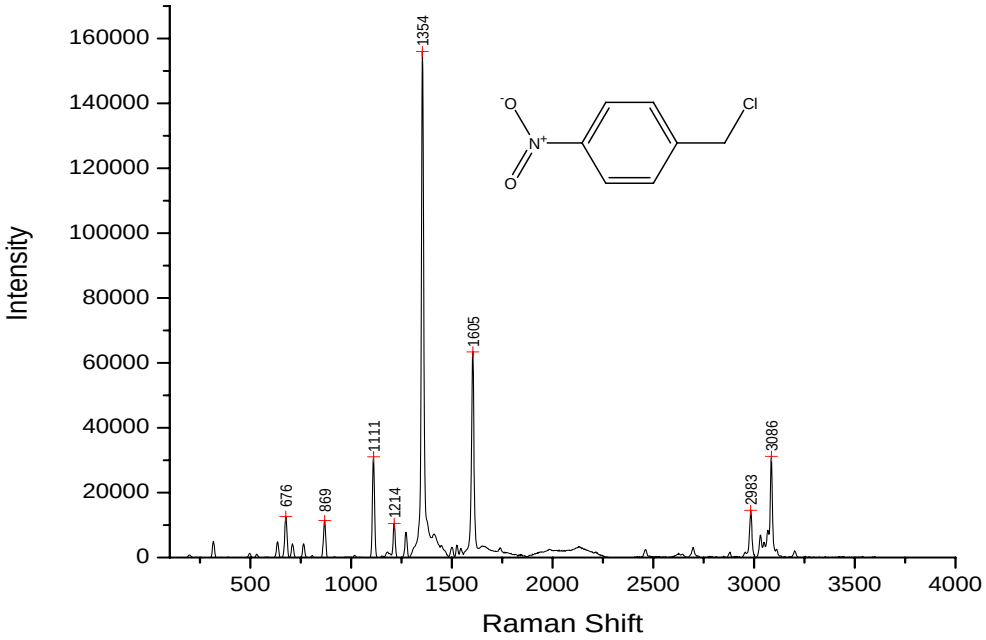

Figure A–50. Raman Spectrum of p-Nitrobenzyl Chloride

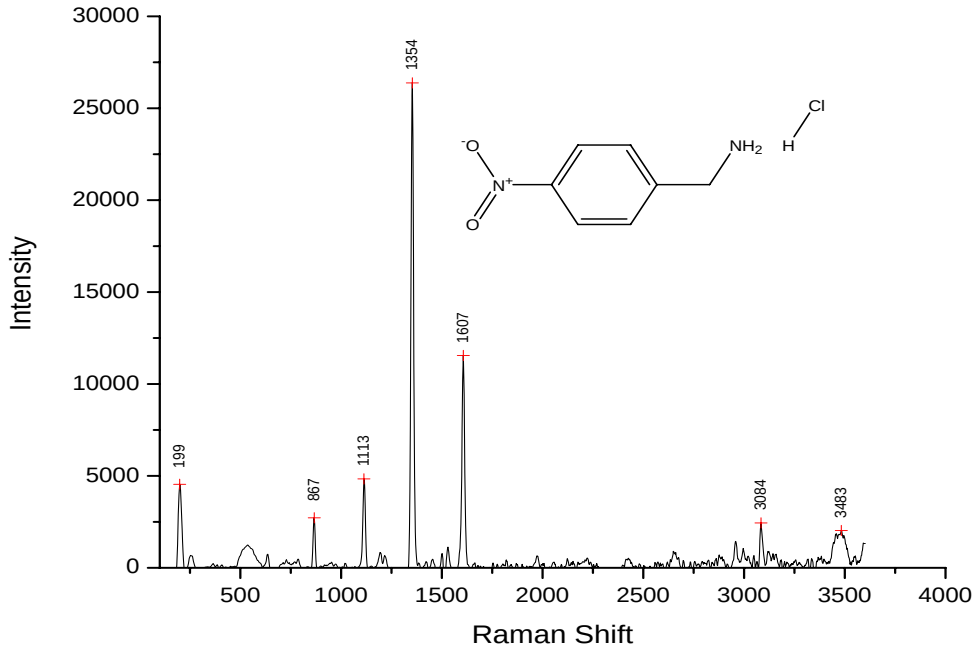

Figure A–51. Raman Spectrum of p-Nitrobenzyl Hydrochloride

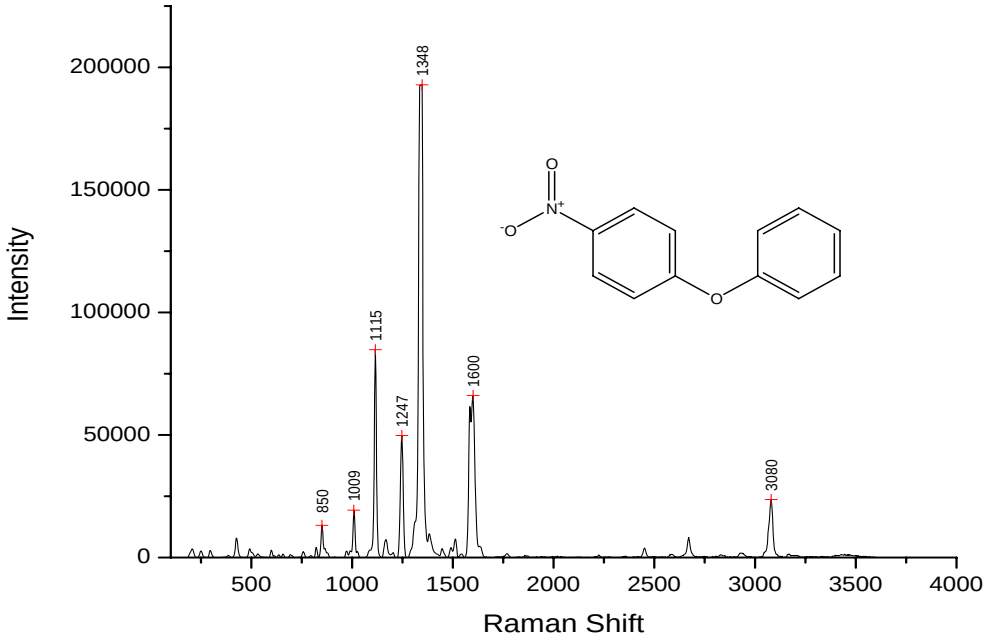

Figure A–52. Raman Spectrum of p-Nitrodiphenyl Ether

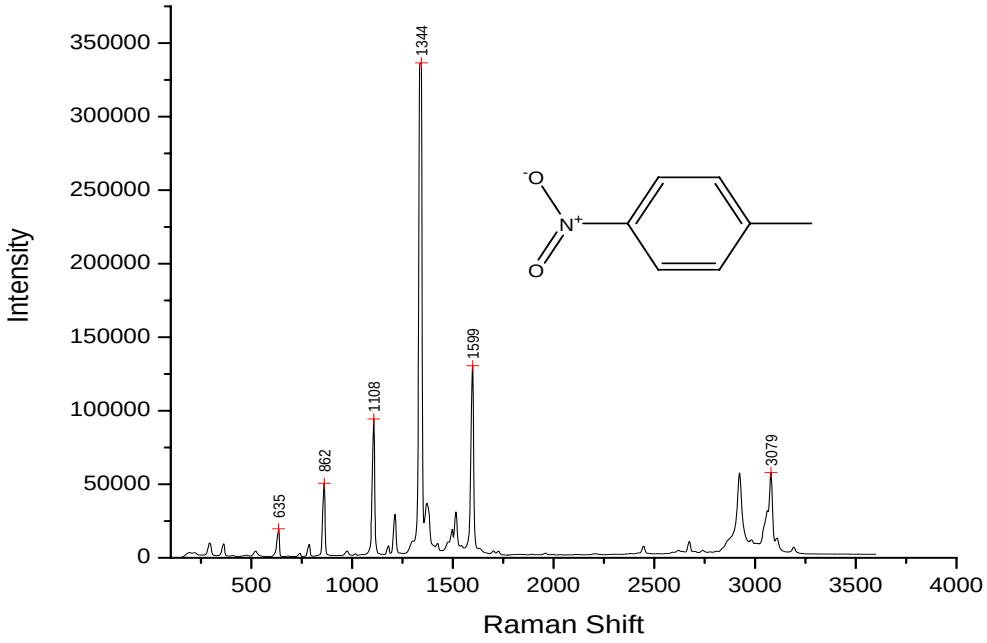

Figure A–53. Raman Spectrum of p-Nitrotoluene

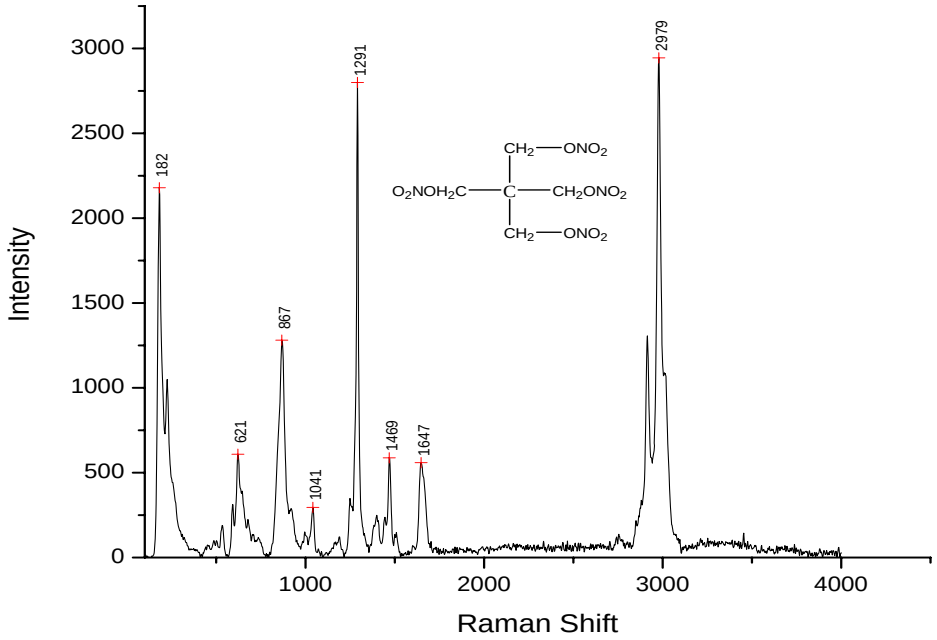

Figure A–54. Raman Spectrum of Pentaerytritoltetranitrate

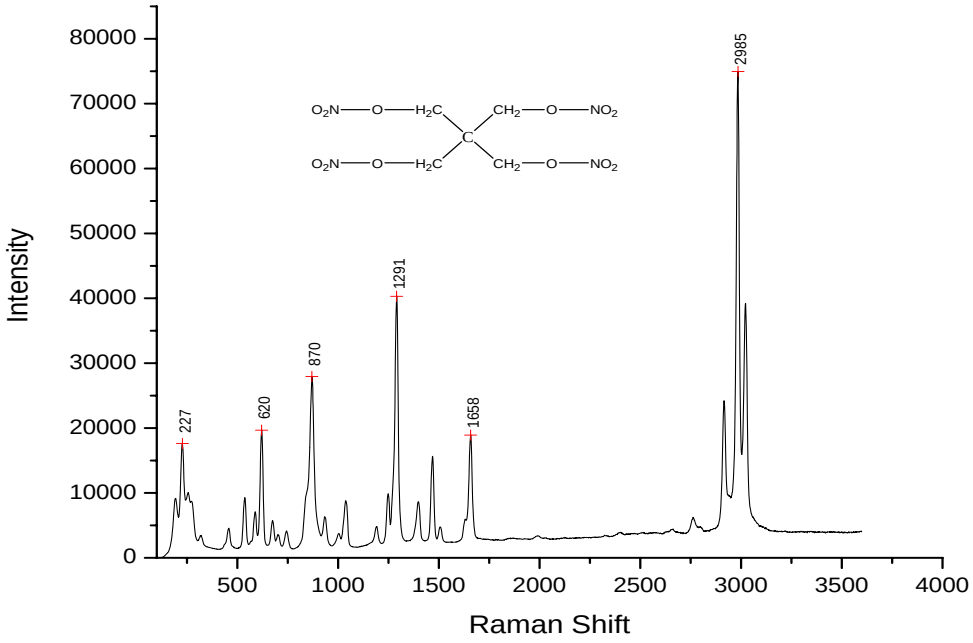

Figure A–55. Raman Spectrum of PETN

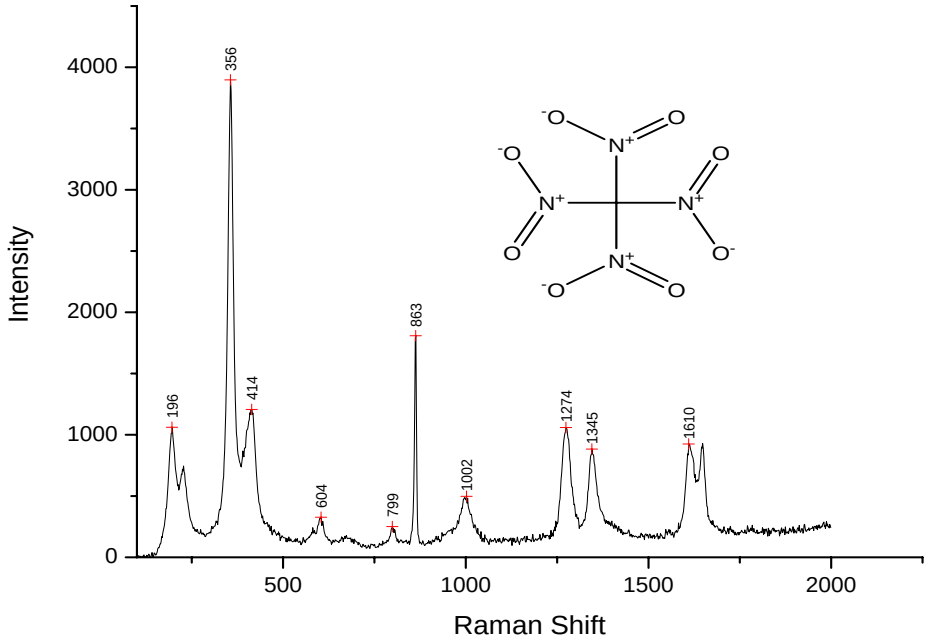

Figure A–56. Raman Spectrum of Tetranitromethane

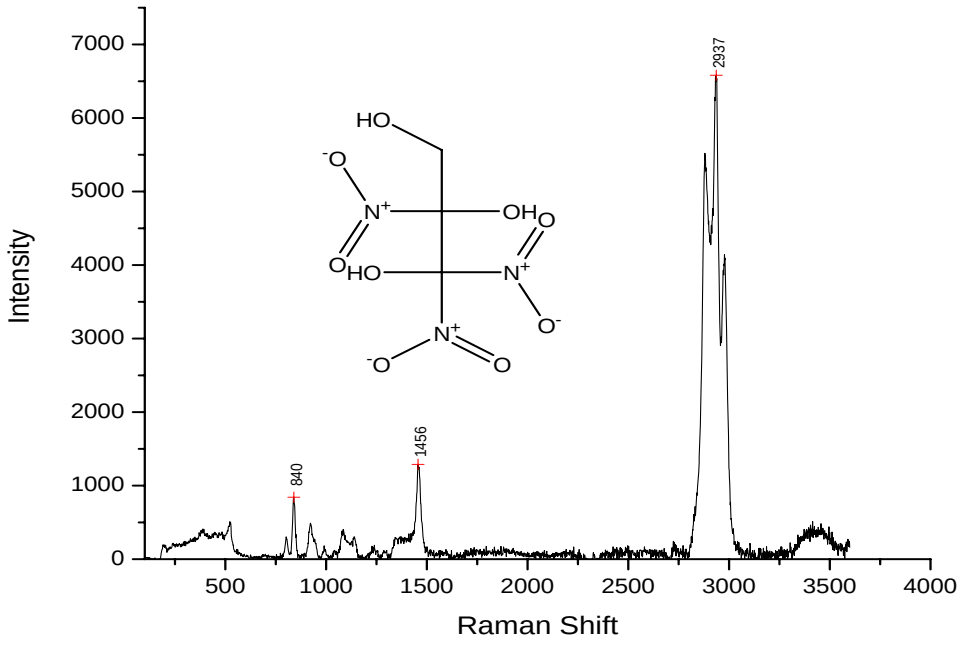

Figure A–57. Raman Spectrum of Tirnitroglycerine

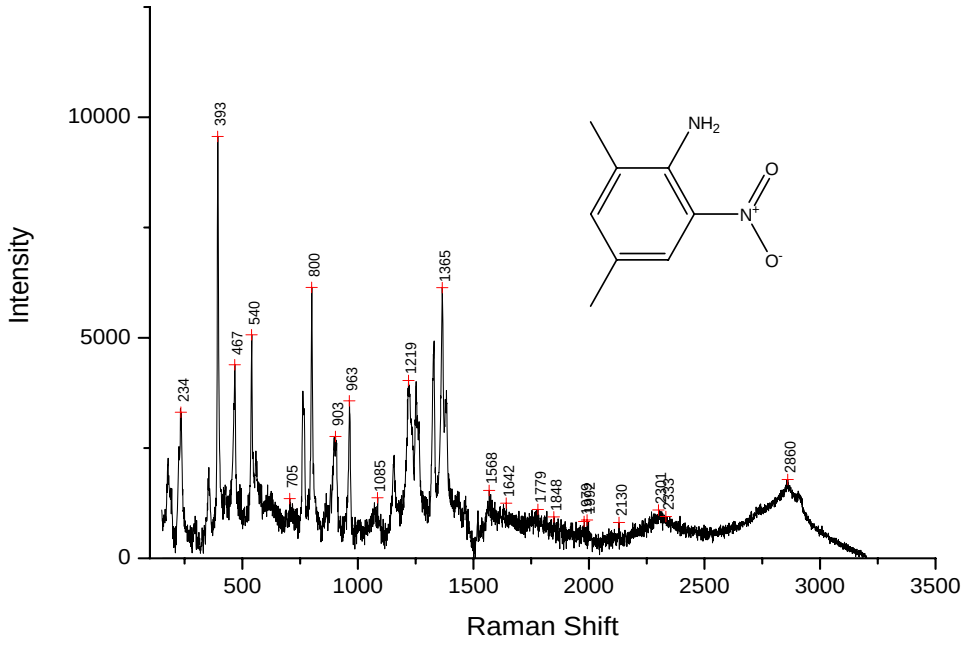

Figure A–58. Raman Spectrum of 5-Nitro-4-Amino-1,3-Dimethylbenzene

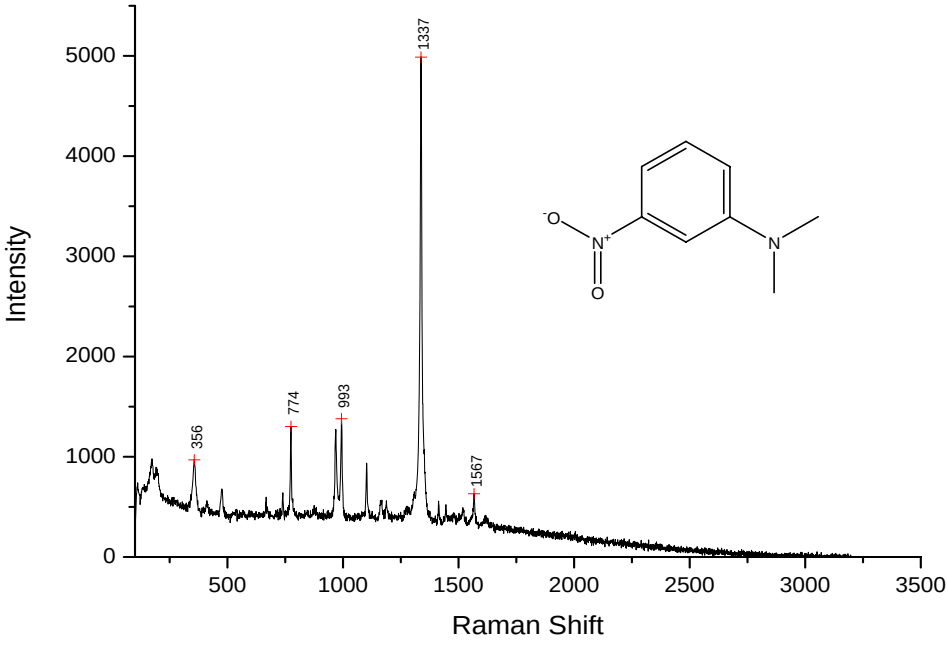

Figure A–59. Raman Spectrum of m-Nitrodimethylaniline

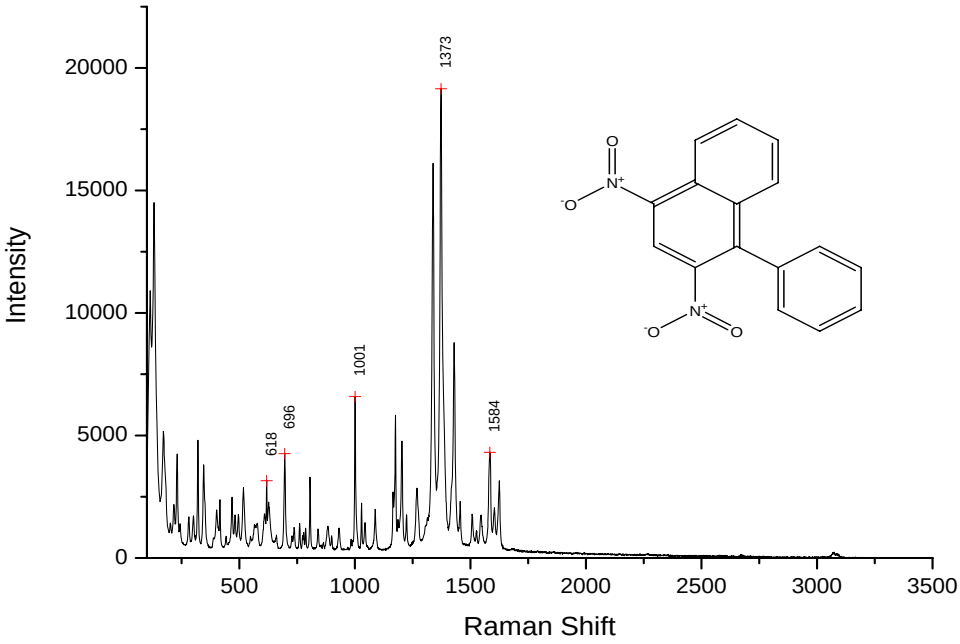

Figure A–60. Raman Spectrum of N-(2,4-Dinitro-1-Naphthyl)-Benzene

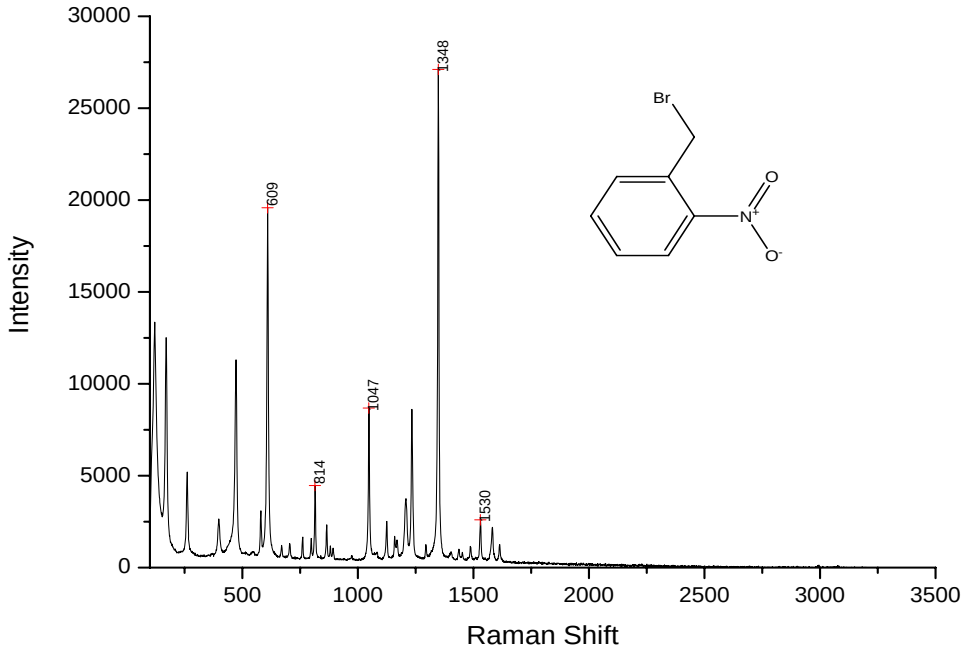

Figure A–61. Raman Spectrum of o-nitrobenzyl bromide

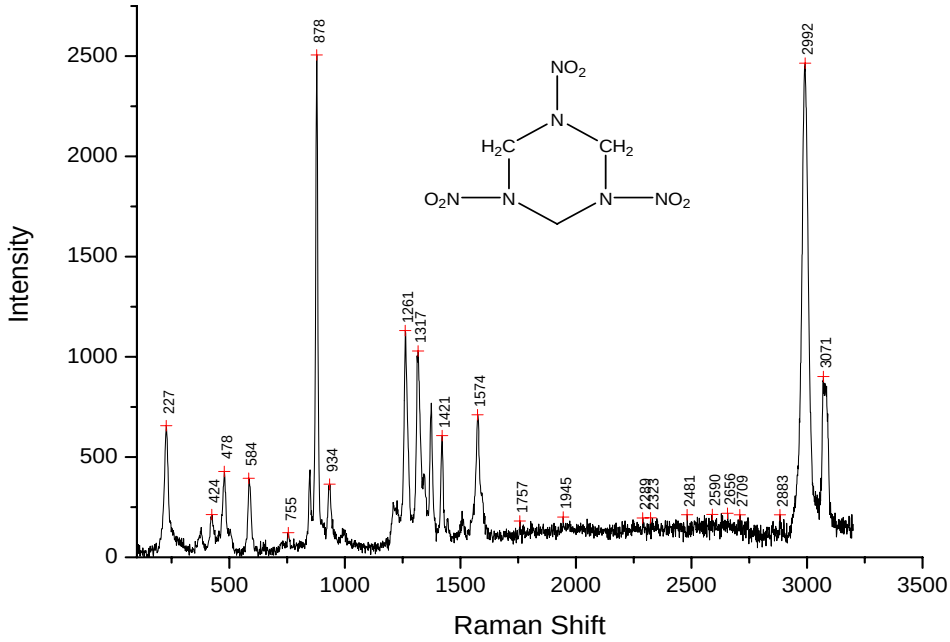

Figure A–62. Raman Spectrum of RDX

APPENDIX B
INFRARED SPECTRA

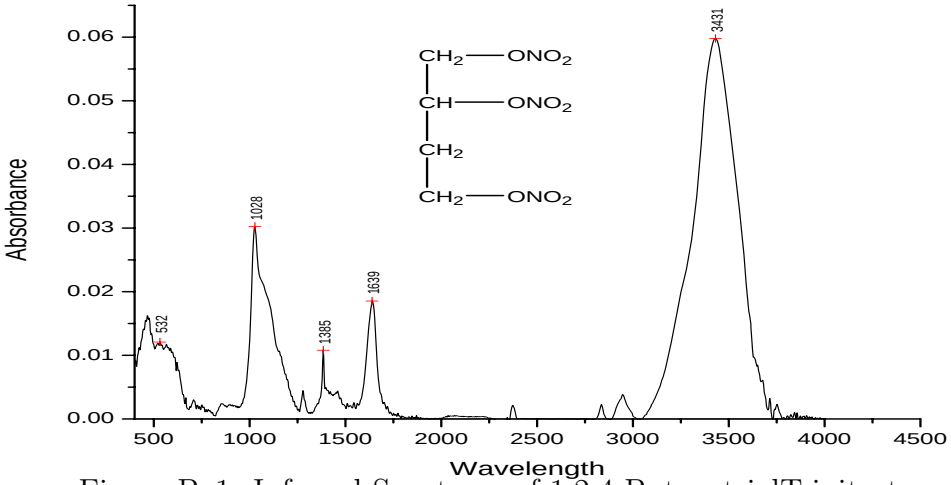

Figure B–1. Infrared Spectrum of 1,2,4-ButanetriolTrinitrate

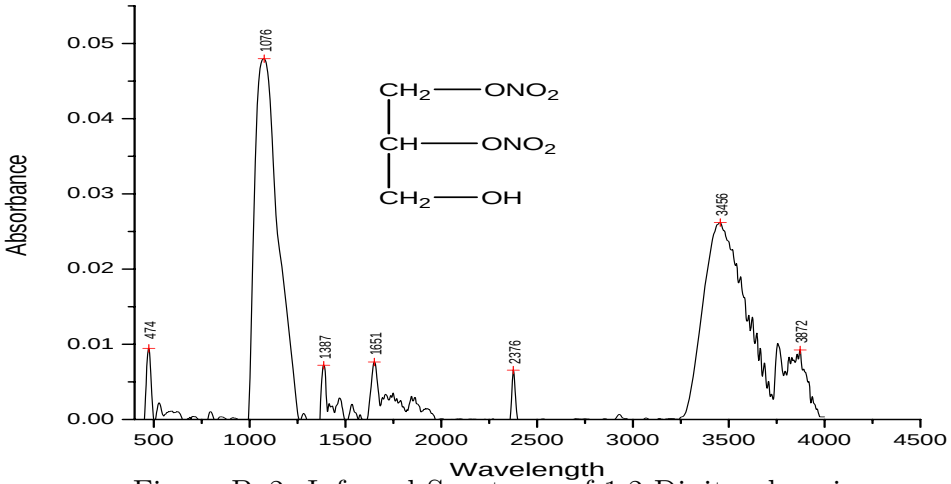

Figure B–2. Infrared Spectrum of 1,2-Dinitroglycerin

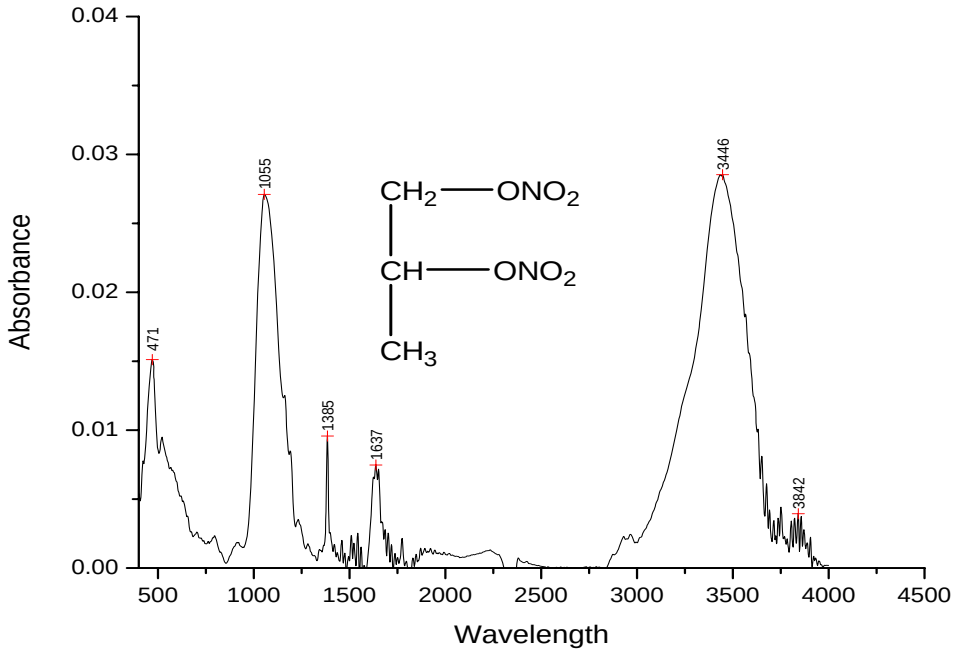

Figure B–3. Infrared Spectrum of 1,2-Pentanediol Dinitrate

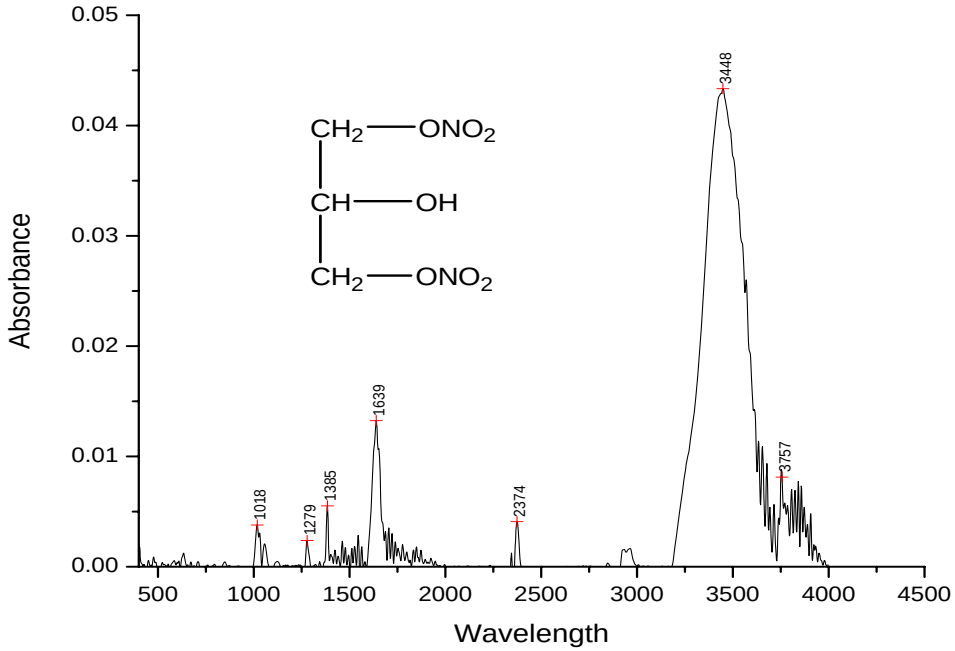

Figure B–4. Infrared Spectrum of 1,3-Dinitroglycerin

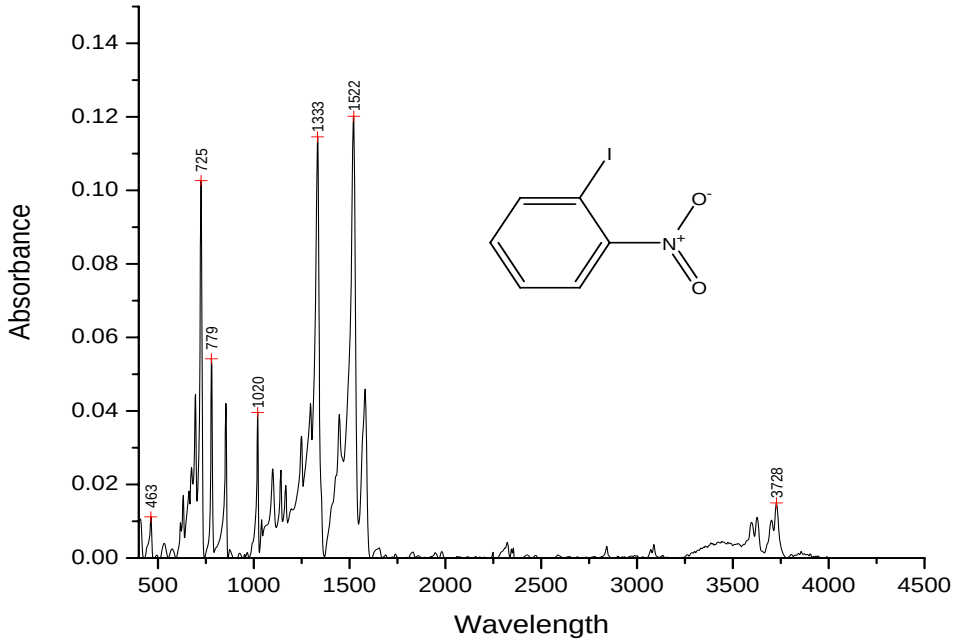

Figure B–5. Infrared Spectrum of 1-Iodo-2-Nitrobenzene

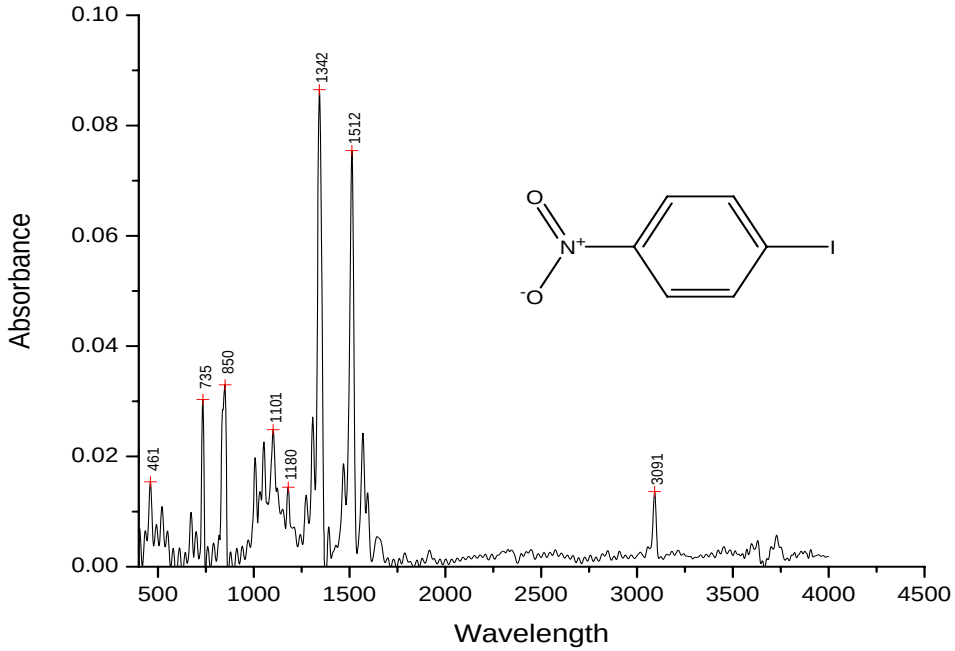

Figure B–6. Infrared Spectrum of 1-Iodo-4-Nitrobenzene

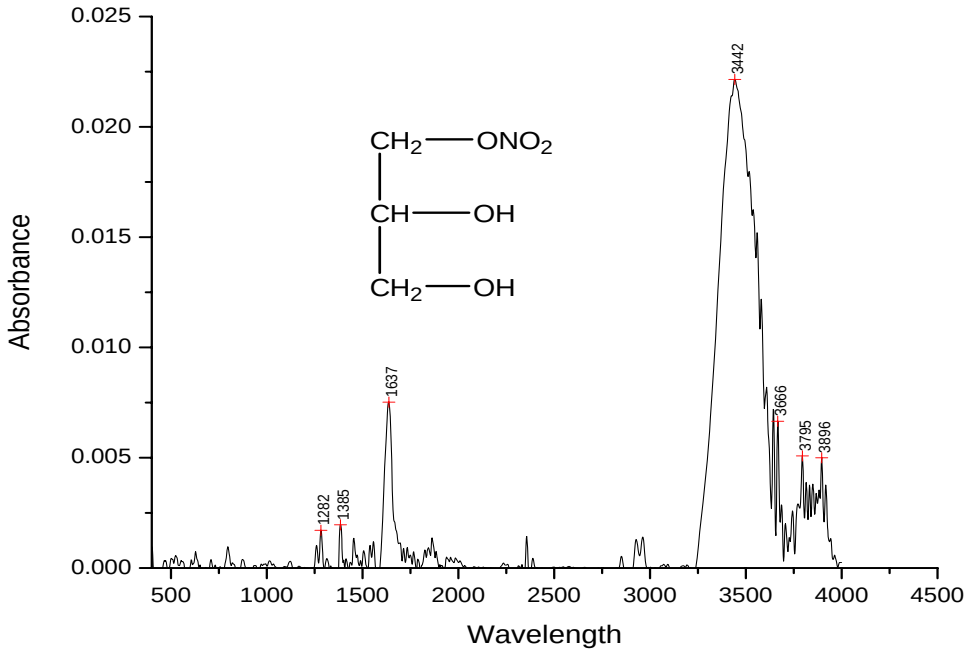

Figure B–7. Infrared Spectrum of 1-Mononitroglycerin

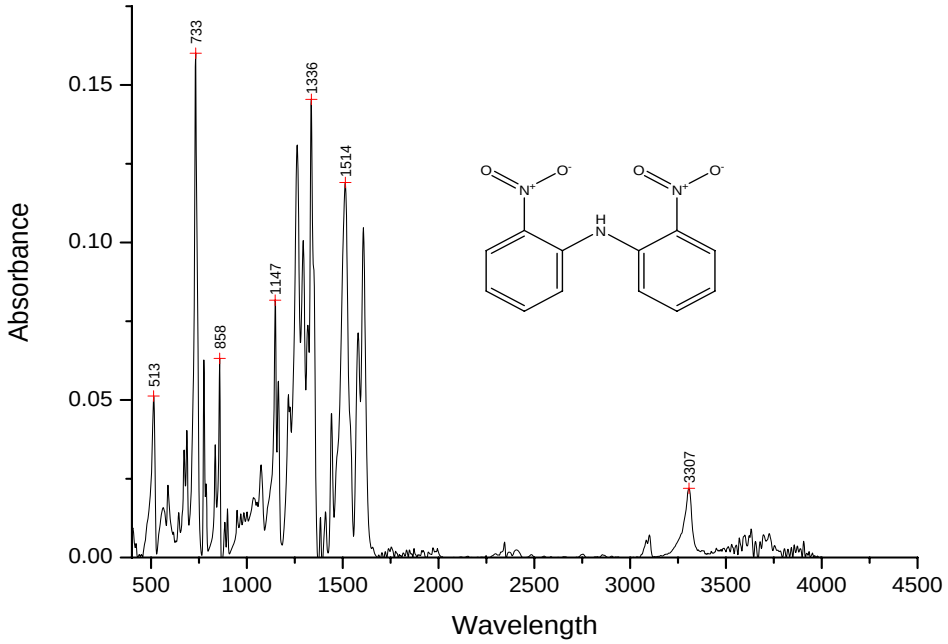

Figure B–8. Infrared Spectrum of 2,2-Dinitrodiphenylamine

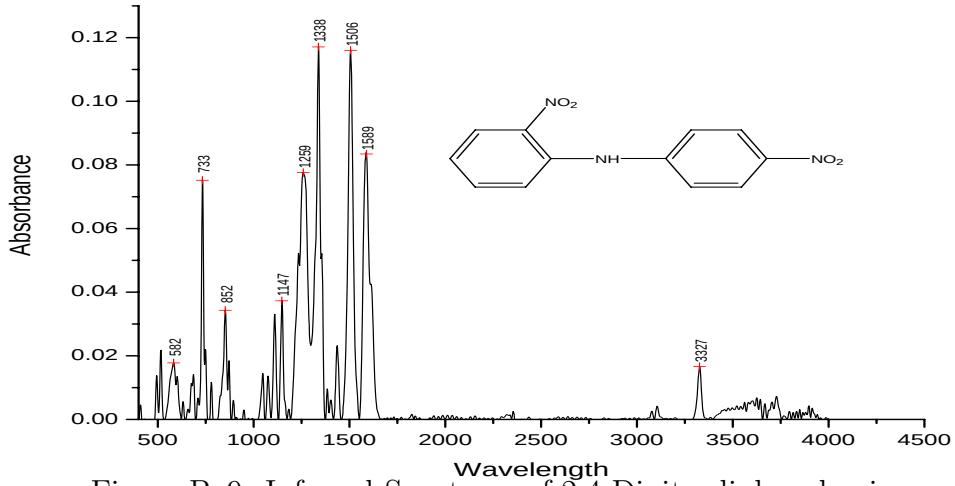

Figure B–9. Infrared Spectrum of 2,4-Dinitrodiphenylamine

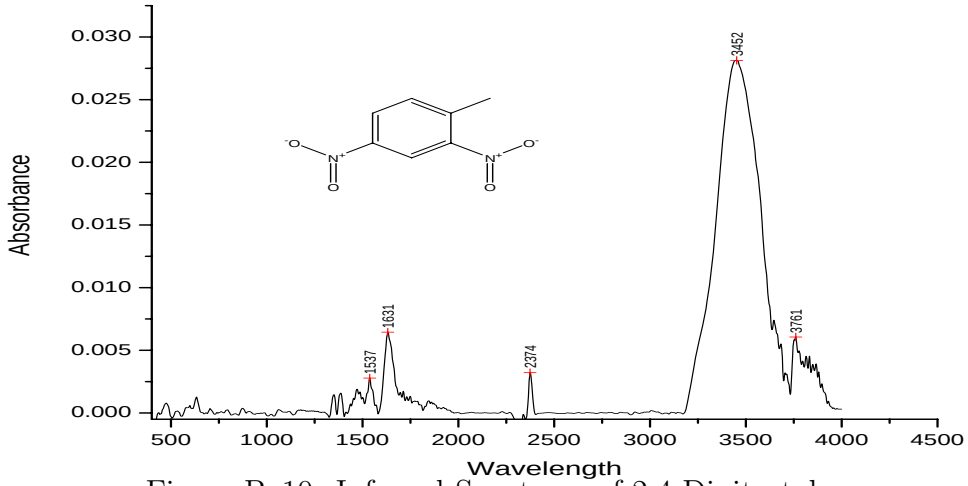

Figure B–10. Infrared Spectrum of 2,4-Dinitrotoluene

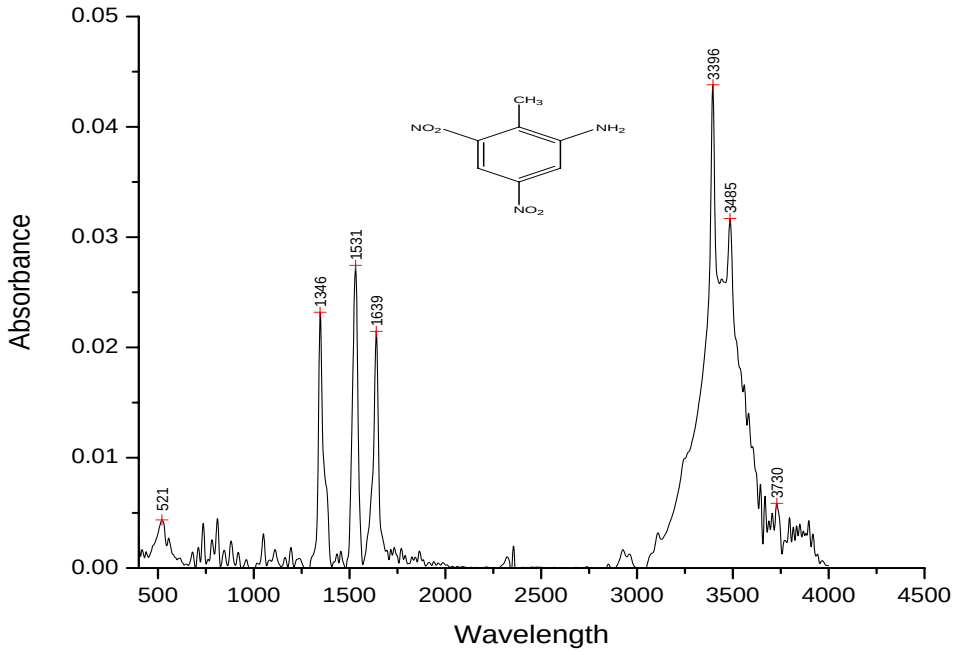

Figure B–11. Infrared Spectrum of 2-Amino-4,6-dinitrotoluene.

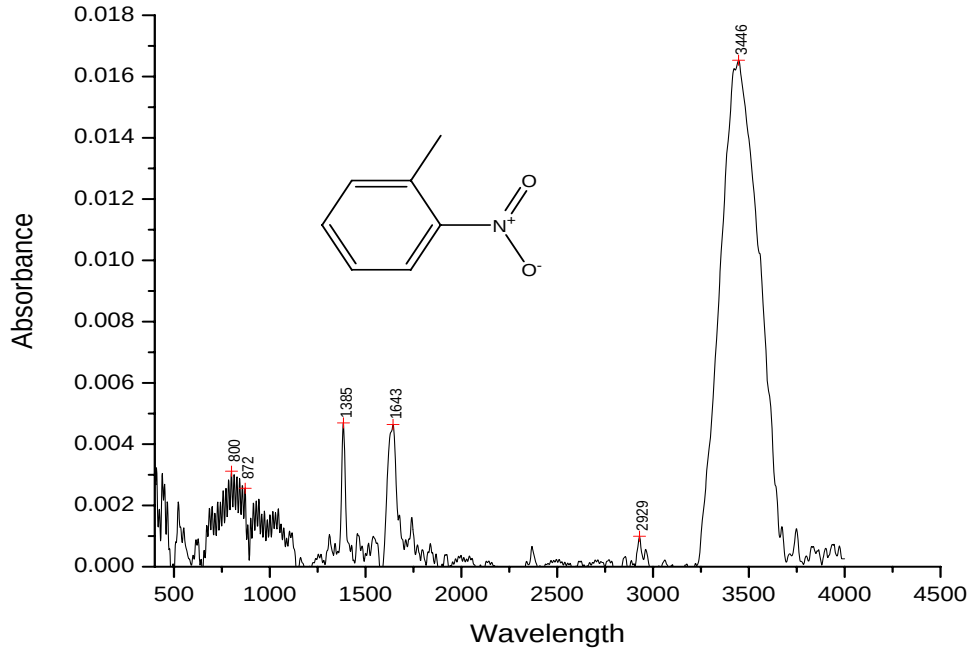

Figure B–12. Infrared Spectrum of 2-Nitrotoluene

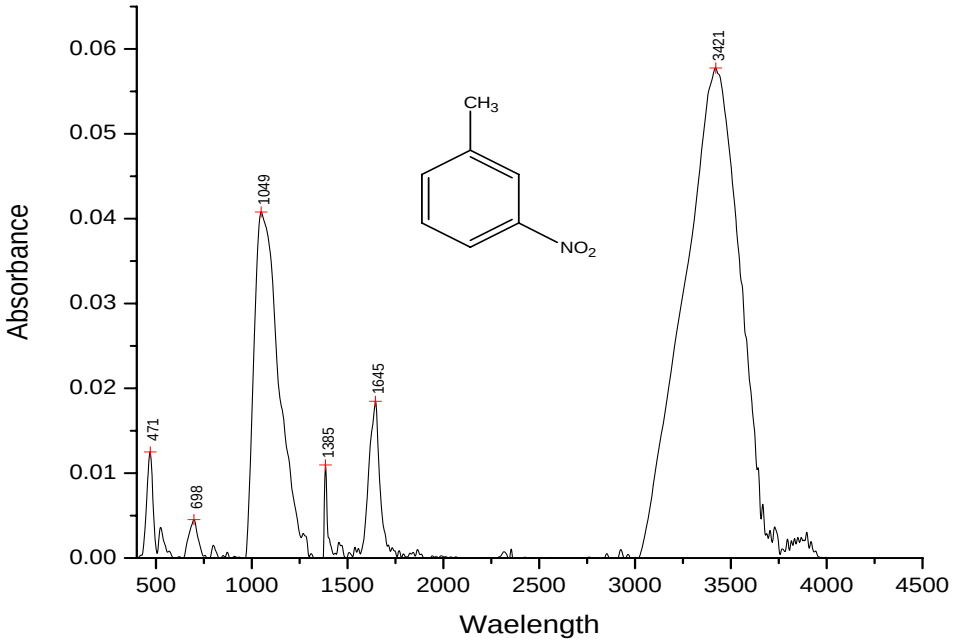

Figure B–13. Infrared Spectrum of 3-Nitrotoluene

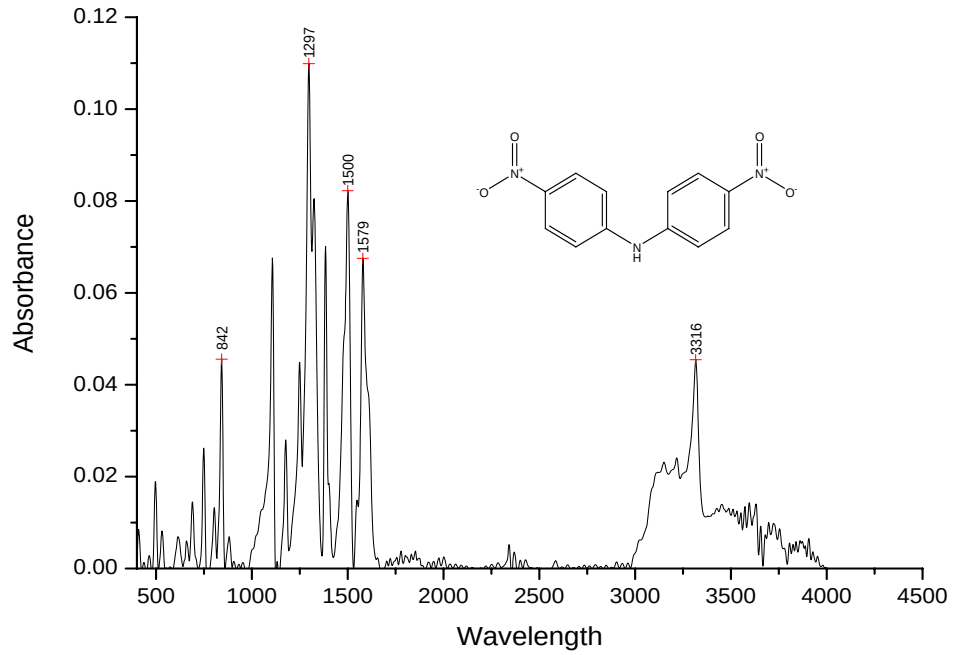

Figure B–14. Infrared Spectrum of 4,4-Dinitrodiphenylamine

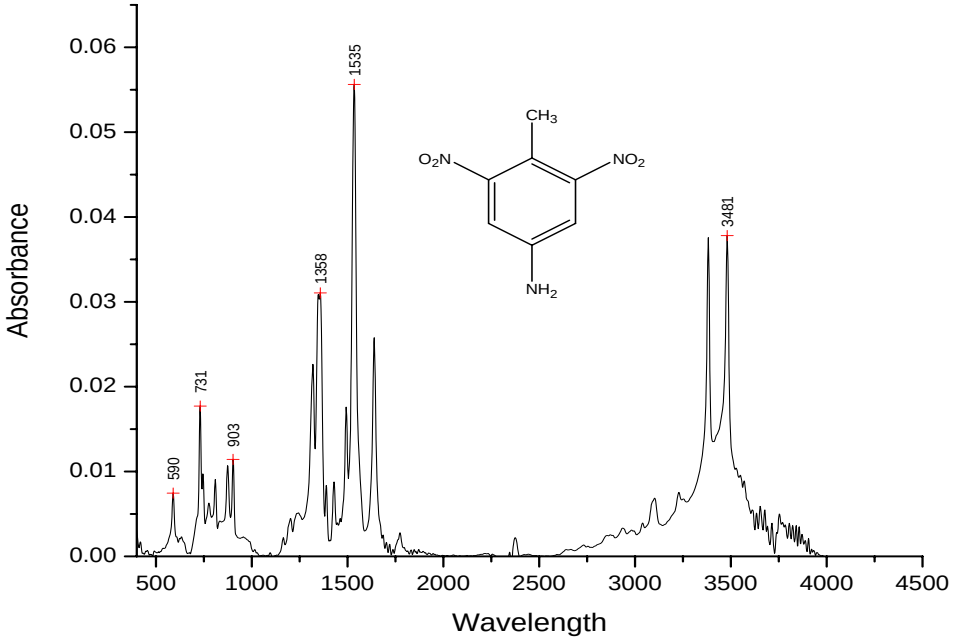

Figure B–15. Infrared Spectrum of 4-Amino-2,6-Dinitrotoluene

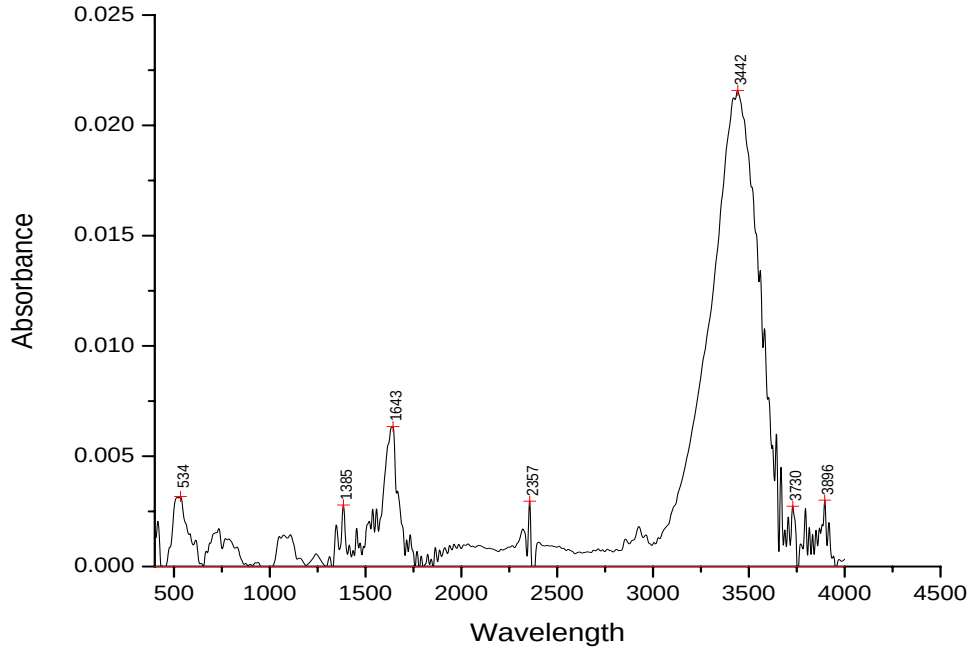

Figure B–16. Infrared Spectrum of 4-Nitrotoluene

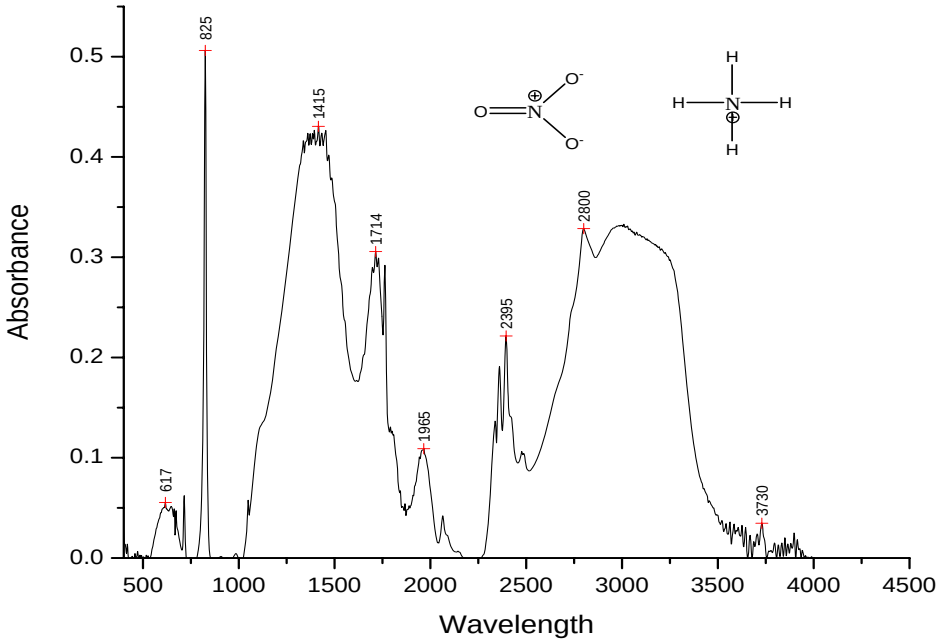

Figure B–17. Infrared Spectrum of Ammonium Nitrate

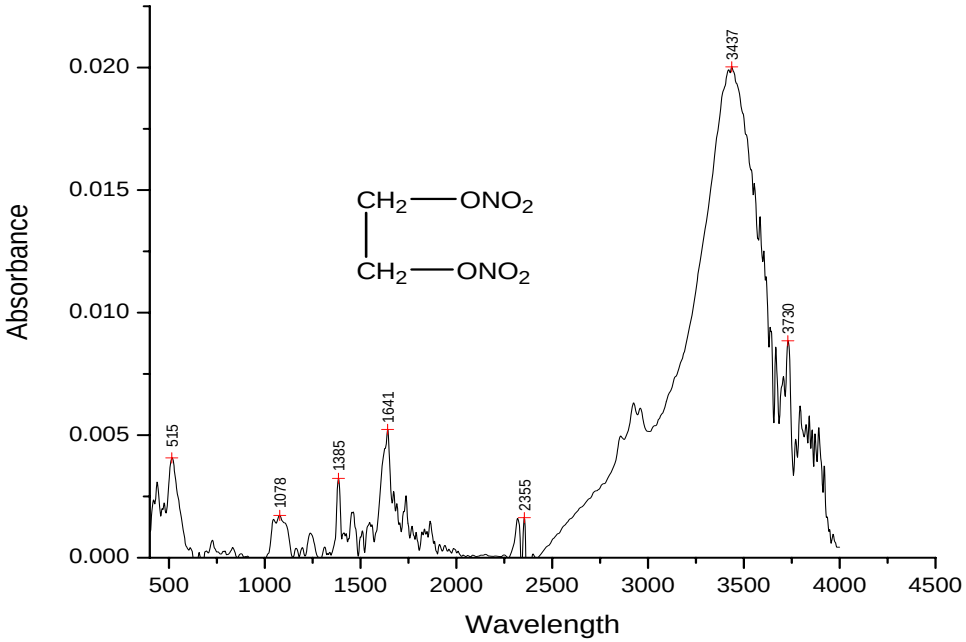

Figure B–18. Infrared Spectrum of Dinitroethylenglycol

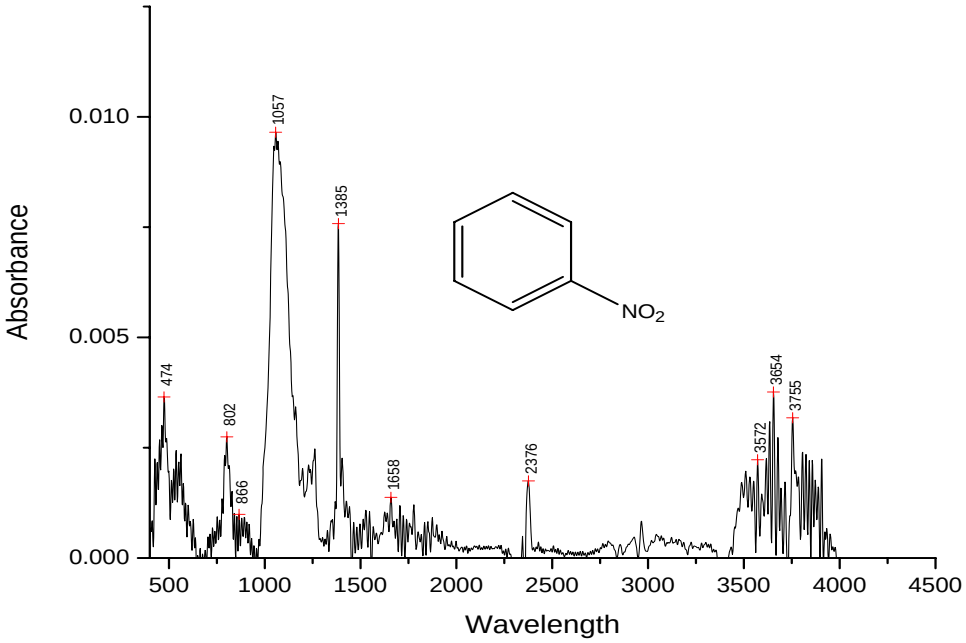

Figure B–19. Infrared Spectrum of Nitrobenzene

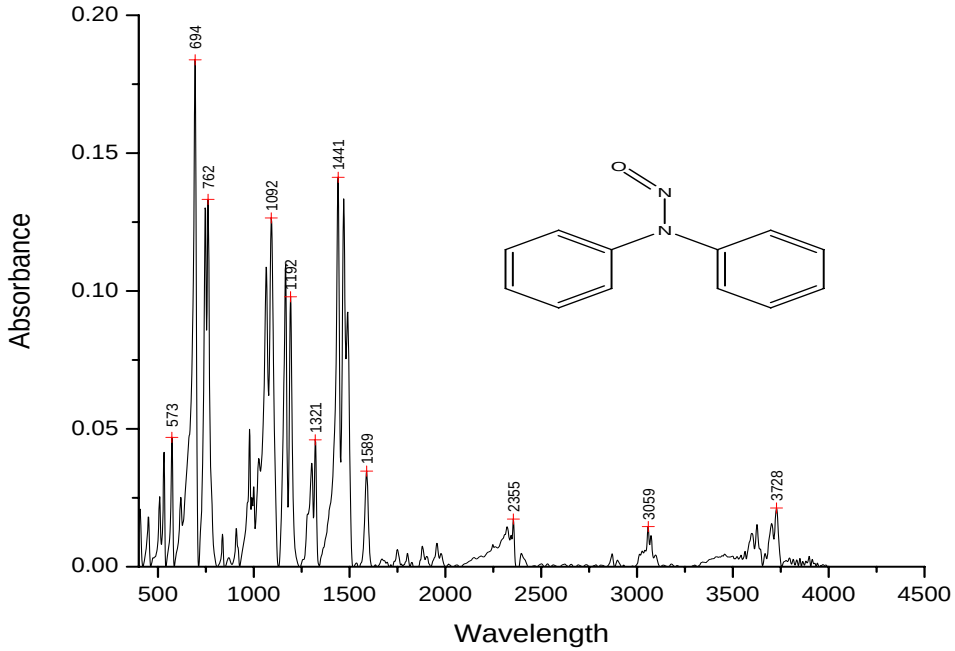

Figure B–20. Infrared Spectrum of N-Nitrosodiphenylamine

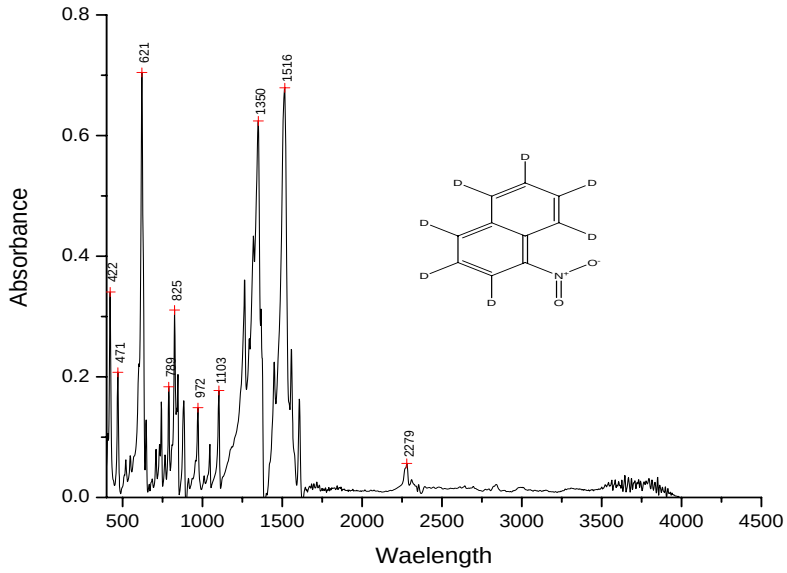

Figure B–21. Infrared Spectrum of 1-nitronaphtalene d-7

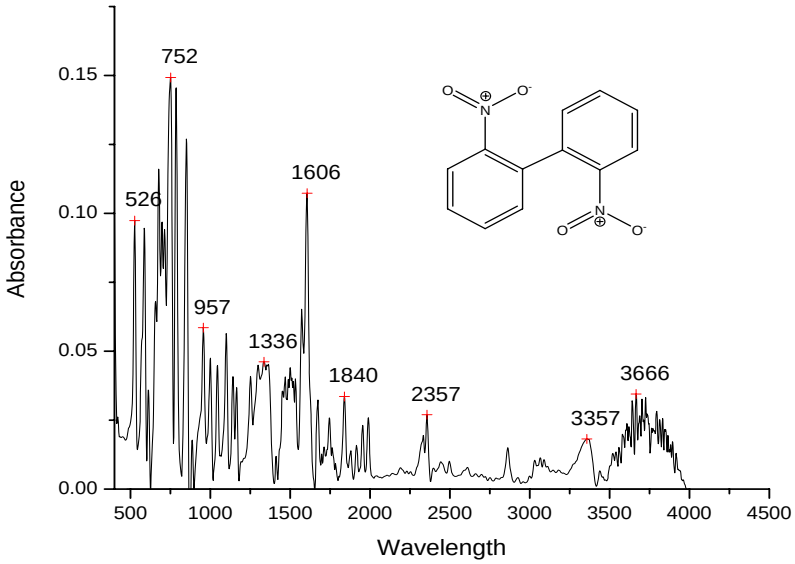

Figure B–22. Infrared Spectrum of 2,2-dinitrobiphenyl

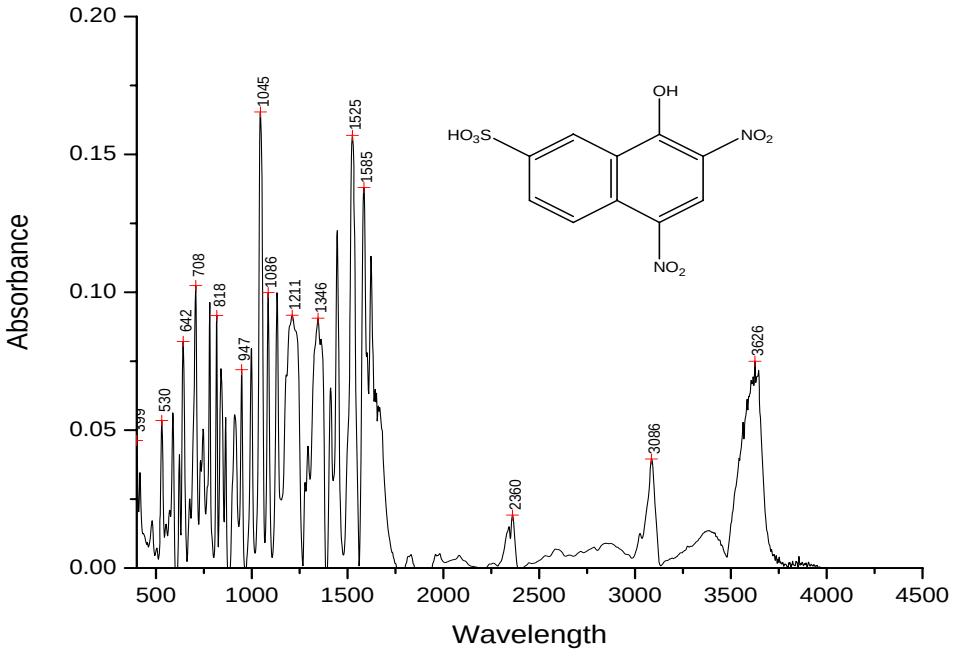

Figure B–23. Infrared Spectrum of 2,4-dinitro-1-naphtol-7-sulfonic acid

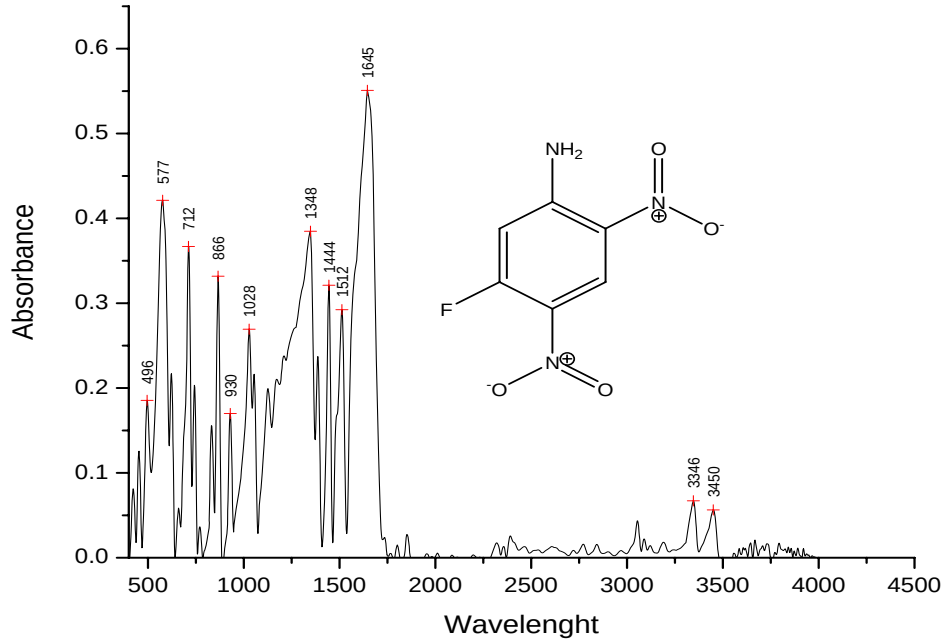

Figure B–24. Infrared Spectrum of 2,4-Dinitro-5-Fluoroaniline

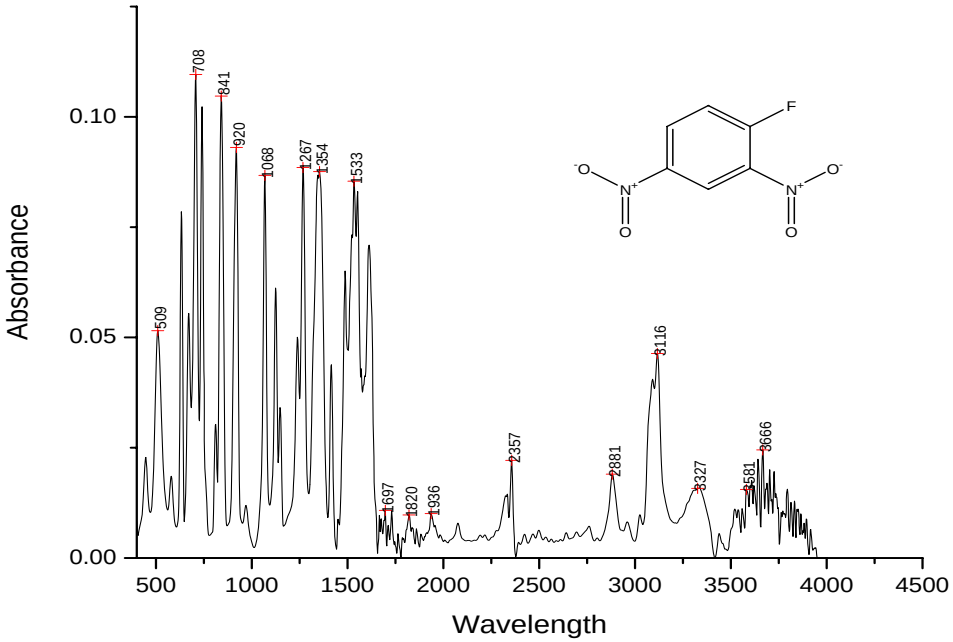

Figure B–25. Infrared Spectrum of 2,4-Dinitrofluorobenzene

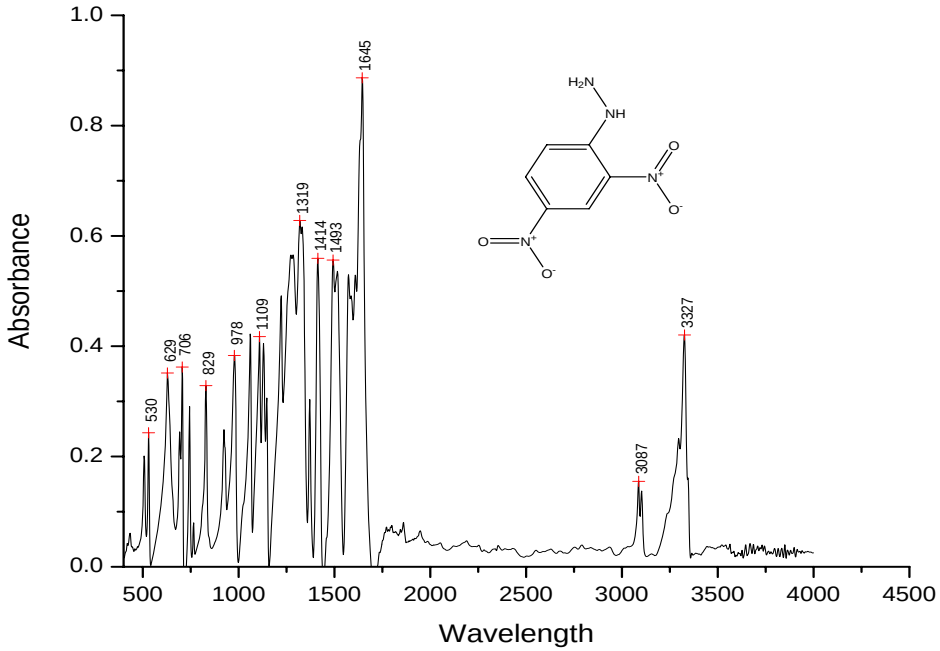

Figure B–26. Infrared Spectrum of 2,4-Dinitrophenylhydrazine

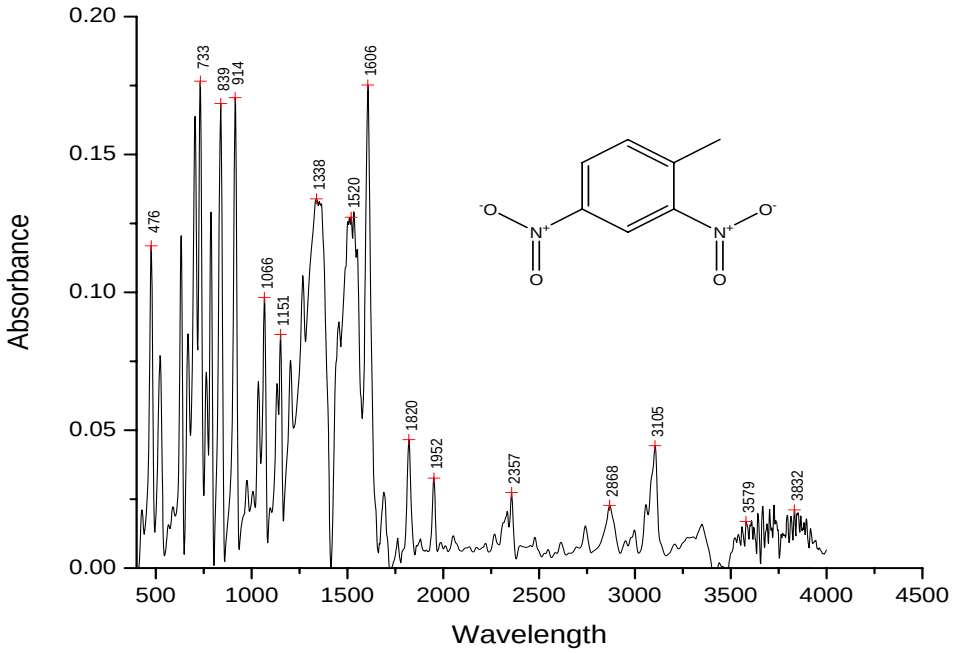

Figure B–27. Infrared Spectrum of 2,4-DNT

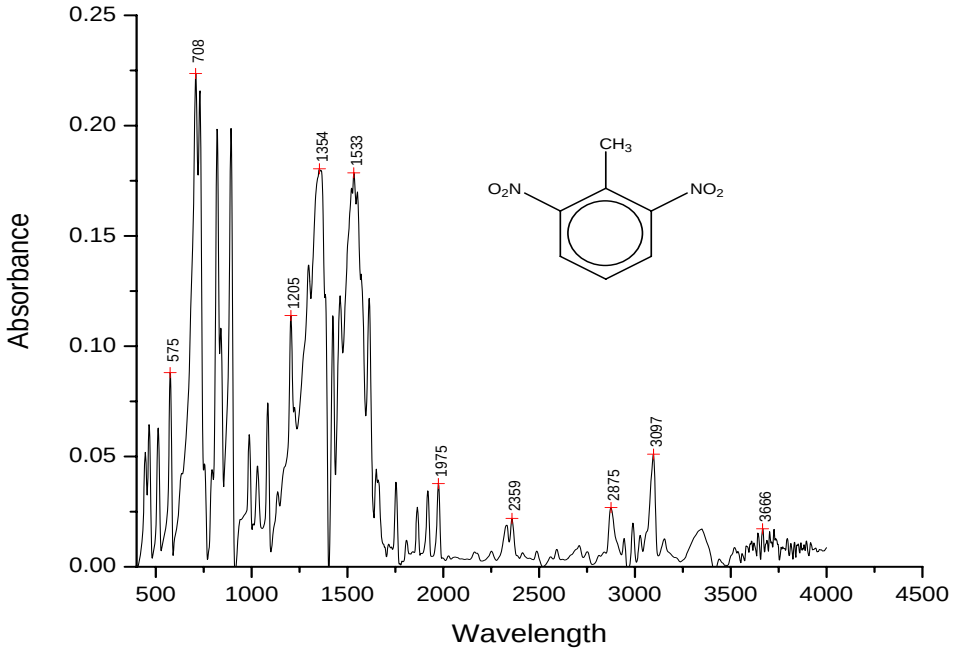

Figure B–28. Infrared Spectrum of 2,6-DNT

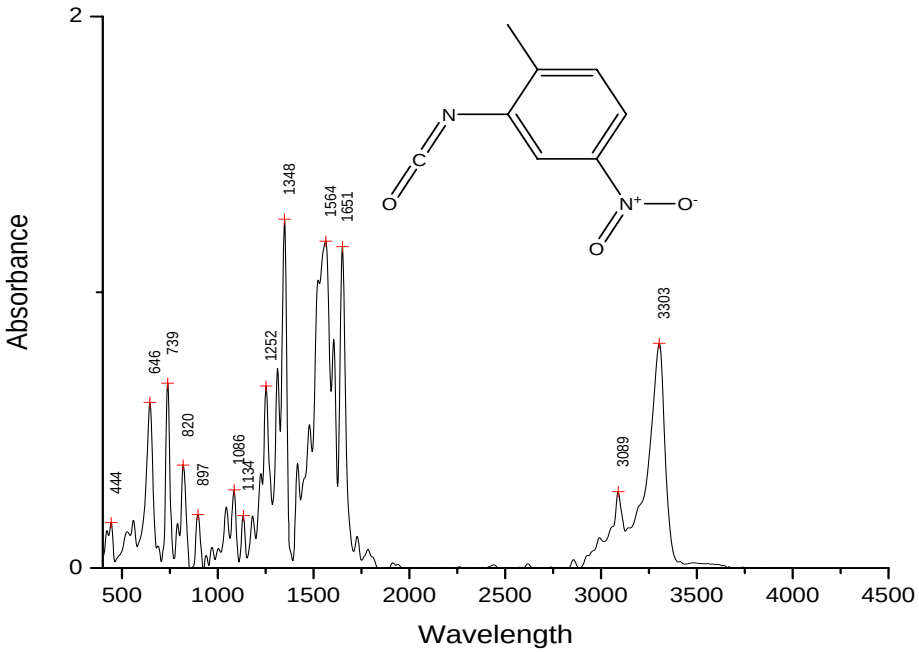

Figure B–29. Infrared Spectrum of 2-methyl-5-nitrophenylisocyanate

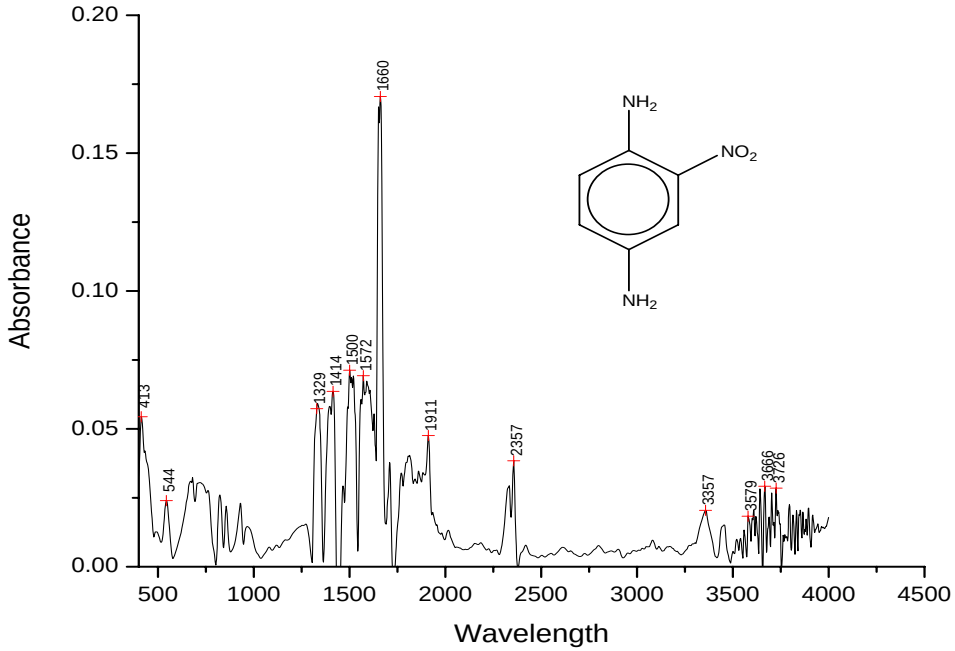

Figure B–30. Infrared Spectrum of 2-nitro-1,4-diaminobenzene

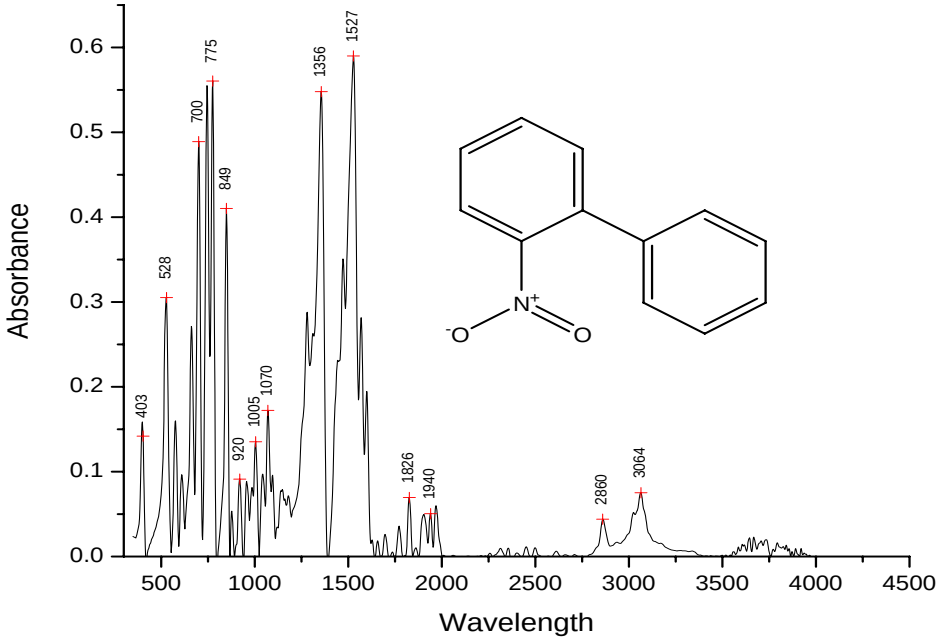

Figure B–31. Infrared Spectrum of 2-nitrobiphenyl

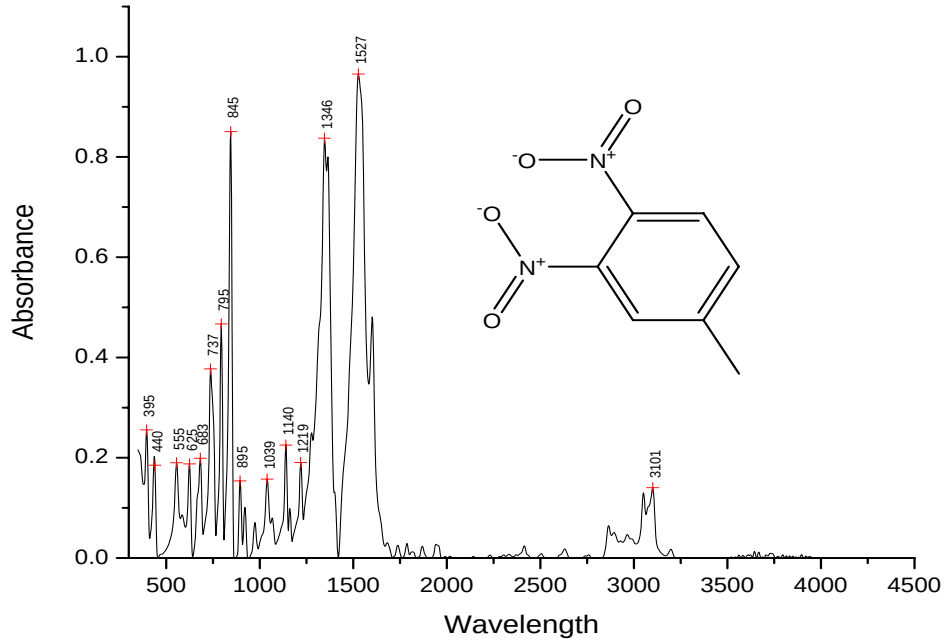

Figure B–32. Infrared Spectrum of 3,4-dinitrotoluene

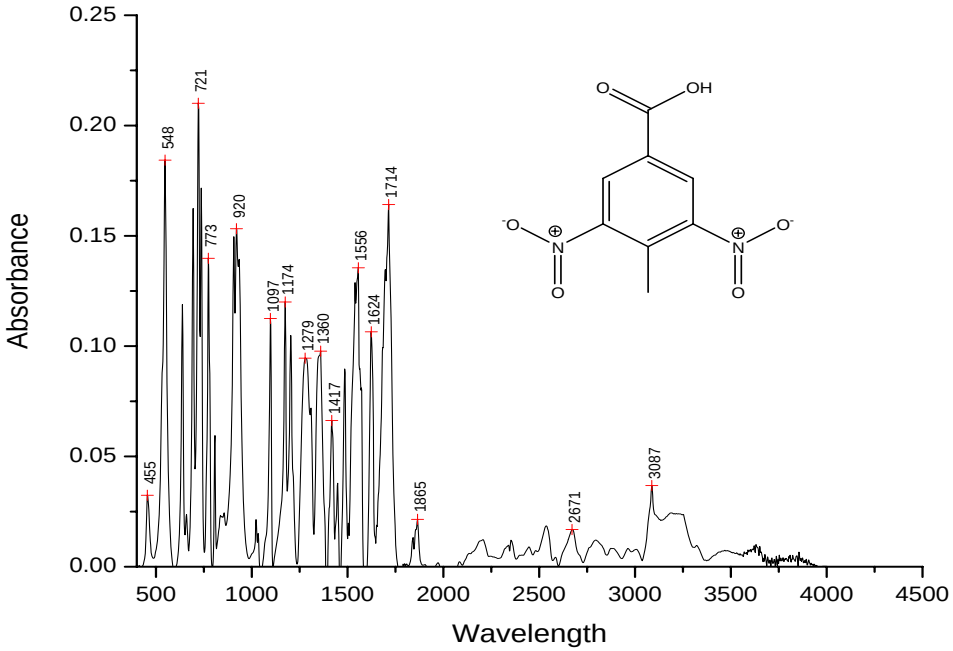

Figure B–33. Infrared Spectrum of 3,5-dinitro-4-methylbenzoic acid

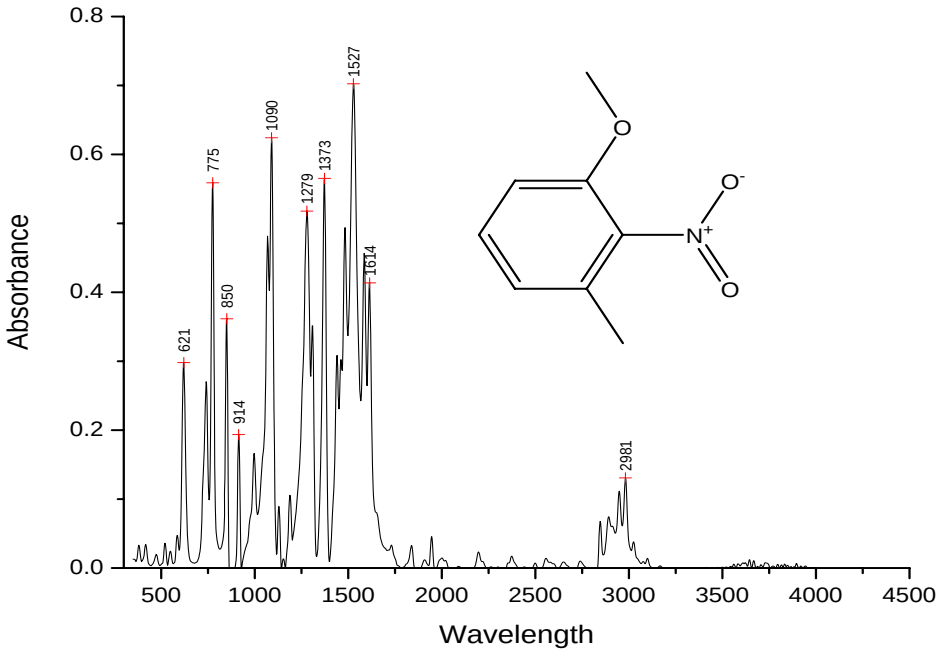

Figure B–34. Infrared Spectrum of 3-methyl-2-nitroanisole

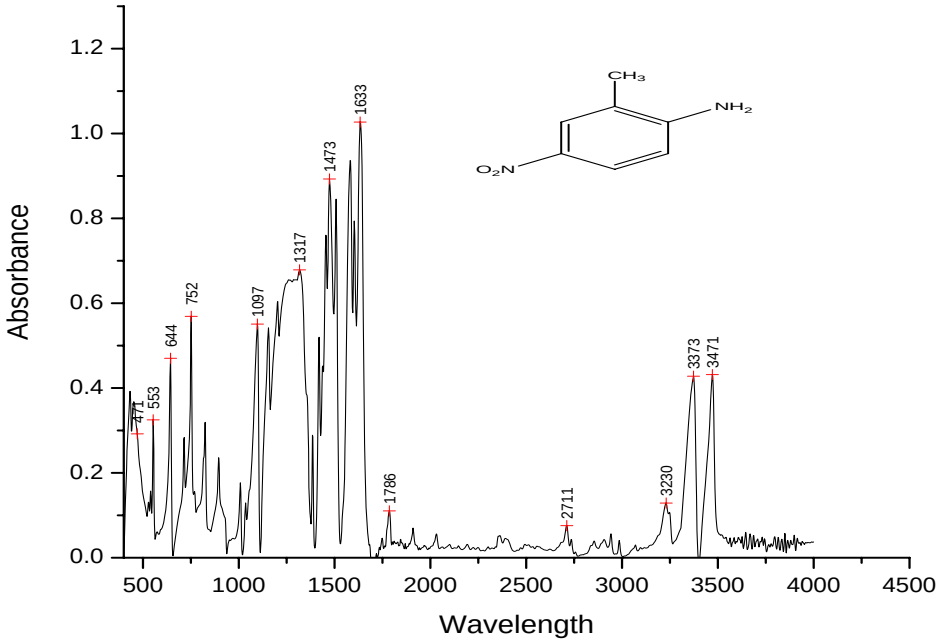

Figure B–35. Infrared Spectrum of 5-nitro-2-aminotoluene

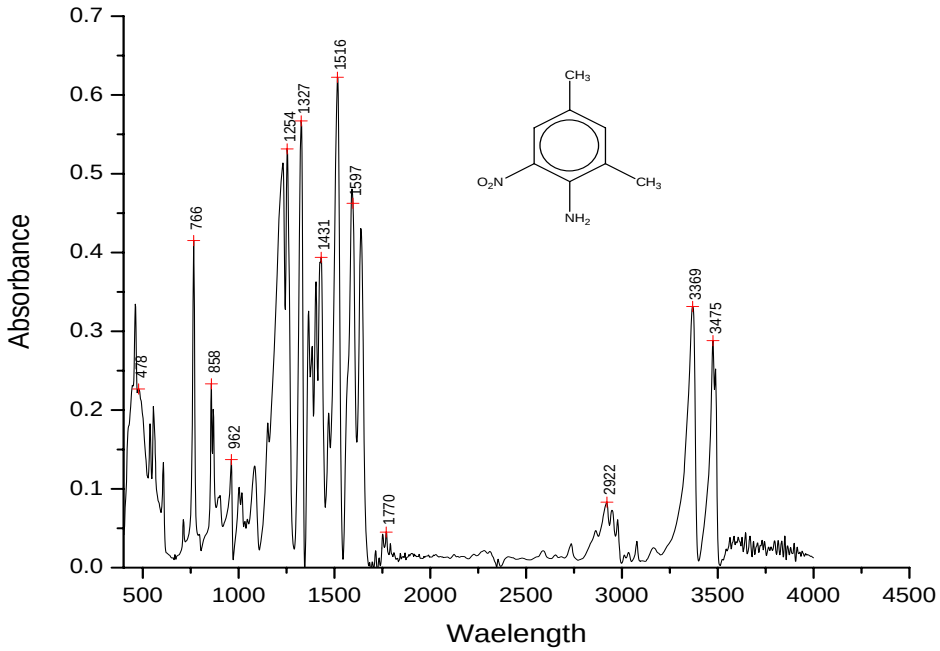

Figure B–36. Infrared Spectrum of 5-nitro-4-amino-1,3-dimethylbenzene

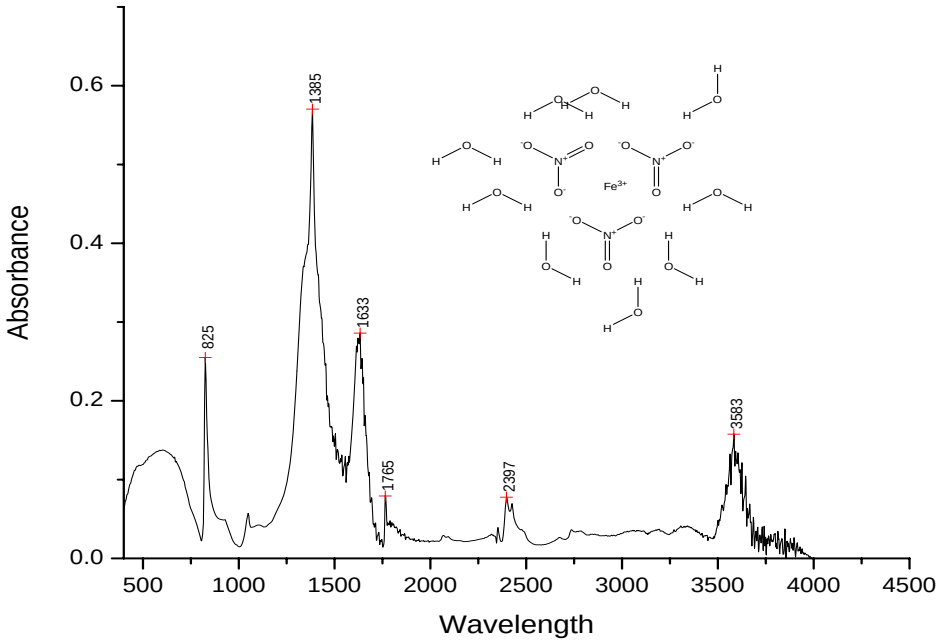

Figure B–37. Infrared Spectrum of Iron(III)nitrate nonahydrate

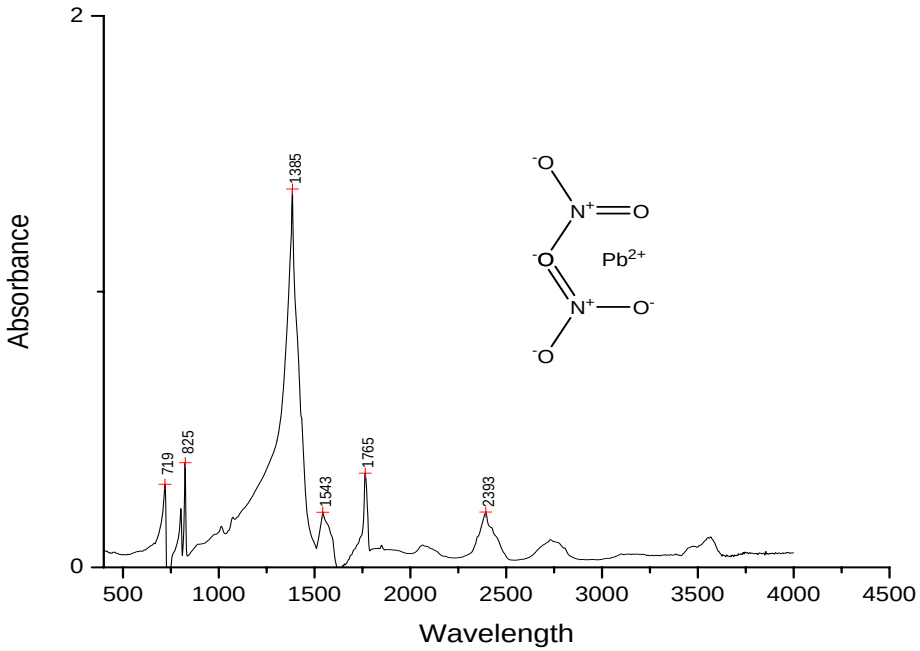

Figure B–38. Infrared Spectrum of Lead Nirate

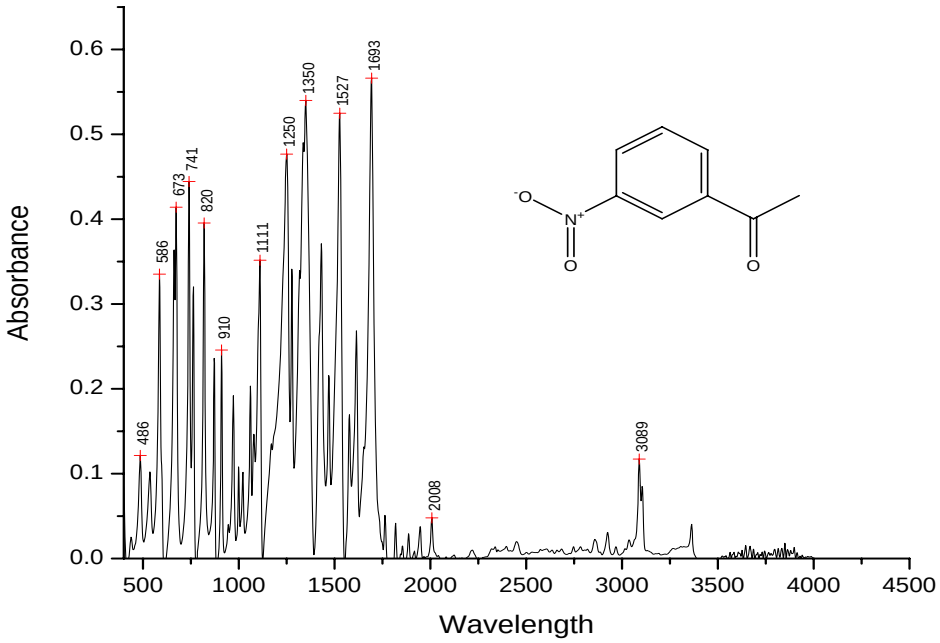

Figure B–39. Infrared Spectrum of m-Nitroacetophenone

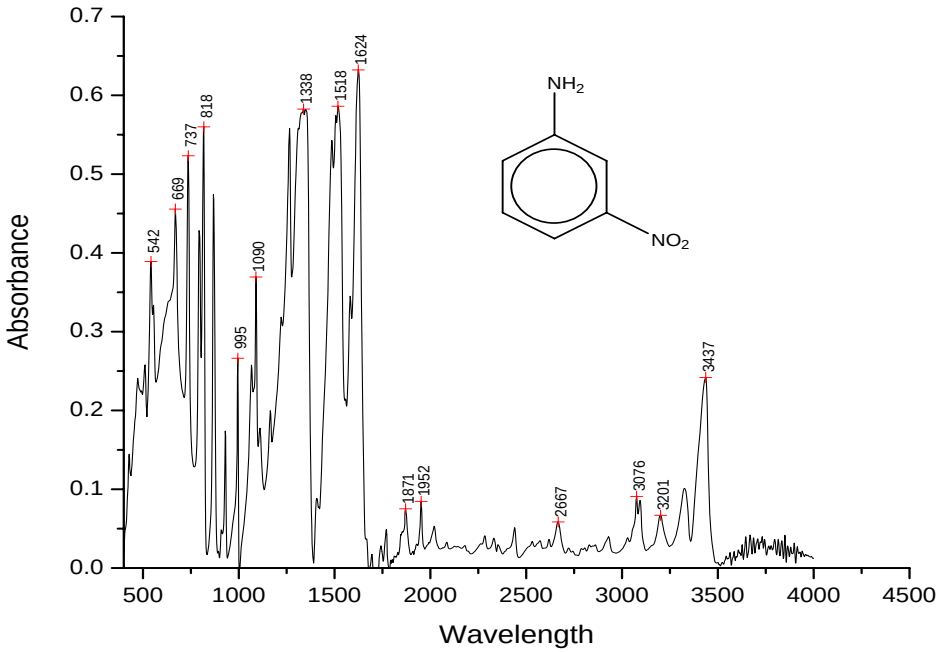

Figure B–40. Infrared Spectrum of m-Nitroaniline

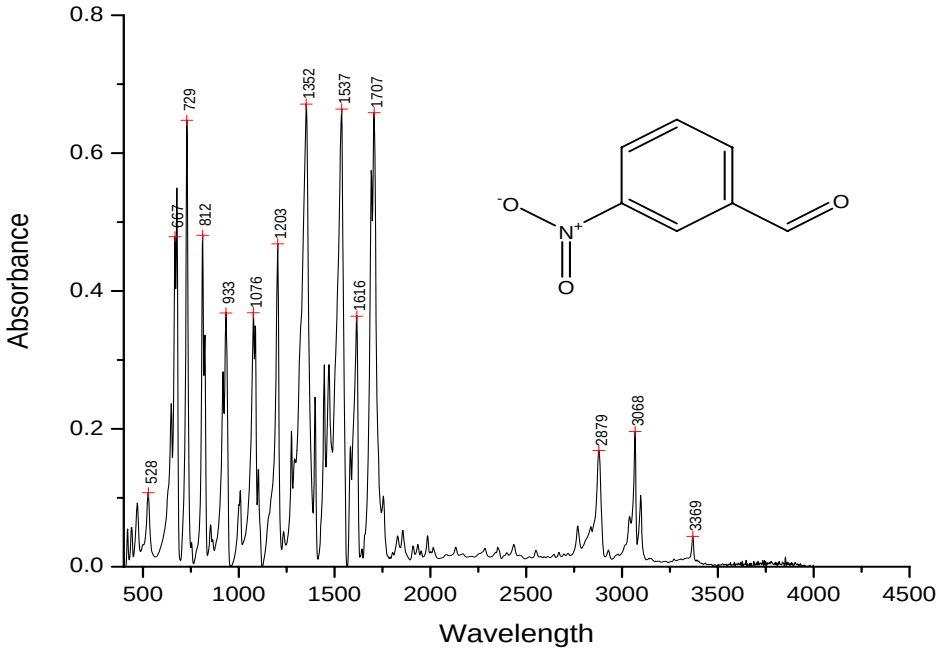

Figure B–41. Infrared Spectrum of m-Nitrobenzaldehide

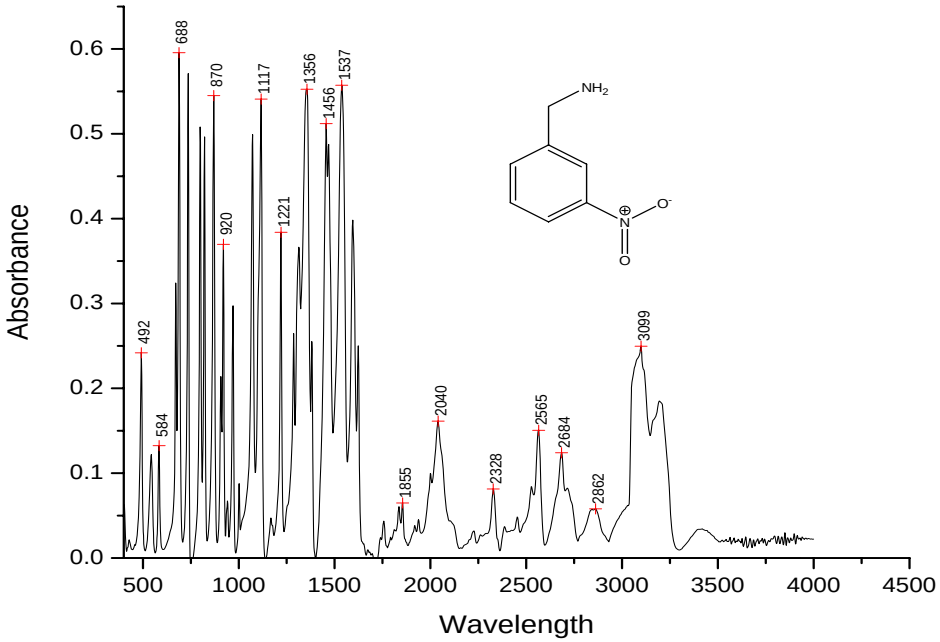

Figure B–42. Infrared Spectrum of m-Nitrobenzylaminehydrochloride

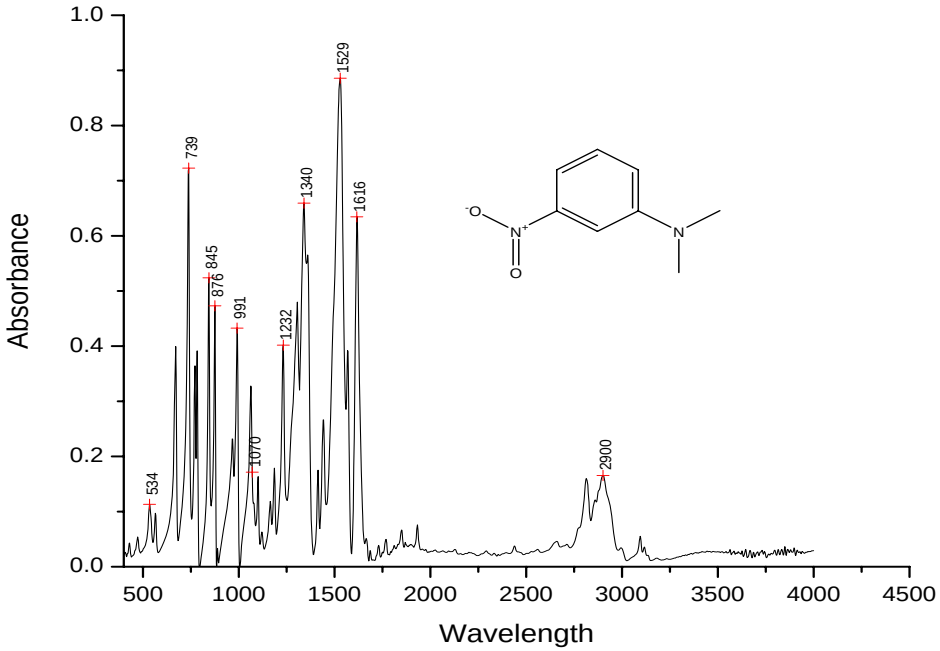

Figure B–43. Infrared Spectrum of m-nitrodimethylaniline

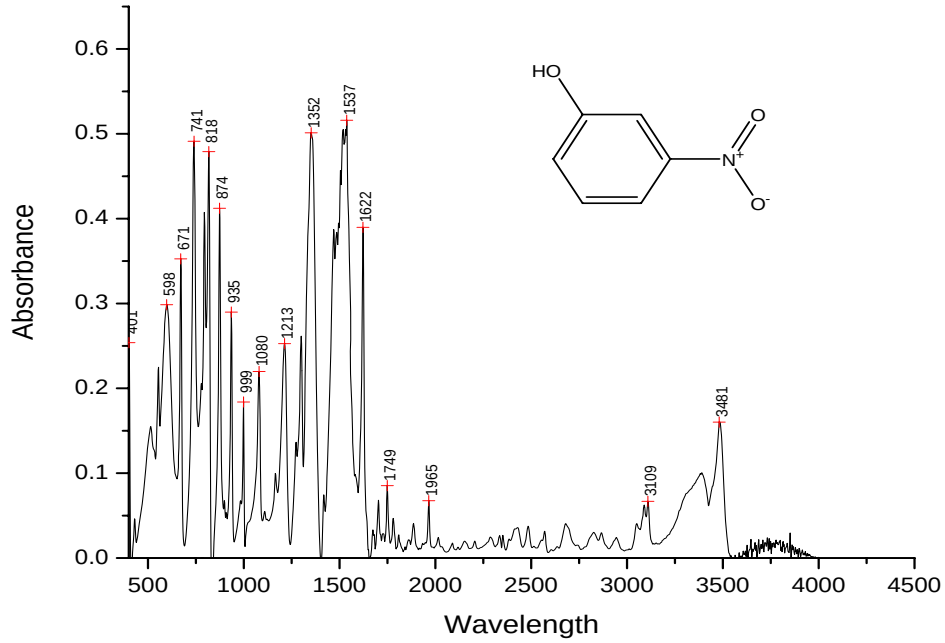

Figure B–44. Infrared Spectrum of m-Nitrophenol

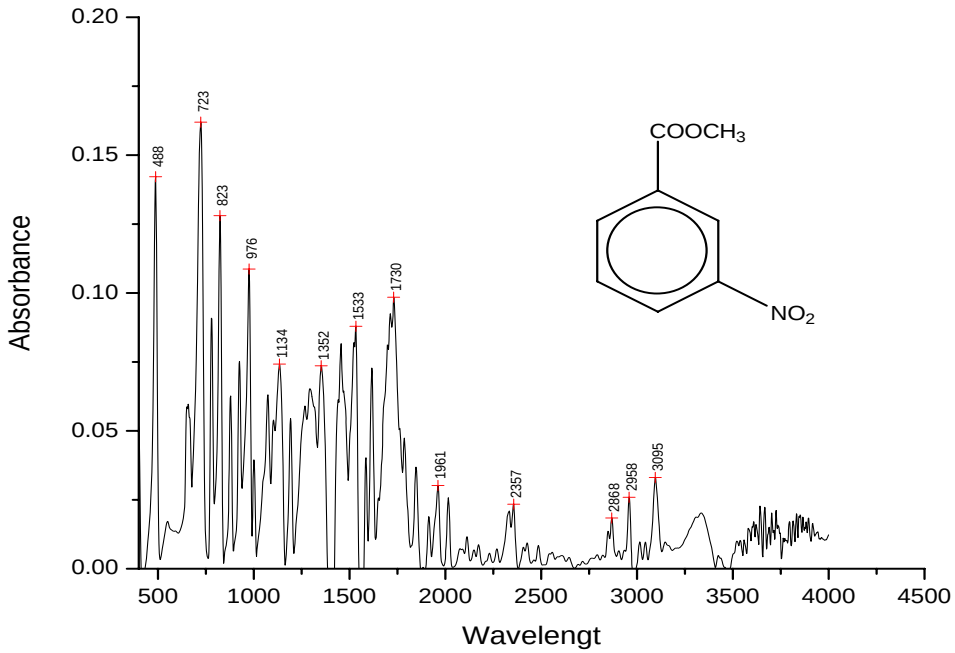

Figure B–45. Infrared Spectrum of Methyl-m-nitrobenzoate

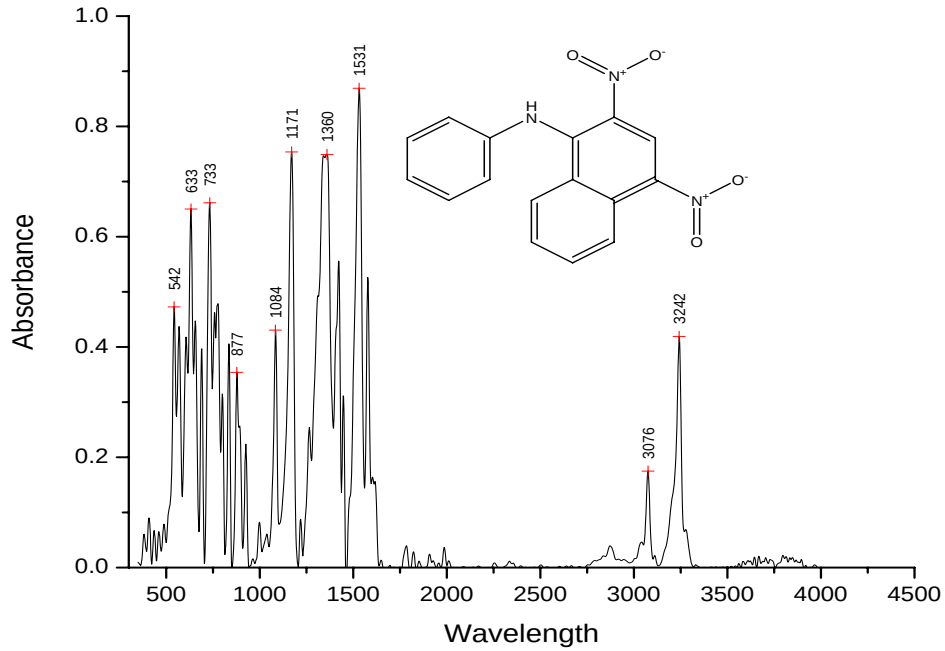

Figure B–46. Infrared Spectrum of N-(2,4-dinitro-1-naphthyl)-benzenamine

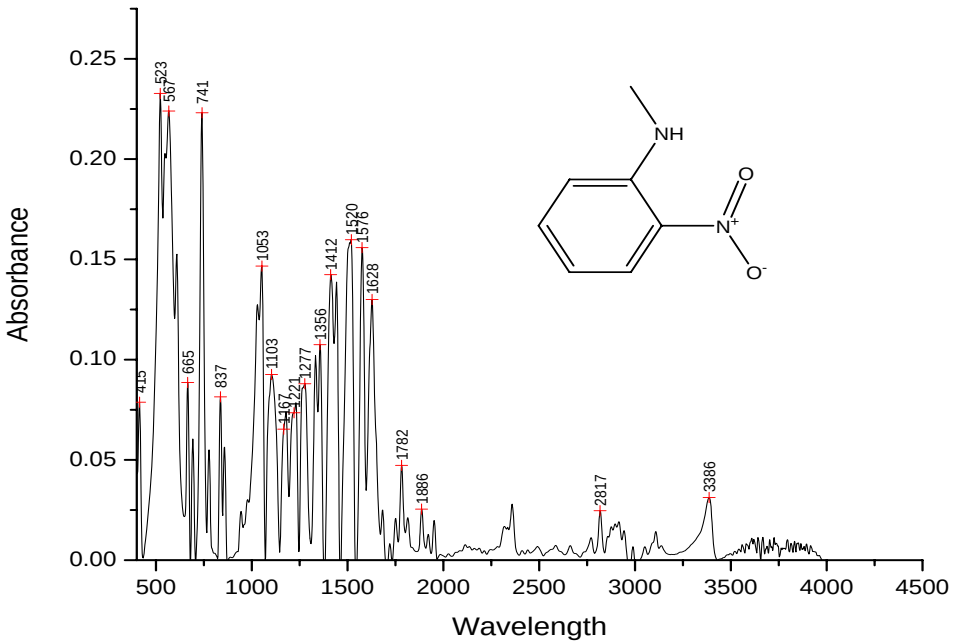

Figure B–47. Infrared Spectrum of n-methyl-o-nitroanilina

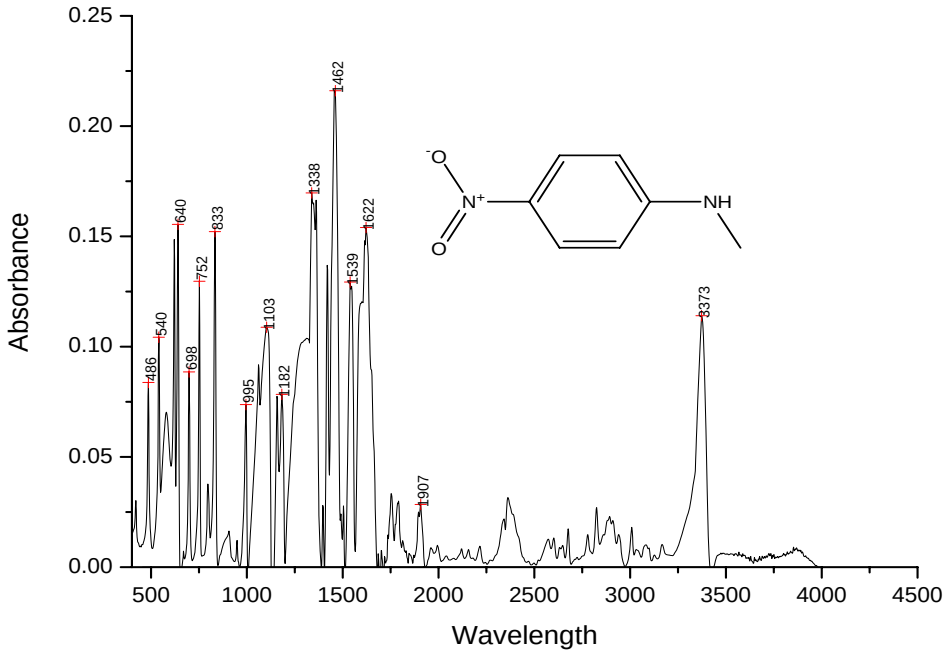

Figure B–48. Infrared Spectrum of n-methyl-p-nitroanilina

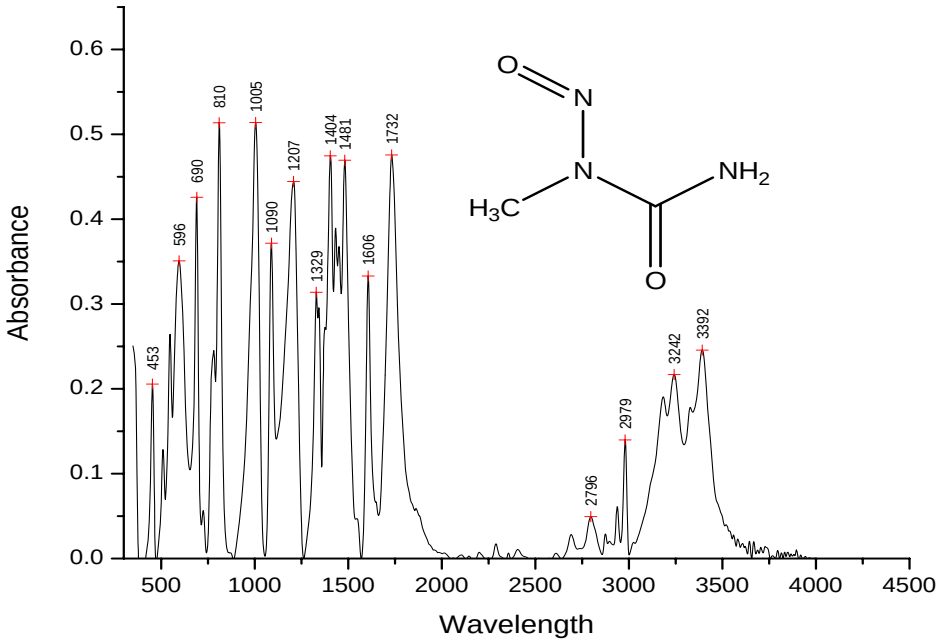

Figure B–49. Infrared Spectrum of N-Nitroso-N-Ethylurea

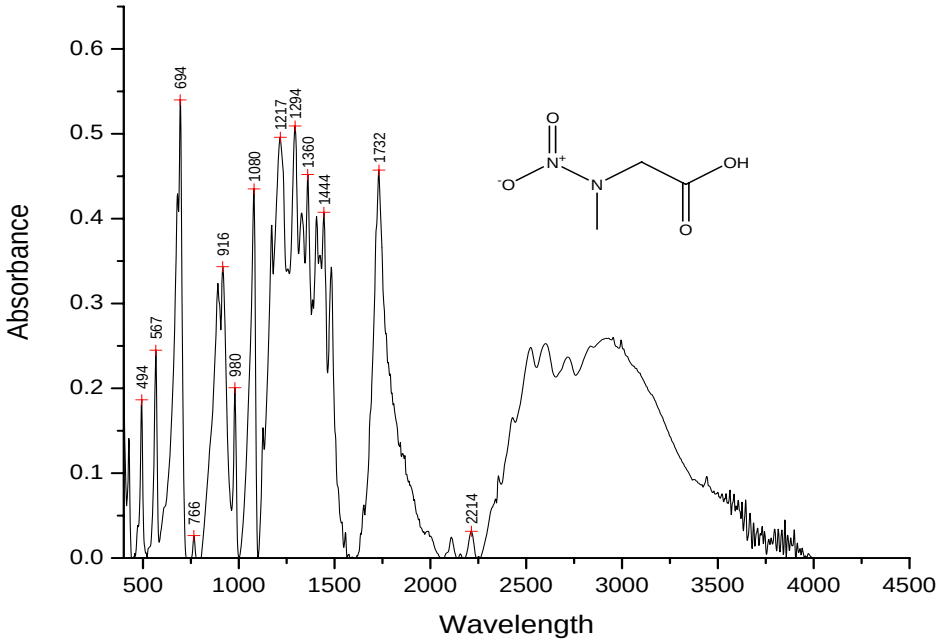

Figure B–50. Infrared Spectrum of n-nitrosoarcosine

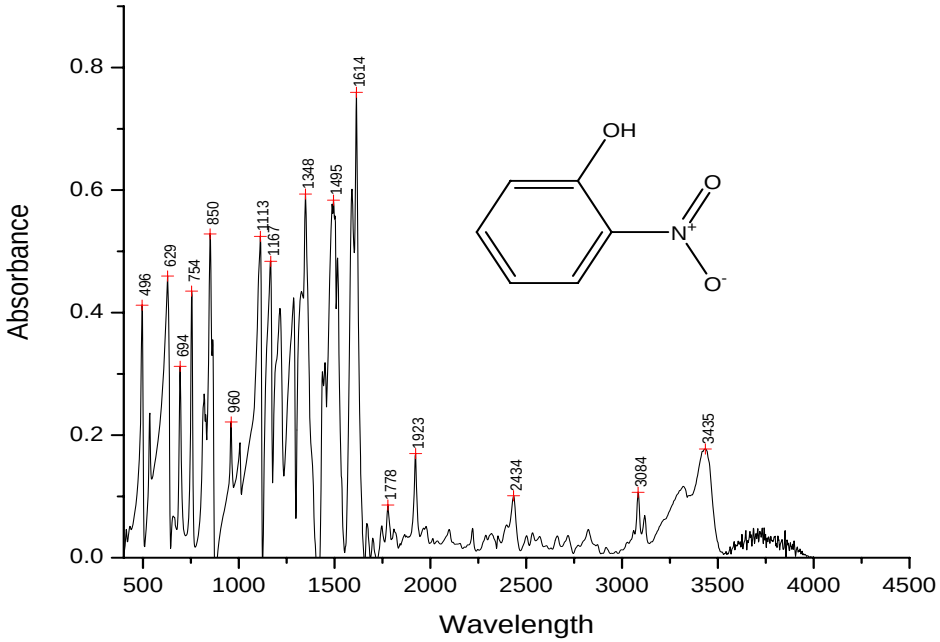

Figure B–51. Infrared Spectrum of nirophenol

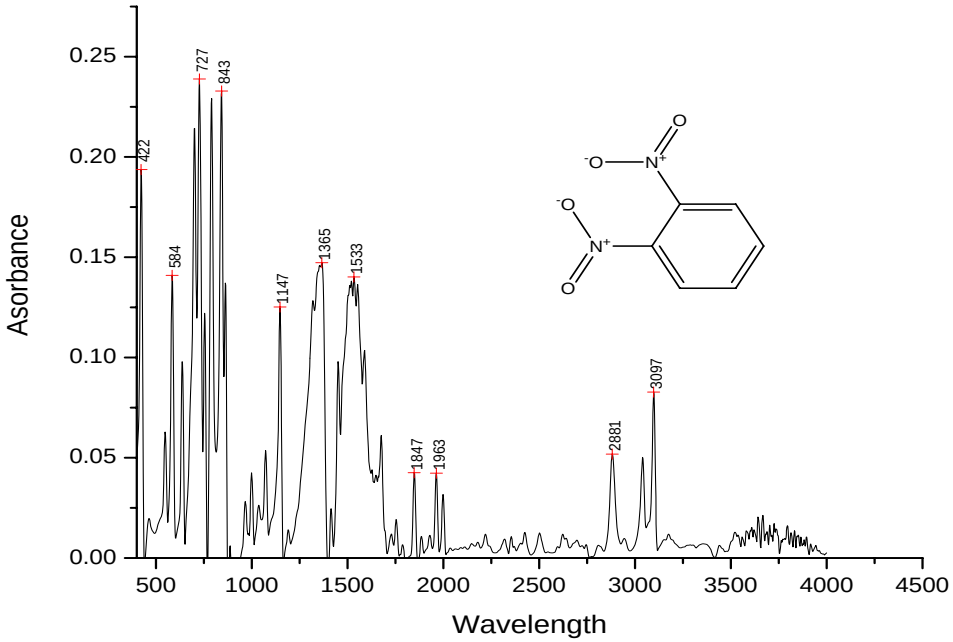

Figure B–52. Infrared Spectrum of o-dinitrobenzene

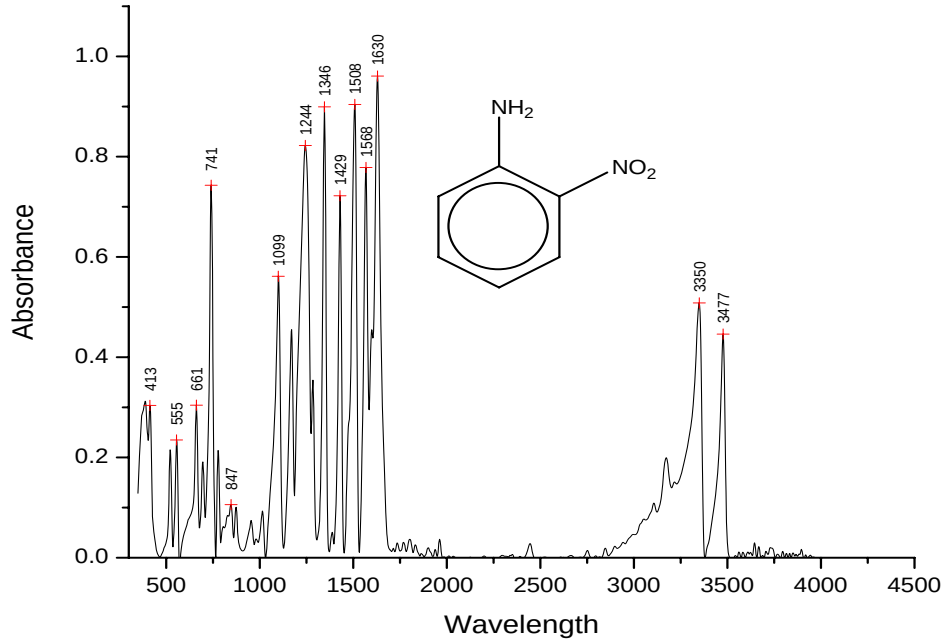

Figure B–53. Infrared Spectrum of O-Nitroaniline

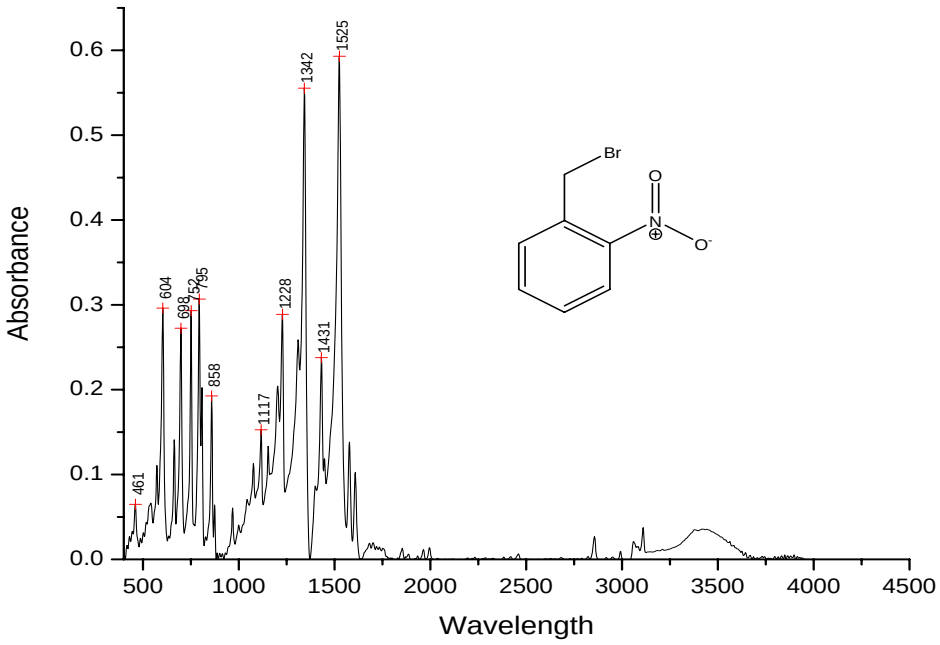

Figure B–54. Infrared Spectrum of o-Nitrobenzylbromide

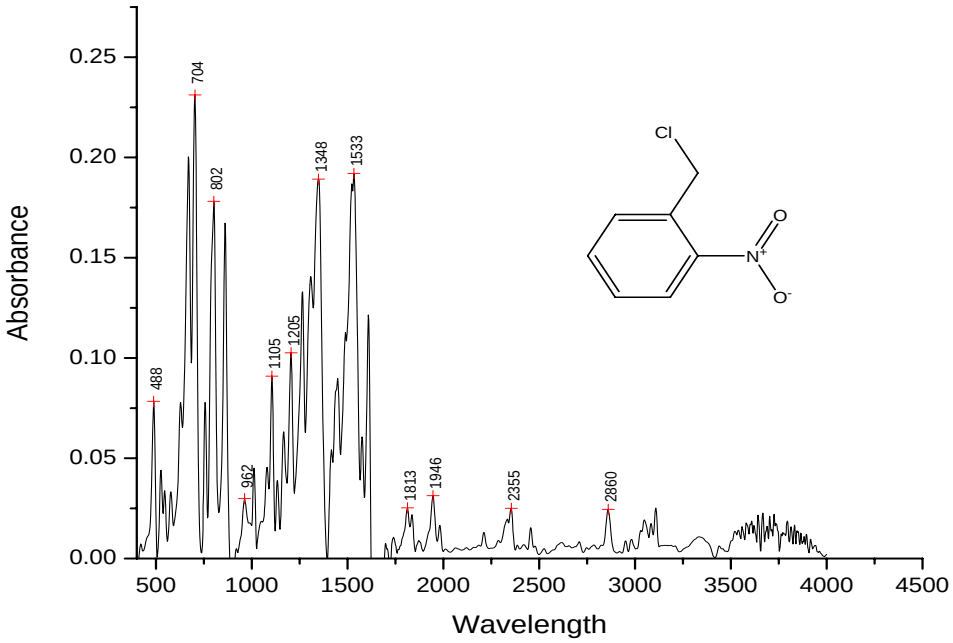

Figure B–55. Infrared Spectrum of o-nitrobenzylchloride

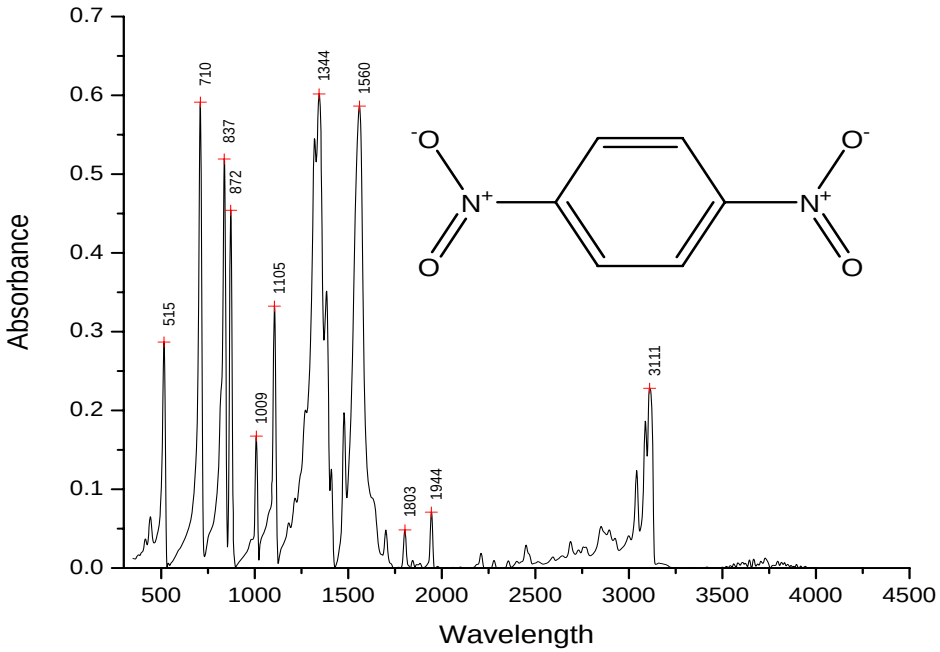

Figure B–56. Infrared Spectrum of p-Dinitrobenzene

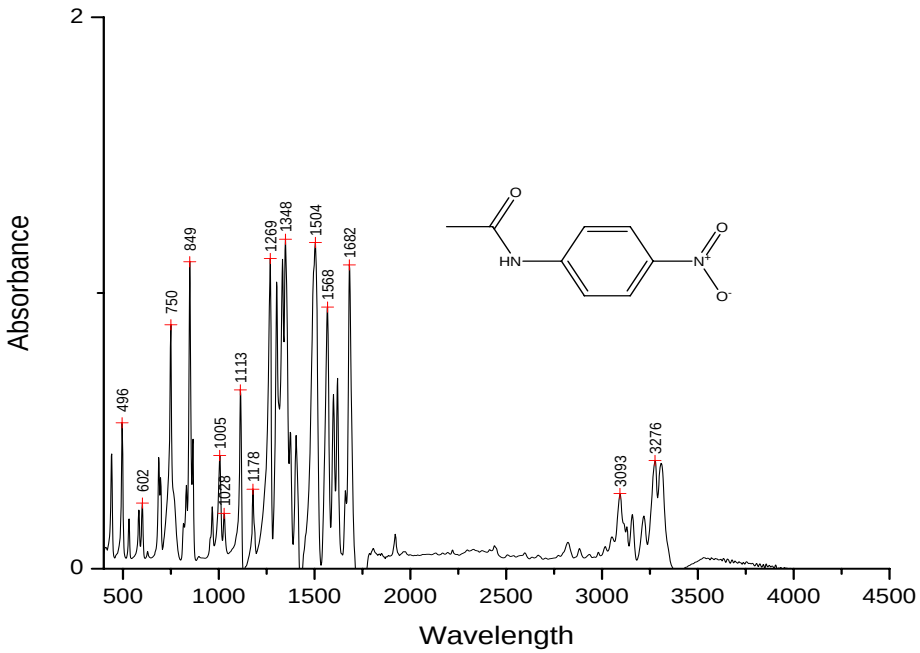

Figure B–57. Infrared Spectrum of p-Nitroacetanilide

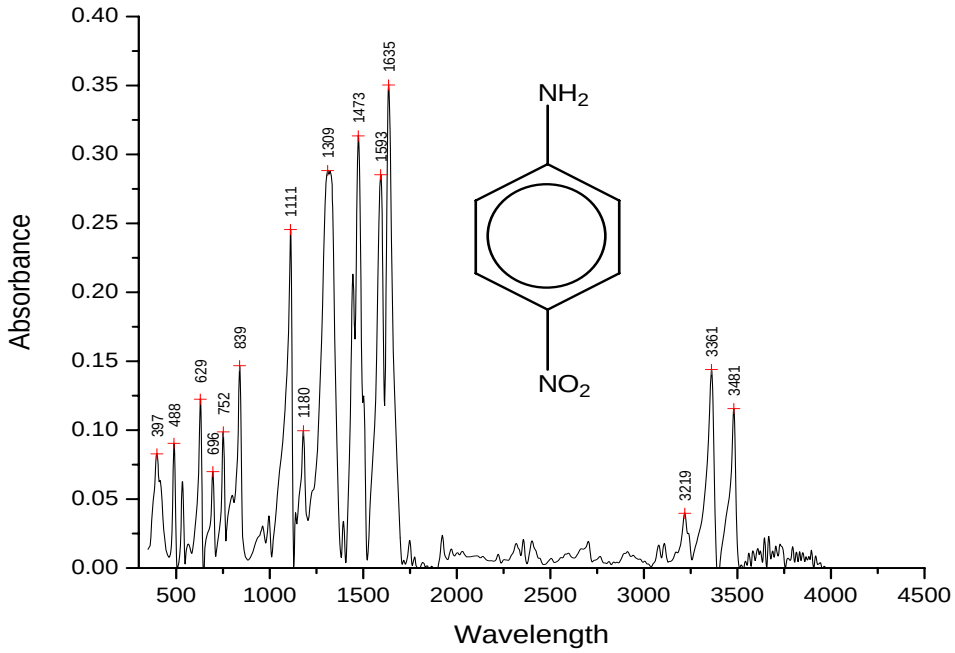

Figure B–58. Infrared Spectrum of p-Nitroaniline

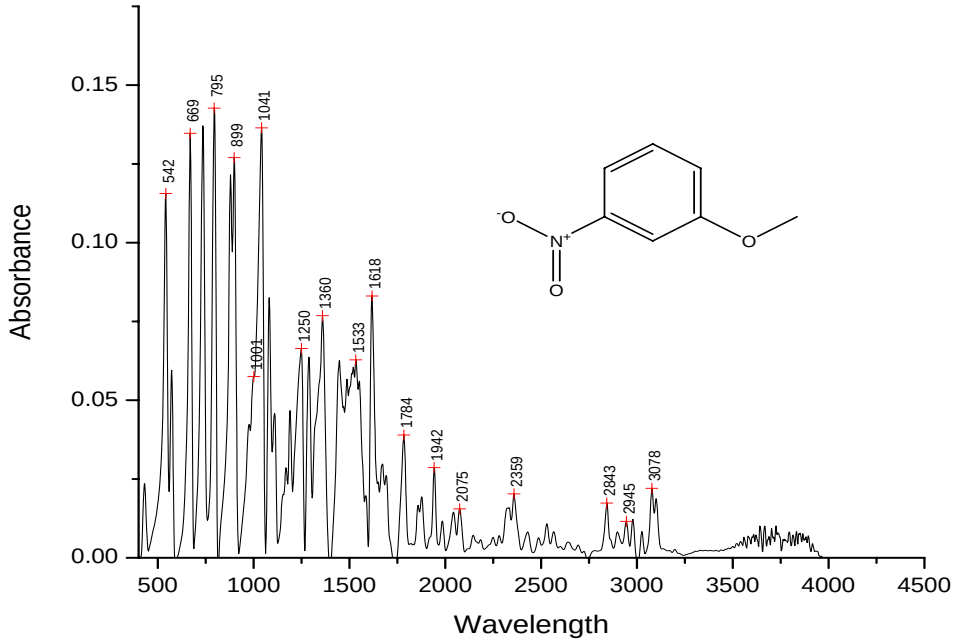

Figure B–59. Infrared Spectrum of p-Nitroanisole

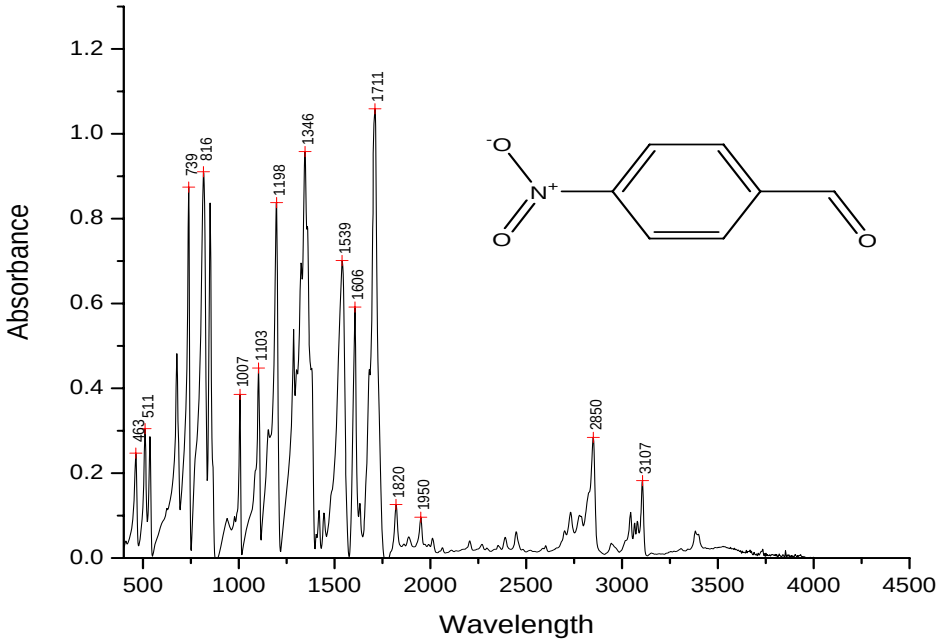

Figure B–60. Infrared Spectrum of p-Nitrobenzaldehide

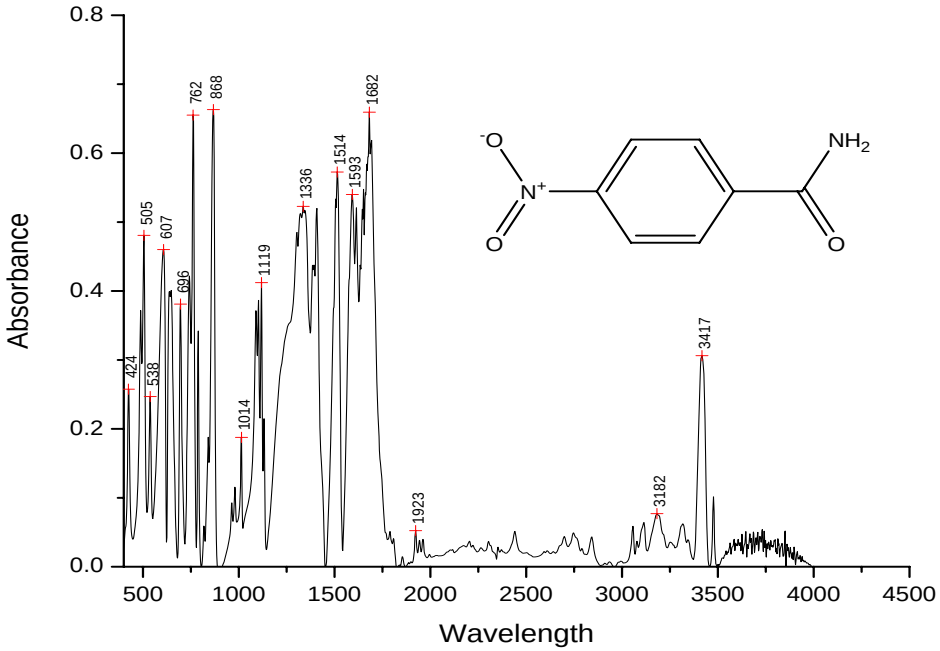

Figure B–61. Infrared Spectrum of p-Nitrobenzamide

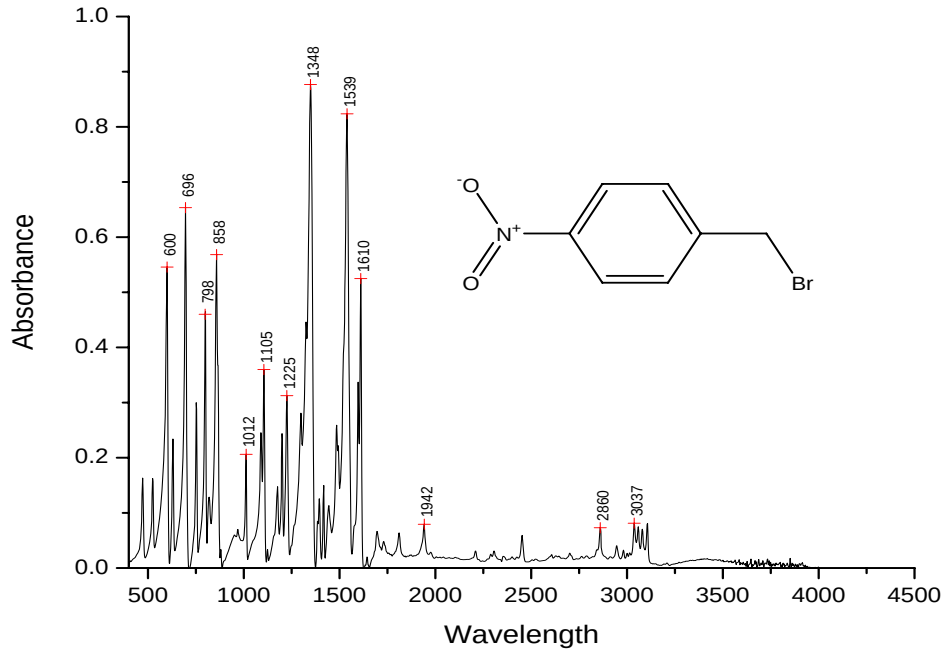

Figure B–62. Infrared Spectrum of p-Nitrobenzylbromide

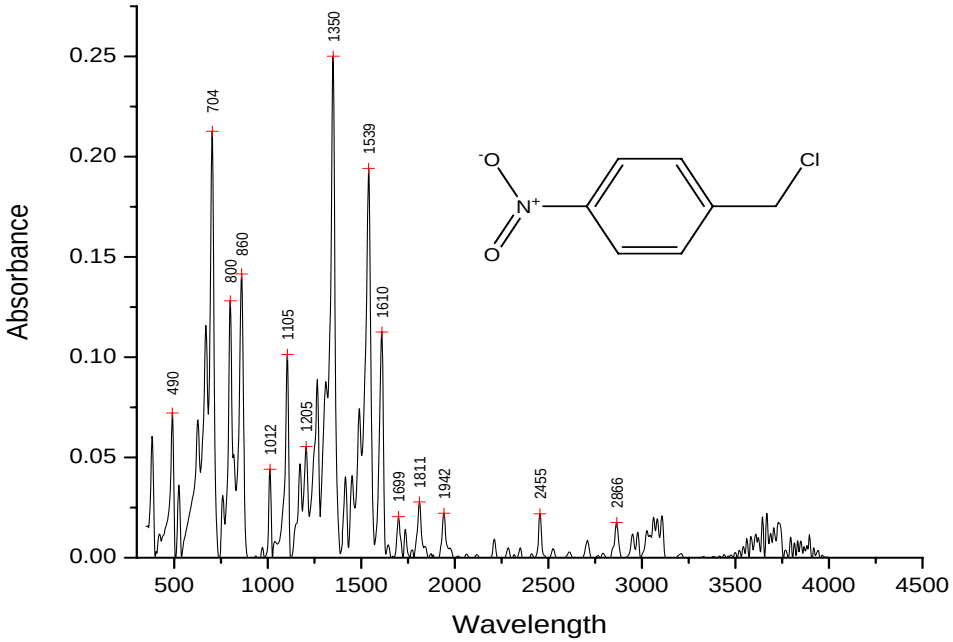

Figure B–63. Infrared Spectrum of p-Nitrobenzyl Chloride

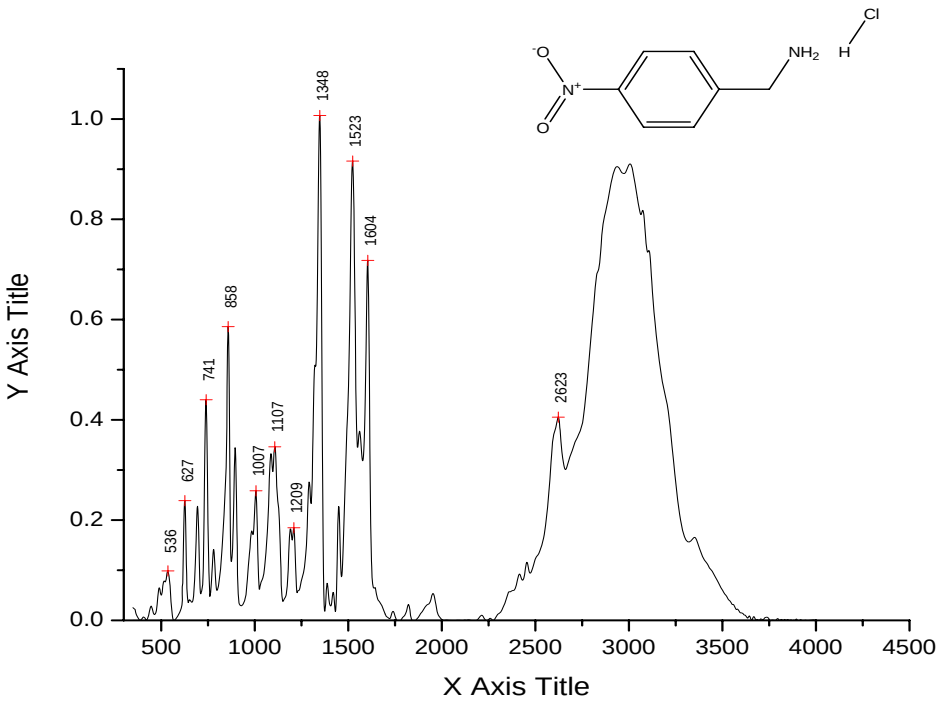

Figure B–64. Infrared Spectrum of p-Nitrobenzylaminehydrochloride

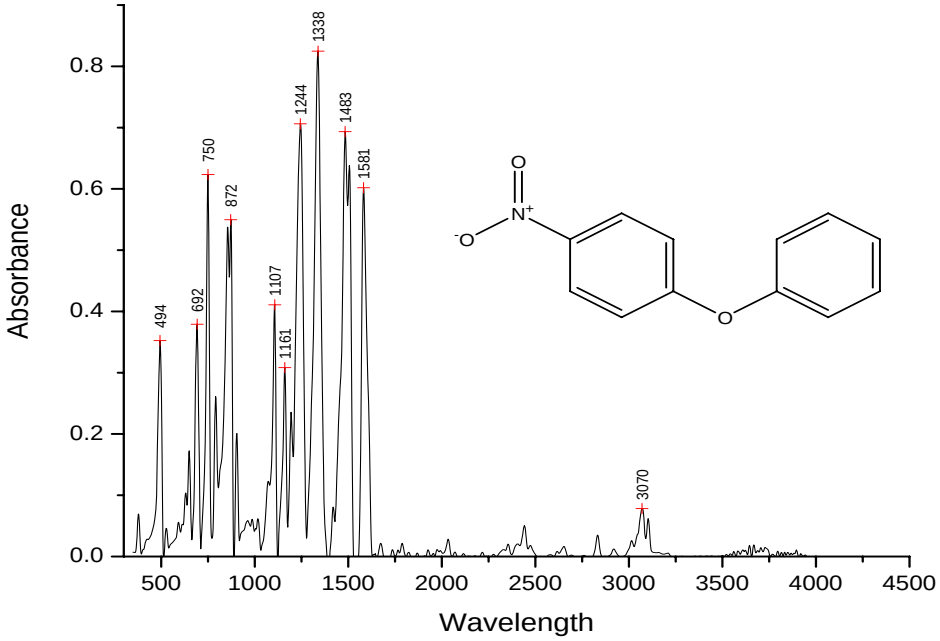

Figure B–65. Infrared Spectrum of p-Nitrodiphenyl ether

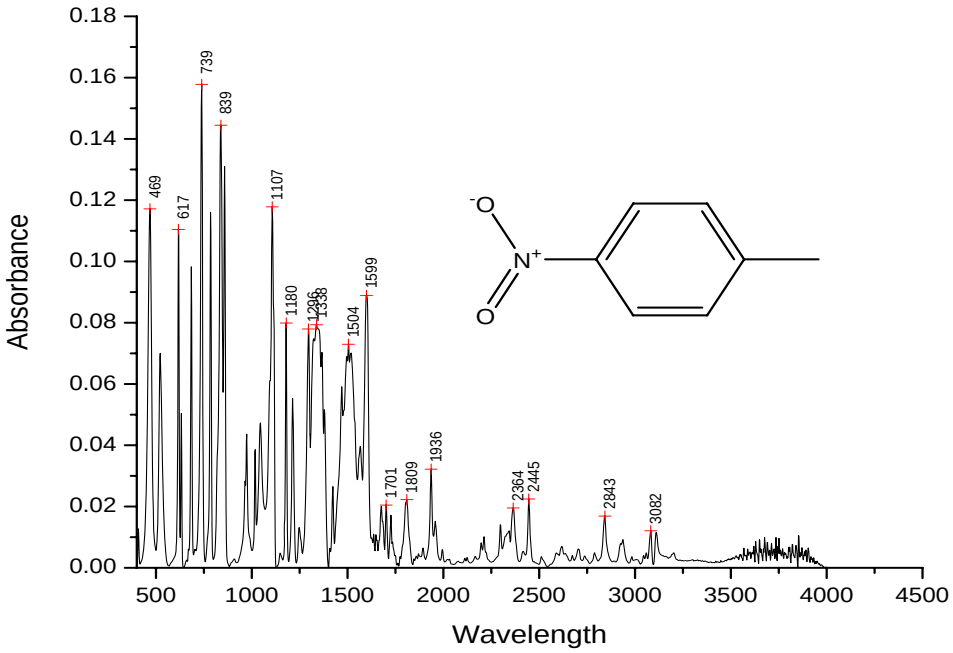

Figure B–66. Infrared Spectrum of p-Nitrotolueno

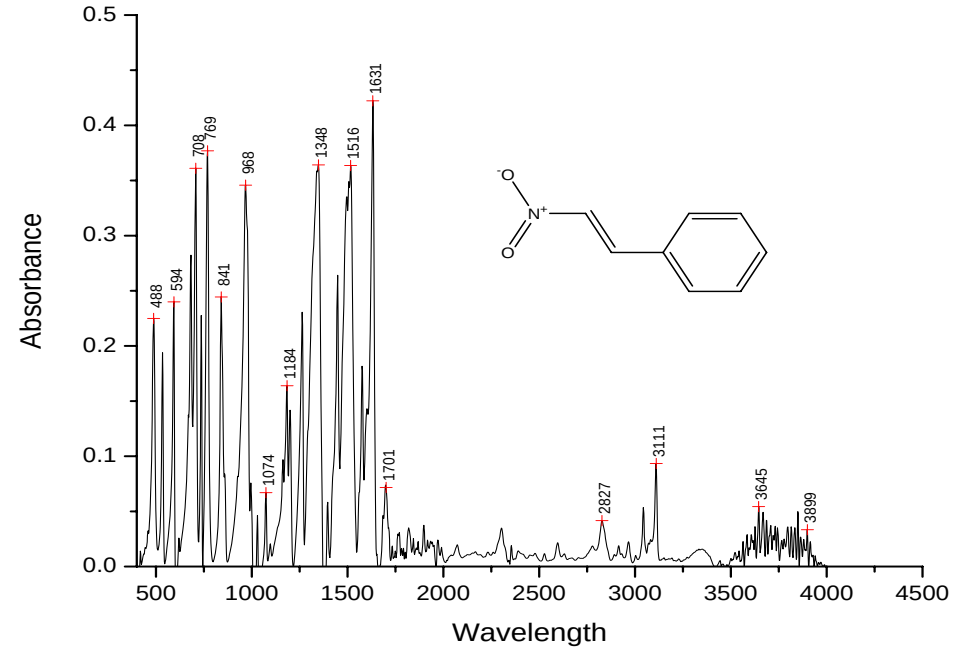

Figure B–67. Infrared Spectrum of Trans-Beta-Nitrostyrene